JAEA-Research
2024-009
DOI:10.11484/jaea-research-2024-009

JAEA-Research

Heat Transfer Coefficients Model for SIMMER-III and SIMMER-IV

David J. BREAR, Satoru KONDO, Joji SOGABE, Yoshiharu TOBITA and Kenji KAMIYAMA

Fast Reactor Cycle System Research and Development Center
Oarai Research and Development Institute

October 2024

Japan Atomic Energy Agency

日本原子力研究開発機構

国立研究開発法人日本原子力研究開発機構　研究開発推進部　科学技術情報課
〒 319-1112　茨城県那珂郡東海村大字村松 4 番地 49
E-mail: ird-support@jaea.go.jp

JAEA-Research 2024-009

Heat Transfer Coefficients Model for SIMMER-III and SIMMER-IV

David J. BREAR[*1], Satoru KONDO[*2], Joji SOGABE, Yoshiharu TOBITA[*3] and Kenji KAMIYAMA[+]

Fast Reactor Cycle System Research and Development Center
Oarai Research and Development Institute
Japan Atomic Energy Agency
Oarai-machi, Higashiibaraki-gun, Ibaraki-ken

(Received June 6, 2024)

The SIMMER-III/SIMMER-IV computer codes are being used for liquid-metal fast reactor (LMFR) core disruptive accident (CDA) analysis. The sequence of events predicted in a CDA is often influenced by the heat exchanges between LMFR materials, which are controlled by heat transfer coefficients (HTCs) in the respective materials. The mass transfer processes of melting and freezing, and vaporization and condensation are also controlled by HTCs. The complexities in determining HTCs in a multi-component and multi-phase system are the number of HTCs to be defined at binary contact areas of a fluid with other fluids and structure surfaces, and the modes of heat transfer taking into account different flow topologies representing flow regimes with and without structure. As a result, dozens of HTCs are evaluated in each mesh cell for the heat and mass transfer calculations.

This report describes the role of HTCs in SIMMER-III/SIMMER-IV, the heat transfer correlations implemented and the calculation of HTCs in all topologies in multi-component, multi-phase flows. A complete description of the physical basis of HTCs and available experimental correlations is contained in Appendices to this report. The major achievement of the code assessment program conducted in parallel with code development is summarized with respect to HTC modeling to demonstrate that the coding is reliable and that the model is applicable to various multi-phase problems with and without reactor materials.

Keywords: Multi-phase Flow, Heat Transfer Coefficient, Fluid-fluid Heat Transfer, Fluid-structure Heat Transfer, Film Boiling, Safety Analysis, CDA, SIMMER-III, SIMMER-IV, LMFR

＋ Policy Planning and Administration Department
*1 Formerly International Fellows, Power Reactor and Nuclear Fuel Development Corporation (the present Japan Atomic Energy Agency)
*2 Fast Reactor Cycle System Research and Development Center until March 31, 2023
*3 Karlsruhe Institute of Technology

SIMMER-III 及び SIMMER-IVの熱伝達係数モデル

日本原子力研究開発機構　大洗研究所　高速炉サイクル研究開発センター

David J. BREAR*[1]、近藤 悟*[2]、曽我部 丞司、飛田 吉春*[3]、神山 健司[+]

（2024年6月6日受理）

SIMMER-III/SIMMER-IV は液体金属高速炉の炉心崩壊事故（CDA）の解析に使用する計算コードである。CDA の事象進展は炉心物質間の熱伝達係数（HTC）により大きく影響される。溶融・固化、蒸発・凝縮といった質量移行現象も熱伝達により支配される。複雑な多相・多成分系においては、一つの流体成分と他の流体又は構造材表面との間での多数の異なる HTC を計算する必要がある。また、多相流の流動様式や構造材の配位に従って異なる伝熱モードを考慮する必要もある。結果として、各計算セルごとに数十の HTC が計算される。

本報告書には、SIMMER-III/SIMMER-IV の HTC モデルの役割、選定した HTC 相関式とその技術的背景、流動様式の取扱いと HTC の内挿方法、検証及び妥当性確認の成果概要を記載する。

大洗研究所：〒311-1393 茨城県東茨城郡大洗町成田町4002 番地
＋ 経営企画部
*1 当時、動力炉・核燃料開発事業団 国際特別研究員
*2 高速炉サイクル研究開発センター（2023 年 3 月 31 日まで在籍）
*3 カールスルーエ工科大学

Contents

目　次

List of Tables

List of Figures

This is a blank page.

1. Introduction

The SIMMER-III and SIMMER-IV computer codes couple a two-/three-dimensional, multi-velocity field, multi-phase, multi-component, Eulerian fluid dynamics module with a space- and time-dependent neutronics model and a structure model[1)-7)]. The codes have been used for liquid-metal fast reactor (LMFR) core disruptive accident (CDA) analyses, which typically involve significant temperature responses and phase changes of LMFR core materials and their influence on the reactor neutronic state. In order to model complex multi-phase flow physical processes, mass and energy conservation equations are solved for the density components and energy components, respectively. With many improved and advanced features successfully implemented, the codes have replaced the former SIMMER-II code[8)], developed at the Los Alamos National Laboratory. SIMMER-IV is the three-dimensional code, which retains essentially the same modeling as the two-dimensional SIMMER-III, except for the fluid convection algorithm and the additional structure wall treatment in SIMMER-IV. In the remainder of this report, only the code name SIMMER-III is referred to in many parts, unless noted differently.

In the fluid-dynamics algorithm, intra-cell heat and mass transfer processes are treated separately from inter-cell fluid convection. Complexities associated with different flow topologies and structure configuration in a multi-component, multi-velocity-field system are the main reason of this separation. The important heat and mass transfer paths are modeled by calculating the heat fluxes to and across the binary contact interface for each pair of interacting materials. Since the heat fluxes are controlled by heat transfer coefficients (HTCs), the HTCs in the code can play an important role in predicting the evolution of an accident sequence. This report describes the fluid-side HTC model and the structure-side HTCs are treated in the structure model documented elsewhere[5)].

Although the models and experience in the previous codes, SIMMER-II[8)] and AFDM[9), 10)], were heavily utilized, there have been significant development and improvement in the flamework of SIMMER-III. The resultant HTC model has the following salient and advanced features over the previous SIMMER-II or AFDM:

- Extensive literature review: Available papers and reports up to the early 1990s were fully reviewed on relevant experimental data, engineering correlations and multi-phase computer codes. The collected information has been used to select the standard and optional theories and correlations.
- Full SIMMER-III/SIMMER-IV components: Each of the 8 fluid energy components can transfer heat to other fluid energy components plus three structure surfaces in SIMMER-III (five for SIMMER-IV). This requires the computation of up to 73 HTCs (89 HTCs for SIMMER-IV) in each mesh cell.
- Multi-phase flow topology treatment with smooth transition: The contact modes between energy components depend on multiphase flow topology (flow regimes). The HTCs are first determined for well-defined flow topologies, such as bubbly, annular and dispersed flow regimes. The HTCs for ill-defined flow topologies, such as transition and slug flow regimes, are calculated by suitable interpolation of the HTCs of well-defined flow regimes.

- Improved treatment of fluid particles: The special effects of enhancement of heat transfer due to internal circulation and surface oscillation of fluid particles are modeled.
- Droplet-droplet heat transfer: The HTC for droplet-droplet contact in the dispersed flow is modeled, assuming short-timescale collision, based on the SIMMER-II approach.
- Film-boiling HTC: If the conditions for film boiling are satisfied for a hot dispersed-phase liquid in contact with a more volatile liquid, film-boiling HTCs are calculated.
- Flexible input specifications: All the parameters of HTC correlations are specified by user input variables, whilst their recommended and default values for the standard LMFR materials are built in the code. Simple multipliers are also available for easily scaling the HTCs.

The HTC model and its use for SIMMER-III was first documented in the 1990s as an informal technical report, together with a series of backing documents that reviewed the then available heat-transfer correlations and the relating models in the other multiphase codes. The purpose of this report, therefore, is to re-compile related and scattered documents into a new research report to be useful for SIMMER-III/SIMMER-IV users. The main body of the report is a concise summary of the implemented HTC correlations and the use of the model. The overview of fluid-dynamics model and role of the HTC model is briefly described in Chapter 2. The scope and limitations of the model are also discussed. Chapter 3 contains a list of the implemented heat transfer correlations, and the interpolation procedures used. Although the details of the verification and validation (V&V) of the model are beyond the scope of this report, the achievements of SIMMER-III assessment program[11), 12)] with respect to HTC modeling are summarized in Chapter 4. Chapter 5 provides brief program description and the use of HTC. A more complete description of the physical basis of the heat transfer correlations and available correlations is contained in Appendices which are attached to this report.

2. Overview and Purpose of Heat-Transfer Coefficients Model

2.1. Overview of Fluid Dynamics Algorithm

In SIMMER-III/SIMMER-IV, conservation equations are written for independent variables in a unit volume, and the mass and energy are represented by the macroscopic (smear) density, $\bar{\rho}_m$, and specific internal energy, e_M, respectively. The density components are subscripted by m, the energy components by M, and $\bar{\rho}_m = \alpha_M/v_M$. The conservation equations involving fluid mass, momentum and internal energy are:

$$\frac{\partial \bar{\rho}_m}{\partial t} + \nabla \cdot \left(\bar{\rho}_m \boldsymbol{v}_q\right) = -\Gamma_m \tag{1}$$

$$\frac{\partial \bar{\rho}_q \boldsymbol{v}_q}{\partial t} + \sum_{m\in q} \nabla \cdot \left(\bar{\rho}_m \boldsymbol{v}_q \boldsymbol{v}_q\right) + \alpha_q \Delta p - \bar{\rho}_q \boldsymbol{g} + K_{qS}\boldsymbol{v}_q - \sum_{q'} K_{qq'}\left(\boldsymbol{v}_{q'} - \boldsymbol{v}_q\right) - \boldsymbol{VM}_q = \sum_{q'} \Gamma_{qq'}\left[H\left(\Gamma_{qq'}\right)\boldsymbol{v}_q + H\left(\Gamma_{q'q}\right)\boldsymbol{v}_{q'}\right] \tag{2}$$

$$\frac{\partial \bar{\rho}_M e_M}{\partial t} + \sum_{m\in M} \nabla \cdot \left(\bar{\rho}_m e_m \boldsymbol{v}_q\right) + p\left[\frac{\partial \alpha_M}{\partial t} + \nabla \cdot \left(\alpha_M \boldsymbol{v}_q\right)\right] - \frac{\bar{\rho}_M}{\bar{\rho}_m}\left[\sum_q K_{q'q}\left(\boldsymbol{v}_q - \boldsymbol{v}_{q'}\right)\cdot\left(\boldsymbol{v}_q - \boldsymbol{v}_{q'q}\right) + K_{qS}\boldsymbol{v}_q \cdot \left(\boldsymbol{v}_q - \boldsymbol{v}_{qS}\right) + \boldsymbol{VM}_q \cdot \left(\boldsymbol{v}_q - \boldsymbol{v}_{GL}\right)\right] = Q_N + Q_M(\Gamma_M) + Q_H(h, a, \Delta T) \tag{3}$$

where $\Gamma's$, $K's$ and $Q's$ are the mass transfer rates, the momentum exchange functions and the heat transfer rates, respectively.

The overall fluid-dynamics solution algorithm is based on a time-factorization four-step algorithm, in which intra-cell interfacial area source terms, heat and mass transfer, and momentum exchange functions are determined in Step 1, separately from inter-cell fluid convection In Steps 2, 3 and 4. Step 1 solves Eqs. (1) and (3) for intra-cell heat and mass transfers with ignoring the convection terms. Steps 2, 3 and 4 solve fluid convection by integrating Eqs. (1) - (3) with ignoring the source terms on the right-hand sides. First Step 2 explicitly estimates the end-of-time-step variables to initialize for the pressure iteration. Step 3 performs the pressure iteration that obtains consistent end-of-time-step velocities and pressure. Finally Step 4 performs consistent mass, momentum and energy convection based on the semi-implicit algorithm.

2.2. SIMMER-III/SIMMER-IV Components

All materials are represented by components: density components are used to calculate the mass conservation equations; and energy components the energy conservation equations. The complete lists of the structure-, liquid- and vapor-field components are shown in Tables 1 and 2. In these tables, the lower-case subscripts denote density components while the upper-case subscripts denote energy components. The fuel components are divided into fertile and fissile in their mass (density components) to represent different

enrichment zones in the core. However, the two materials are assumed to be intimately mixed, and hence the single temperature (energy components) is assigned.

It is noted the only difference between SIMMER-III and SIMMER-IV is the number of can walls; i.e. the front and back can walls are modeled in a three-dimensional code in addition to left and right can walls.

2.3. Role of HTCs in SIMMER-III/SIMMER-IV

The mass and energy conservation equations solved in Step 1 are derived from Eqs. (1) and (3) by neglecting the convection terms. The mass conservation equation is written as:

$$\frac{\partial \bar{\rho}_m}{\partial t} = -\Gamma_m \,, \tag{4}$$

which means the change in mass with time corresponds to the mass-transfer rate from the component *m*. Similarly, the energy equation is written as:

$$\frac{\partial \bar{\rho}_M e_M}{\partial t} = Q_N + Q_M(\Gamma_M) + Q_H(h,\ a,\ \Delta T), \tag{5}$$

where the three terms on the right-hand side of Eq. (5) denote the energy transfer rates per unit volume due to nuclear heating, mass transfer and heat transfer, respectively. The energy transfer rate due to heat transfer is a function of HTC, heat-transfer area and temperature difference between the two components exchanging energy. In addition to the energy equation, HTCs are also required for determining the rates of mass transfer because vaporization/condensation (V/C) and melting/freezing (M/F) processes are driven by heat transfer and the energy balance at the binary contact interface between a pair of interacting energy components.

The calculative flow of the fluid-dynamics Step 1 is illustrated in Fig. 1. HTCs are necessary to calculate heat and mass transfers between energy components. Each of the 8 fluid energy components (7 liquid-field components and vapor mixture) can transfer heat to other fluid energy components plus three structure surfaces (five for SIMMER-IV). Thus, heat transfer occurs across up to 52 binary contact interfaces (68 for SIMMER-IV), and requires the computation of up to 73 HTCs (89 HTCs for SIMMER-IV) in each mesh cell. Some HTCs are used to calculate heat transfer across more than one interface, which means that the number of independent HTCs is less than 73. For example, a single HTC is appropriate for a solid particle no matter with which liquid component it interacts. As a result, 44 HTCs (48 for SIMMER-IV) are currently used to compute heat and mass transfer in each mesh cell, as shown in Fig. 2 (Fig. 3 for SIMMER-IV). It is noted again that the structure-side HTCs are computed in the structure model.

HTCs are defined for 52 binary contacts between the energy components and contribute to 30 V/C paths and 20 M/F paths. The coefficients control heat transfer between the bulk and interface (surface) temperatures for each liquid energy component and for the vapor mixture. The heat and mass transfer calculations are performed in the M/F and V/C routines after HTCs are determined. At selected binary contact interfaces, non-equilibrium phase changes are calculated from the balance of heat fluxes at the interface. The interface ID numbers, and the number of mass transfer paths at each interface, are also described in Figs. 2 and 3.

The fluid HTCs are used to calculate non-equilibrium mass transfer processes. This means that heat transfer must occur by direct contact of interacting components, i.e. by conduction and convection. Thermal radiation heat transfer is currently not modeled (except as part of the film boiling model).

2.4. HTC Modeling Approach

The HTCs are based on quasi-steady-state heat transfer correlations. The correlations take account of the Prandtl number range of the interacting fluids, which is particularly important when calculating heat transfer in liquid metals.

Solid particles are treated as rigid spheres, and heat transfer is controlled by conduction. Liquid droplets and gas bubbles were also treated as rigid spheres but the effects of internal circulation and oscillation of fluid particles are also treated. In the latter case conduction is augmented by convection in the fluid particles. In the dispersed flow regime, the heat transfer between moving droplets can be calculated as a function of the contact times.

Forced convection heat transfer from continuous phase liquids or gas to solid particles is calculated using correlations obtained from forced flow over spheres. Fluid spheres are treated as rigid spheres at low Reynolds number, but at higher Reynolds numbers alternative correlations are used to take account of internal circulation in the fluid particles. When the velocity difference between the continuous and dispersed phases is low the forced convection heat transfer can be augmented by natural convection heat transfer. Heat transfer between continuous phase liquid or gas and structure is calculated using correlations obtained for forced convection single-phase flows in pipes.

A model to calculate HTCs in the event of film boiling around a hot droplet or particle in a continuous phase coolant liquid is also available in SIMMER-III. The model can significantly reduce heat fluxes due to the insulating effect of the vapor blanket.

The HTCs are defined for the bubbly, annular and dispersed flow regimes. HTCs in intermediate flow regimes are computed by interpolation between well-defined flow regimes. The interpolation is performed using logarithmic averaging to smooth the transition between flow regimes. In addition, the HTCs of two liquid components are interpolated between the continuous and discontinuous phase HTCs when neither liquid forms a dominant continuous phase. This avoids sudden changes in heat transfer caused by small alterations in volume fractions of the components.

2.5. Scope and Limitations in Calculating HTCs

The energy components are described by a single (bulk) temperature, so HTCs must be computed without knowing the space-dependent temperature distributions in the interacting components. In addition, the temperature history of the components is not followed, so it is impossible to properly simulate transient HTCs. HTCs must be obtained from quasi-steady state correlations which make use of local, instantaneous flow and temperature conditions. Thus, the application to highly transient heat transfer problems must be made carefully.

The correlations used to calculate the heat transfer rates must be sufficiently general so that they can be applied to fluids with a wide range of physical properties. In particular the heat transfer correlations must be applicable to liquid metals, which have very low Prandtl numbers. Heat transfer correlations must also be applicable to a wide range of flow conditions.

The geometry of the structure may not be well-defined. Structure can conceivably represent a tube, a bundle of fuel pins, the walls of a container or a flat plate. The HTCs which describe heat transfer from fluid to structure cannot be made specific to a particular geometry. Use of a hydraulic diameter is well justified for a channel flow which is confined by structure walls. However, there is an uncertainty to determine a heat-transfer lengthscale in a pool flow in contact with structure.

3. Heat Transfer Coefficients Models

This chapter describes the heat transfer correlations and interpolation procedures which are implemented in SIMMER-III. The background of engineering correlations and the relevant experimental data base are discussed in detail in Appendices to this report to justify the selection of the models adopted in the code.

3.1. Overview of HTC Models

The HTC models are based on quasi-steady-state Nusselt number correlations in well-defined topologies. The well-defined topologies are:

- Discontinuous components (i.e. solid or fluid particles), which are treated as spheres.
- Continuous liquid in bubbly flow, or gas in dispersed flow, which surrounds particles and fills a channel.
- A liquid film on structure.

The format of the heat transfer correlations appropriate to the above topologies are described in Section 3.2. The recommended Nusselt number correlations are justified in more detail in Appendices which are attached to this report.

For ill-defined flow regimes, and for topologies where there is no single continuous liquid, the HTCs are calculated by interpolation between the values of HTCs evaluated for the well-defined topologies. These interpolation procedures are described in Section 3.3.

3.2. Heat Transfer Correlations

The HTC correlations used in SIMMER-III are listed below:

H_P	rigid particle internal HTC
H_{FP}	fluid particle (droplet or bubble) internal HTC
H_{CPP}	HTC in a continuous phase fluid to a particle
H_{CPS}	HTC in a continuous phase fluid to structure
H_{AFS}	HTC from a liquid film to structure
H_{DPS}	HTC in a droplet or solid particle to structure
H_{DF}	HTC between moving droplets in dispersed flow
H_{FB}	film boiling HTCs

In the following section, subscript "i" denotes the energy component for which the HTC is being calculated, and subscript "j" denotes the component being interacted with.

The constants used in the correlations are all user-input variables. In the following equations they are denoted as a, b, c, …, k. The relationship between the constants and the input variables is defined in Table 3. The recommended and default values for the constants are shown in Table 4.

The heat transfer to structure requires a special consideration on how to determine a lengthscale used in the HTC correlations. There is a recent development on this subject that is described in Section 3.2.6.

3.2.1. Rigid particles - internal heat transfer

The HTC in solid particles and non-circulating, non-oscillating fluid particles is:

$$H_{P,i} = \frac{K_i}{2R_i} a_i \,, \tag{6}$$

where K and R are thermal conductivity and radius of the particle, respectively, and a_i's are user-input constants with the defaulted value of 10 assuming heat conduction to the mass centroid of the particle. Equation (6) describes conduction heat transfer inside a rigid particle, using a constant Nusselt number. A transient Nusselt number is ideally required to describe heat transfer from a rigid particle, but transient HTCs are beyond the scope of SIMMER-III. The limitations of using a constant Nusselt number to represent heat transfer inside a particle are discussed in Appendix A.

3.2.2. Circulating and oscillating fluid particles - internal heat transfer

The HTC in a circulating droplet is calculated only if its Reynolds number Re_i lies between input parameters Re_{ic} and Re_{os}:

$$H_{FP,i} = H_{P,i}\left\{1 + j_{i,1}\left[1 + \tanh\left(j_{i,2}\ln\left(\frac{\mathrm{Pe}_i^*}{j_{i,3}}\right)\right)\right]\right\} \text{ , for } \mathrm{Re}_{ic} < \mathrm{Re}_i \le \mathrm{Re}_{os} \,, \tag{7}$$

where j_i's are user-input constants and Pe_i^* is modified Peclet number of the fluid i defined as:

$$\mathrm{Pe}_i^* = \frac{\mathrm{Pe}_i}{1+\kappa} = \frac{2R_i V_{ij}}{\alpha_i(1+\kappa)} \,, \tag{8}$$

where α_i is the thermal diffusivity of the fluid i, $\kappa = \mu_{dp}/\mu_{cp}$ is the viscosity ratio and V_{ij} is the velocity difference. The HTC in an oscillating fluid particle is calculated only if its Reynolds number exceeds input parameter Re_{os}:

$$H_{FP,i} = H_{P,i} k_i \text{ , for } \mathrm{Re}_{os} < \mathrm{Re}_i \,, \tag{9}$$

where k_i's are user-input constants, and $H_{P,i}$ is defined by Eq. (6). Equations (7) and (9) effectively enhance the rigid particle Nusselt number by a multiplying factor. Equation (7) describes the increase of internal heat transfer in a circulating fluid particle according to the Kronig-Brink formula. Note that the HTC of a gas bubble is not enhanced according to Eq. (7) because the effect is negligible. Equation (9) represents the effect of oscillations on internal heat transfer by a simple multiplication factor. Equations (7) and (9) are justified in Appendix C. These fluid particle correlations are switched on and off by control option input.

3.2.3. Heat transfer in CP fluid to particles

Heat transfer in The HTC due to forced convection of a CP (Continuous Phase) liquid or gas (denoted by subscript "i") to rigid particles (denoted by subscript "j") is:

$$H_{CPP,i} = \frac{K_i}{2R_j}\left[b_i + e_{i,1}\mathrm{Re}_j^{e_{i,2}}\mathrm{Pr}_i^{e_{i,3}}\left(1 + e_{i,4}\mathrm{Re}_j^{e_{i,5}}\right)\right], \tag{10}$$

where b_i and e_i's are user-input constants. Equation (10) is composed of a conduction term, b_i, which describes the minimum heat transfer rate from a particle to a stagnant liquid, and a forced convection term, the e_i's. The forced convection heat transfer term is derived from measurements of quasi-steady state heat transfer from stationary spheres, and treats heat transfer across both the front laminar boundary layer of the particle and the wake at the rear. The correlation is discussed in more detail in Appendix B.

If the particles are fluid particles which are circulating or oscillating, and the particle-to-external liquid viscosity ratio is less than 2 ($\kappa < 2$), a different correlation can be used:

$$H_{CPP,i} = \frac{K_i}{2R_j}\left\{b_i + i_{i,1}\mathrm{Pe}_j^{i_{i,2}}\left[1 - \frac{\left(i_{i,3} + i_{i,4}\kappa^{i_{i,5}}\right)}{\mathrm{Re}_j^{1/2}}\right]^{i_{i,6}}\right\}, \tag{11}$$

where b_i is the same constant as in Eq. (10), and i_i's are user-input constants. Equation (11) describes the heat transfer from a sphere in potential flow and predicts higher heat transfer rates than Eq. (10) because of the thinner boundary layer around circulating fluid particles. Note that Eq. (11) is not applied to liquid droplets in gas because in this system it is always the case that $\kappa > 2$. Equation (11) is used in place of Eq. (10) only if it yields a higher value of $H_{CPP,i}$. The correlation is discussed in more detail in Appendix C. The calculation is switched on and off using input control option.

Heat transfer to the particles by natural convection driven by thermal expansion can also be calculated using the following correlation:

$$H_{CPP,i} = \frac{K_i}{2R_j}\left[b_i + f_{i,1}\left(\mathrm{Gr}_j\mathrm{Pr}_i^{f_{i,3}}\right)^{f_{i,2}}\right], \tag{12}$$

where b_i is the same constant as in Eq. (10) and f_i's are user-input constants. Equation (12) describes the natural convection heat transfer from a sphere driven by a temperature difference between the sphere surface and the CP fluid bulk temperature. The Grashof number Gr_j is calculated using an estimate of the interface temperature for the two components in place of the sphere surface temperature. The interface temperature is not allowed to exceed the saturation temperature of the volatile liquid for a non-equilibrium V/C interface, nor allowed to fall below the melting point of the hot liquid at a non-equilibrium M/F interface. Equation (12) is used in place of Eqs. (10) and (11) only if it yields a higher value of $H_{CPP,i}$. The correlation is discussed in more detail in Appendix D. The calculation is switched on and off using input control option.

3.2.4. Heat transfer in CP fluid to structure

The HTC for gas/vapor in the dispersed flow regime exchanging heat with structure is:

$$H_{CPS,i} = \frac{K_i}{D_h}\left[c_i + g_{i,1}\mathrm{Re}_{D_h}^{g_{i,2}}\mathrm{Pr}_i^{g_{i,3}}\right], \tag{13}$$

where c_i and g_i's are user-input constants. The lengthscale of the Reynolds number of the continuous phase $\mathrm{Re}_{D_h}^{g_{i,2}}$ is represented by the hydraulic diameter. Equation (13) is composed of a conduction term c_i, which describes the minimum heat transfer in laminar flow, and a term obtained from measurements of forced convection turbulent flow in tubes. The correlation is discussed in more detail in Appendix E.

The HTC for bubbly flow CP liquid exchanging heat with structure is:

$$H_{CPS,i} = \frac{K_{mix}}{D_h}h_1 + \frac{K_i}{D_h}\left(g_{i,1}\mathrm{Re}_{D_h}^{g_{i,2}}\mathrm{Pr}_i^{g_{i,3}}\right), \tag{14a}$$

where

$$K_{mix}^{h_2} = \left(\sum_{i=1}^{7}\alpha_i K_i^{h_2} + \alpha_{g,bub}K_g^{h_2}\right)\Big/\alpha_{bub}\,. \tag{14b}$$

and h_1, h_2 and g_i's are user-input constants. Equation (14a) contains a term obtained from measurements of forced convection turbulent flow in tubes, the same as Eq. (13). The other term is the heat conduction from a multi-component mixture having conductivity K_{mix}, assuming fluid components are uniformly mixed in a mesh cell. The correlation is further discussed in Appendix E.

The HTC for a liquid film in annular flow exchanging heat with structure is:

$$H_{CPS,i} = \frac{K_i}{W_i}\left[d_i + g_{i,1}\mathrm{Re}_{D_h}^{g_{i,2}}\mathrm{Pr}_i^{g_{i,3}}F\right], \text{ where } F = \left(\frac{2W_i}{D_h}\right)^{0.743}\frac{\left[1-\frac{8}{15}\right]}{\left[1-\frac{8}{15}\left(\frac{2W_i}{D_h}\right)\right]} \tag{15}$$

where W_i is the liquid film thickness, d_i's and g_i's are user-input constants, and F is a multiplication factor. Equation (15) is composed of a conduction term d_i which describes the minimum heat transfer, and a term describing convection heat transfer from turbulent film flow. The origin of the correlation is described in Appendix E.

3.2.5. Heat transfer from droplets and solid particles to structure

An HTC between solid particles and structure is calculated only if the particles exceed the maximum packing fraction, since above the maximum packing fraction the topology of the "particles" is more like solder than rigid spheres:

$$H_{DPS,i} = \frac{K_{mix}}{D_h}h_1 \text{ for } \frac{\alpha_{pp}}{(1-\alpha_{st})} \geq \alpha_{MP}\text{, or} \tag{16a}$$

$$H_{DPS,i} = 0 \text{ for } \frac{\alpha_{pp}}{(1-\alpha_{st})} < \alpha_{MP}\,, \tag{16b}$$

where K_{mix} is defined in Eq. (14) and α_{MP} is the maximum packing fraction. Equation (16) describes conduction heat transfer for a multi-component mixture. The correlation is discussed in more detail in Appendix E.

The HTC between droplets and structure depends on whether the flow is turbulent or laminar:

$$H_{DPS,i} = \frac{K_{mix}}{D_h} h_1 \text{ for } \mathrm{Re}_{CP} < 3000 \text{ (laminar), or} \tag{17a}$$

$$H_{DPS,i} = \frac{K_i}{2R_i} a_i \text{ , for } \mathrm{Re}_{CP} \geq 3000 \text{ (turbulent).} \tag{17b}$$

The expression for laminar flow in Eq. (17a) corresponds to conduction heat transfer for a multi-component mixture. The expression for turbulent flow describes conduction heat transfer inside a single rigid particle. These correlations are discussed in more detail in Appendix E.

3.2.6. Lengthscale of heat transfer to structure

In the above correlations on heat transfer to structure, a heat-transfer lengthscale D_h is normally represented by a hydraulic diameter defined in the structure configuration model[5] as

$$D_h = \frac{4A_{flow}}{P_{flow}}, \tag{18}$$

where A_{flow} and P_{flow} are the flow cross-sectional area and the wetted perimeter of flow, respectively. The use of this definition is a reasonable choice for a channel flow that is confined in structure walls. However, when a liquid pool is in contact with the structure wall, there is an uncertainty in determining the lengthscale for heat transfer, because the standard definition of hydraulic diameter is no longer applicable. In the SIMMER-III structure model[5], D_h is set to the mesh cell width in such cells in contact with the pool wall.

$$D_h = (1 - \alpha_S)\Delta r , \tag{19}$$

where Δr is the width of the mesh cell in contact with structure in a pool flow. The continuous liquid to structure heat transfer, for example, the first term of Eq. (14a) becomes the heat conduction between cell center and structure surface by setting Nusselt number (h_1) to 2. This treatment is also consistent with the use of a newly developed inter-cell heat-transfer model (Section 4.9.1 of Ref. 1)), in which heat transfer between cell centers are modeled. Thus, $h_1 = 2$ is recommended for pool configuration, whilst default value of $h_1 = 5$ is still recommended for channel flow configurations. Note that the hydraulic diameter is set to a large value (10^{20}) in mesh cells with no structure ($\alpha_S = 0$).

When there is a large temperature difference between fluids and structure, the effect of transient heat transfer becomes important. Although it is beyond the scope of SIMMER-III quasi-steady-state HTC model, a simple time constant model has been developed for parametrically examining this effect. The effective heat transfer lengthscale is represented by a thermal penetration length, similarly to the structure surface node representation, as

$$D_h = 2\delta_M = 2\sqrt{3}\sqrt{\frac{K_M \upsilon_M}{c_M}}\tau_M\,, \tag{20}$$

where K_M, υ_M and c_M are the thermal conductivity, specific volume, and specific heat of the fluid mixture, and τ_M is the input time constant to simulate the effect of transient heat transfer.

3.2.7. Droplet-droplet heat transfer in dispersed flow

The HTC for droplet-droplet contact in the dispersed flow regime is:

$$H_{DF,i} = \frac{K_i}{2R_i}\frac{-3\alpha_i\tau_{ij}^c}{2R_i^2}\Big/\ln\left[\frac{6}{\pi^2}\sum_{n=1}^{\infty}\frac{1}{n^2}\exp\left(\frac{-n^2\pi^2\alpha_i\tau_{ij}^c}{R_i^2}\right)\right], \tag{21}$$

where the contact timescale for each pair of droplets is estimated by:

$$\tau_{ij}^c = \frac{2(R_i + R_j)}{\Delta V_{ij}}\,, \tag{22}$$

Equation (21) is a rough estimate of the enhanced (transient) heat transfer between droplets which are in contact for very short times. The resulting HTC, $H_{DF,i}$, is used only if it yields a higher value than H_P given by Eq. (6). The derivation is described in Appendix A. The calculation is switched on and off using input control option.

3.2.8. Film boiling

If the conditions for film boiling are satisfied for a hot DP (Discontinuous Phase) liquid in contact with a more volatile CP liquid, film boiling HTCs are calculated for both CP and DP liquids: $H_{FB,i}$ and $H_{FB,j}$, respectively. The basis of the film boiling model is described in detail in Appendix F. The calculation is switched on and off using input control option.

3.2.9. HTC multipliers

It is convenient to have the capability from user-input to increase or reduce the HTCs calculated using the empirical formulae by simple multiplying factors. Although all the HTCs can be scaled using user-input coefficients, simple multipliers for all the HTCs are also available. There is also a multiplier, which modifies the convection heat transfer from a liquid film. This is useful to mitigate heat transfer from a high-velocity liquid film.

3.3. Interpolation Procedures

The heat transfer correlations described in Section 3.2 are for well-defined topologies. However, there are circumstances in which suitable correlations are not available: (a) flow regimes which are topologically ill-defined (e.g. transition and interpolated flow), (b) a multi-component liquid mixture in which no single component comprises the continuous liquid phase, and (c) boiling regimes for a hot droplet in a coolant when the film boiling condition is not satisfied. HTCs in these conditions are calculated from practical, rather than physical, considerations: the HTCs are calculated by interpolation between topologies with well-defined HTCs.

3.3.1. Interpolation by log-averaging

An example of interpolation is in the transition flow regime for a single-component liquid and gas. Transition flow is treated by dividing the mesh cell into two regions, corresponding to bubbly and dispersed flow, respectively. The HTC in the liquid phase is defined as H_B and H_D for the bubbly and dispersed flow regimes, respectively. The value of the HTC in the transition flow regime H_{tran} is assumed to lie somewhere between H_B and H_D.

A linear interpolation between H_B and H_D would be the simplest estimation of H_{tran}, but it does not give a smooth transition when H_B and H_D vary by orders of magnitude. For inter-phase drag in SIMMER-III a sufficiently smooth transition is achieved by using logarithmic averaging of the drag coefficients in the well-defined flow regimes. Therefore, the same procedure has been adopted for interpolating HTCs. For an example, the HTC for the transition flow regime is calculated by:

$$\log H_{tran} = \beta \log H_B + (1-\beta) \log H_D \text{ , where } \beta = \left(\frac{\alpha_D - \alpha}{\alpha_D - \alpha_B}\right) \text{ for } 0 < \beta < 1 \text{ .} \quad (23)$$

Equation (23) gives a sufficiently smooth transition of HTCs between flow regimes. Note that the heat transfer rates need not be smooth since the binary contact areas in the two flow regimes may be very different. However, it is convenient to separate the calculation of HTCs from the calculation of the binary contact areas.

3.3.2. Interpolation between flow regimes

The flow regime map used to calculate HTCs is shown in Fig. 4. The heat transfer correlations described in Section 3.2 are used to define the HTCs in the flow regimes at the four corners of the map: bubbly (H_B), annular (H_A) and dispersed (H_D). HTCs in the remaining flow regimes are calculated by interpolation between the well-defined flow regimes. Two weighting factors, corresponding to the x-axis and y-axis of Fig. 4, respectively, are required in order to perform the log-averaging:

$$\beta = \left(\frac{\alpha_D - \alpha}{\alpha_D - \alpha_B}\right) \text{ , and} \quad (24)$$

$$\chi = 1 - \frac{E_r}{E_U} \text{ ,} \quad (25)$$

where α is the effective void fraction and all other variables are defined in Fig. 4.

The transition flow regime is treated as comprised of bubbly and dispersed flow regions. The HTCs in the transition flow regime are calculated by interpolating between H_B and H_D using Eq. (23).

The HTCs in slug flow are treated as an interpolation between the HTCs in the bubbly and annular flow regimes:

$$\log H_{slug} = \beta \log H_B + (1-\beta) \log H_A \text{ , for } 0 < \beta < 1 \text{ .} \quad (26)$$

There are undoubtedly more physically-based correlations for slug flow, but Eq. (26) is convenient to implement in SIMMER-III. The situation where H_A is zero is treated by scaling H_B linearly with void fraction:

$$H_{slug} = \beta H_B \quad , \quad \text{for } 0 < \beta < 1 \, . \tag{27}$$

The HTCs in annular-dispersed flow are treated by interpolating between the HTCs in the dispersed and annular flow regimes:

$$\log H_{anndsp} = \chi \log H_A + (1 - \chi) \log H_D \quad \text{for } 0 < \chi < 1 \, . \tag{28}$$

There are probably more justifiable correlations for annular-dispersed flow, but the assignation of the liquid film and droplets to the same velocity field in SIMMER-III means that the flow regime must in any case be treated in an averaged way. In the event of H_A having a zero value the HTC in the annular dispersed regime is scaled linearly with entrainment fraction:

$$H_{anndsp} = (1 - \chi) H_D \quad \text{for } 0 < \chi < 1 \, . \tag{29}$$

The interpolated flow regime does not have a well-defined topology at all. The HTCs are obtained by interpolation between the slug and transition flow regimes:

$$\log H_{inerp} = \chi \log H_{slug} + (1 - \chi) \log H_{tran} \quad \text{for } 0 < \chi < 1 \, . \tag{30}$$

If the value of H_{slug} is zero, then the linear scaling described by Eq. (26) is used for interpolated flow.

3.3.3. Two continuous liquid phases

A discontinuity in heat transfer rates for a mixture of two liquid energy components can be avoided by interpolating between the CP and DP HTCs for each component. The procedure is analogous to the treatment of HTCs in the transition flow regime described above, where HTCs are calculated by log-averaging the bubbly and dispersed flow HTCs. However, in this case the gas phase is replaced by another liquid component *Ln*.

Let liquid energy component *m* be the first (dominant) continuous phase (the CP) and component *n* the second continuous phase (the CP2). The bubbly region of a mesh cell is treated by subdividing it into two sub-regions: one sub-region where the CP is the continuous liquid, and a smaller sub-region where the CP2 is the continuous liquid. The HTC for liquid energy component *m* is interpolated between its CP HTC and its DP HTC according to a weighting factor based on relative liquid volume fractions. The weighting factor is:

$$\gamma = \frac{(\tilde{\alpha}_m - \alpha_{B1})}{(\alpha_{B2} - \alpha_{B1})} \text{ , where } \tilde{\alpha}_m = \frac{\alpha_m}{\alpha_m + \alpha_n} \text{ for } 0 < \gamma < 1 \, , \tag{31}$$

where α_m is the volume fraction of liquid *m*, and α_{B1} and α_{B2} are the input constants which define the transition regime between two continuous liquids. The criterion for a single liquid CP is $\tilde{\alpha}_m \geq \alpha_{B2}$, in which case the liquid phase is dominated by liquid component *m* and no interpolation is necessary. However, if $\alpha_{B1} < \tilde{\alpha}_m < \alpha_{B2}$ then the liquid phase can be viewed as a mixture of continuous liquids *m* and *n* and the interpolation procedure is invoked.

Let the CP HTC for liquid energy component *m* be $H_{m,CP}$, and its DP HTC be $H_{m,DP}$, then the interpolated HTCs for the two CP liquid energy components are:

$$\log H_m = \gamma \log H_{m,CP} + (1-\gamma) \log H_{m,DP} \quad \text{for } 0 < \gamma < 1 \text{ , and} \tag{32}$$

$$\log H_n = \gamma \log H_{n,DP} + (1-\gamma) \log H_{n,CP} \quad \text{for } 0 < \gamma < 1 \text{ .} \tag{33}$$

3.3.4. The SIMMER-III boiling curve

Consider a hot DP droplet in contact with a CP coolant. If the interface temperature does not exceed the saturation temperature of the coolant, no vaporization occurs and the HTCs in the CP and DP components are calculated using H_{CPP} and H_{FP}, respectively, as described in Section 3.2. If the conditions are such that film boiling occurs the respective HTCs, $H_{FB,i}$ and $H_{FB,j}$, are calculated by the film boiling model (which is described in Appendix F). The two sets of HTCs can differ by more than an order of magnitude, because of the reduction of heat transfer rates in film boiling.

The situation in which vaporization occurs at a droplet surface, but the film boiling condition is not satisfied, is treated by interpolation between the HTCs for no vaporization and the film boiling HTCs in the following way.

- Boiling is assumed to occur when the interface temperature for two liquid components exceeds the saturation temperature of the more volatile component.
- Single-phase HTCs are nevertheless used to compute heat fluxes up to a temperature which can be identified with the departure from nucleate boiling temperature (DNBT).
- The minimum film boiling temperature (MFBT) defines the conditions for film boiling. The MFBT is partly determined by input, and partly by the minimum vapor film thickness. The derivation of the MFBT is described in Appendix F.
- Heat fluxes are interpolated between the DNBT and MFBT using logarithmic averaging of the heat flux at the DNBT and the heat flux at the MFBT.

The "boiling heat flux" is converted to HTCs, $H_{FB,i}$ and $H_{FB,j}$. This treatment of the boiling curve is a convenient solution, and is not intended to be a physical representation of the heat transfer process, especially in the nucleate boiling regime. The SIMMER-III boiling curve underestimates boiling heat transfer from a solid sphere because single-phase HTCs are used in the "nucleate boiling regime".

4. Verification and Validation

4.1. SIMMER-III Assessment Program

A verification and validation (V&V) program for SIMMER-III has been planned since the beginning of the code development. The program, called the “code assessment program”, was conducted in two steps, Phase 1 and Phase 2. The Phase 1 assessment is intended to verify individual fluid-dynamics models of the code, whilst Phase 2 is for comprehensive validation for integral and inter-related accident phenomena, such as transient fuel motion during the transition phase and high-pressure CDA bubble expansion in the post-disassembly expansion phase. Direct application of the code to complex accident phenomena involves many inter-related processes to be solved simultaneously and is not always productive. Thus, the present stepwise approach is advantageous, since in Phase 1 the coding is largely debugged and verified, and each major model is validated separately.

The program was conducted in collaboration with German and French colleagues under the joint research agreement on SIMMER-III. The results and achievement were jointly synthesized and fully documented in the reports[11), 12)].

The results of the assessment are briefly summarized below with respect of V&V of the fluid HTC model. It must be noted that the so-called "developmental assessment" has been conducted as new models were proposed and developed. A good example is the HTC model development, where a simple test code was first developed and extensively compared with available experimental data and correlations, on spread sheets, before the model was incorporated in SIMMER-III.

4.2. Phase 1 Assessment

In Phase 1 assessment[11)], SIMMER-III is applied to a variety of fluid-dynamics test problems with the objective that the individual models are validated separately as far as possible. The test problems therefore are categorized as: fluid convection algorithm, interfacial areas and momentum exchange functions, heat transfer coefficients, melting and freezing, and vaporization and condensation. In the Phase 1 report, the results of assessment on the HTC modeling were summarized as follows.

Fluids HTCs are modeled by quasi-steady state Nusselt number heat transfer correlations for selected fluid configuration and flow topologies. SIMMER-III calculations of mass transfer during melting/freezing and vaporization/condensation also rely on the HTCs, since the rates of phase transition are determined form an energy balance at the binary contact interface between a pair of energy components. Transient heat transfer coefficients are not modeled. This is known to be inaccurate on short timescales for rigid particles and droplets, and was highlighted by the problem of condensation of steam on a subcooled droplet. Although it is not considered feasible to implement transient correlations into SIMMER-III, the steady-state formulation can be used parametrically to investigate the effect of enhancing the condensation rate.

The vapor bubble collapse problem shows that SIMMER-III can approximately simulate the rate of collapse of subcooled vapor bubbles and that the collapse could be better simulated if heat transfer correlations took account of the internal circulation and mixing in the bubble. This capability has subsequently been implemented in SIMMER-III.

The liquid-structure heat transfer coefficients contributed successfully to the conduction freezing calculations. However, calculations of bulk freezing of fuel indicate the need to model an additional contact thermal resistance between liquid and structure. The implementation of the interface resistance, considering imperfect contact due to surface roughness and liquid supercooling upon freezing inception, have been successfully made later[13].

The analysis of the boiling pool did not result in specific recommendations concerning liquid-wall heat transfer modeling. However, an analysis of the SCARABEE BF2 boiling pool for the Phase 2 assessment[12] indicates that it is desirable to improve the calculation of the local lengthscale and velocity used in the heat transfer correlations.

The SIMMER-III film-boiling model is intended for liquid-liquid heat-transfer, but was successfully applied for a solid sphere in liquid sodium. The application helps to calibrate the model, but also highlighted the fact that there is no physical representation of the boiling curve in SIMMER-III. However, the temperatures which can be reached by LMFR materials in a CDA easily exceed the temperatures achieved in most of the Phase 1 assessment problems.

Not all the test problems studied in Phase 1 were satisfactory; many problem areas were identified and the areas of model improvement were recommended. Model improvements had been continued and some of the test problems were re-calculated in Phase 2.

4.3. Results of Phase 2 Assessment

In Phase 2 assessment[12], SIMMER-III is applied to test problems relevant to key accident phenomena in LMFR: boiling pool dynamics, fuel relocation and freezing, material expansion, fuel-coolant interactions (FCIs), and disrupted core neutronics. The fluid-dynamics test problems are integral and complex in nature, involving various SIMMER-III models. For example, a simulation of FCI requires the models for multi-phase fluid convection, fluid HTCs, flow topology and interfacial area with source terms, momentum exchange functions, and heat and mass transfers. This means the HTC model cannot be validated separately from other models, but is validated together with the heat and mass transfer model. In the synthesis compiled in the Phase 2 report, the results on the assessment concerning the HTC model are evaluated and summarized as follow.

The heat and mass transfer model is a central part of the SIMMER-III code and couples the multiple energy components modeled in the code. Given the binary contact area and heat-transfer coefficient between the two interacting components, the model calculates heat transfer, M/F and V/C. Through the Phase 1 and Phase 2 assessment programs, it was confirmed that the heat-transfer-limited phase transition model is basically valid and is applicable to quasi-steady state and even to highly transient cases.

As to fuel freezing, an improve freezing model, which is also known as the fuel-caps freezing model, has been developed successfully and is shown to be applicable to both fuel freezing and simulant metal freezing[13]. This model encompasses the effect of thermal resistance, taking into account imperfect contact of melt on a wall and supercooling of melt upon freezing inception, and more importantly it can simulate

both the classical bulk and conduction-limited freezing modes occurring simultaneously. The fuel-caps model is implemented in the heat and mass transfer model and the fluid-side HTCs are unchanged.

Various FCI experiments with simulants and reactor materials were analyzed and the overall pressure behaviors and coolant motion were appropriately reproduced. This means the models for HTC, interfacial areas with source terms, momentum exchange, fuel freezing and coolant vaporization were reasonably validated in an integral fashion. The film boiling heat transfer model is available for heat transfer from hot fluid particles (liquid droplets or solid particles) to cold liquid (coolant). The model, based on the minimum film boiling temperature criterion, suitably distinguishes whether film boiling is occurring or there is a direct liquid-liquid contact. This model was successfully applied to the various FCI calculations in the Phase 2 assessment.

The standard calculation of the HTC from the pool fluid to the structure wall is based on combination of heat conduction and Nusselt number engineering correlation for convective heat transfer. Thus, the coefficient is dependent on the representative length of the mesh cell containing the structure wall and hence is dependent on a mesh cell size. The comparison of a calculated heat flux with global experimental data has identified an obvious shortcoming. Unlike a channel flow confined in the wall structure, use of a hydraulic diameter of a standard definition as the representative length is inappropriate.

4.4. Studies after Phase 2

The validation of SIMMER-III has been continued after the completion of the Phase 2 assessment, especially when new knowledge has been made available from later experimental studies. The EAGLE out-of-pile and in-pile experimental program has provided valuable experimental data base simulating LMFR fuel melting and relocation behaviors in relatively large scales[14]. SIMMER-III was used in analyzing selected experiments. It was shown that the experimentally observed timing of structure wall melting was poorly simulated by the code, but was reproduced by increasing the liquid-to-structure heat transfer coefficient by a factor of 3 to 5[15].

One of the causes of this underestimation of the heat transfer to the wall is that the crust fuel layer formed on the structure surface always stays stable in SIMMER modeling and its insulating effect has reduced the heat transfer to the structure. A special model change assuming a direct contact of molten steel with the structure, allowing predominant liquid-steel-to-wall heat transfer, could reproduce the timing of structure failure[16]. Limiting the heat-transfer lengthscale to a mesh cell size was also implemented. A more mechanistic model has been developed to simulate imperfect fuel crust formation in which a part of structure surface is left for liquid-to-structure direct heat transfer[1]. In these model changes, the individual models of HTCs are unchanged. More important shortcoming of the HTC model may come from the fundamental assumption of quasi-steady-state heat transfer. The experimental condition of EAGLE tests is characterized by rapid heating of fuel (or fuel simulant) to generate a molten fuel and steel mixture in a short timescale. This resulted in an extremely large temperature difference between the molten mixture and the structure, where the effect of transient heat transfer becomes more important. Depending on a timescale of heat transfer, the effective lengthscale of heat transfer becomes shorter that the steady-state heat transfer.

5. Brief Program Description

5.1. Input Variables

The relationship between the input variables and the heat transfer correlations described in Section 3.2 is defined by Table 3, while the recommended and default values are presented in Table 4. The input variables are all prefixed by the letter "H" to help identify them as HTC input variables. The following naming convention for the variables has been adopted:

HCDP	ConDuction heat transfer in Particles
HCDLP	ConDuction heat transfer from CP Liquids to Particles
HCDGP	ConDuction heat transfer from CP Gas to Particles
HCDLBS	ConDuction heat transfer from Liquids in Bubbly flow to Structure
HCDLAS	ConDuction heat transfer from Liquids in Annular flow to Structure
HCDGS	ConDuction heat transfer from Gas in dispersed and annular flow to Structure
HFCLP	Forced Convection heat transfer from CP Liquids to Particles
HFCGP	Forced Convection heat transfer from CP Gas to Particles
HNCLP	Natural Convection heat transfer from CP Liquids to Particles
HNCGP	Natural Convection heat transfer from CP Gas to Particles
HFCLS	Forced Convection heat transfer from CP Liquids to Structure
HFCGS	Forced Convection heat transfer from CP Gas to Structure
HCDMXS	ConDuction heat transfer from bubbly flow MiXture to Structure
HKEXP	EXPonent used to calculate the thermal conductivity of a mixture
HREIC	REynolds number denoting onset of Internal Circulation in droplets
HREOS	REynolds number denoting onset of OScillations in droplets
HICLCP	For Internal Circulation in a droplet, heat transfer in the Liquid CP (i.e. the external HTC)
HICLDP	For Internal Circulation in a droplet, heat transfer in the Liquid DP (i.e. the internal HTC)
HOSLDP	Heat transfer in an OScillating droplet (i.e. the Liquid DP)
HOSGBU	Heat transfer in an OScillating Gas BUbble
HTCMUL	HTC MULtiplier

5.2. Calculational Flow

The calculational of HTCs is divided into 8 operations. The first operation defines variables which are used frequently throughout the routine. The subsequent 7 operations calculate the HTCs, for each of which the calculational procedure is similar:

(1) Calculate HTCs for well-defined topologies. These are defined as: the dispersed flow regime, a continuous phase (CP) liquid in the bubbly flow regime, a discontinuous phase (DP) in the bubbly flow regime and a CP liquid film on structure in the annular flow regime.

(2) Calculate HTCs for ill-defined flow regimes and topologies. This is done by interpolation using logarithmic averaging, which is described in Section 3.3. The HTCs for well-defined flow regimes are substituted for the HTCs, H_B, H_D and H_A, in Fig. 4.

The calculational flow takes account of the following points:

- HTCs are calculated only if the flow regime and topology are appropriate, in order not to waste computational time. Similarly, the interpolation procedures are invoked only if required according to the flow regime map.
- The calculation of many HTCs, for fluid particles, natural convection, film boiling etc., can be switched on and off by user-input control options, or are conditional on local flow conditions, and so may not always be performed.
- Usually, no distinction is made between the HTC for a liquid in the dispersed flow regime and as a DP in the bubbly flow regime.
- The film boiling HTCs are calculated in a separate subroutine.

6. Conclusions

This report describes the basis of the heat transfer coefficients (HTC) model in SIMMER-III and SIMMER-IV. The heat transfer correlations with user input data are detailed and the use of the model is briefly described. A more detailed description of the physical basis of the heat transfer correlations used is contained in Appendices which are attached to this report. In consistent with the multiple flow-topology framework, the HTCs in ill-defined flow regimes are suitably interpolated from the well-defined flow regimes. Although the verification and validation of the model is beyond the scope of this report, the major achievement of the SIMMER-III assessment program conducted in parallel with code development is summarized with respect to HTC modeling to demonstrate that the coding is reliable and that the model is appropriately applicable to various multiphase problems with and without reactor materials.

Acknowledgment

The major part of this study was performed in the 1990s when the first author (D. J. Brear) is stationed as an International Fellow at the Oarai Research and Development Institute, JAEA (the former PNC). Useful discussions and suggestions from the then co-researchers, K. Morita, N. Shirakawa, H. Yamano and E. A. Fischer, are gratefully acknowledged. The programming staff at Oarai, including, S. Hosono, M. Sugaya and H. Inoue, have provided indispensable contribution to this study.

References

1) Kondo, S. et al., SIMMER-III and SIMMER-IV: Computer Codes for LMFR Core Disruptive Accident Analysis, JAEA-Research 2024-008, 2024, 235p.

2) Morita, K. et al., SIMMER-III Analytic Equation-of-State Model, JNC TN9400 2000-005, 1999, 57p.

3) Morita, K. et al., SIMMER-III Analytic Thermophysical Property Model, JNC TN9400 2000-004, 1999, 38p.

4) Morita, K. et al., SIMMER-III/IV Heat- and Mass-Transfer Model - Model and Method Description -, JNC TN9400 2003-047, 2003, 116p.

5) Kamiyama, K. et al., SIMMER-III Structure Model - Model and Method Description -, JNC TN9400 2004-043, 2004, 94p.

6) Tobita, Y. et al., Multi-Phase Flow Topology and Interfacial Area Model for SIMMER-III and SIMMER-IV, JAEA-Research 2024-010, 2024, 77p.

7) Tobita, Y. et al., Momentum Exchange Functions Model for SIMMER-III and SIMMER-IV, JAEA-Research 2024-011, 2024, 39p.

8) Bohl, W.R. et al., SIMMER-II: A Computer Program for LMFBR Disrupted Core Analysis, LA-11415-MS, Los Alamos National Laboratory, 1990.

9) Bohl, W.R. et al., AFDM: An Advanced Fluid Dynamics Model, Volume I: Scope, Approach, and Summary, LA-11692-MS, Vol. I, Los Alamos National Laboratory, 1990.

10) Berthier, J. et al., AFDM: An Advanced Fluid Dynamics Model, Volume III: AFDM Heat-Transfer and Momentum-Exchange Coefficients, LA-11692-MS, Vol. III, Los Alamos National Laboratory, 1990.

11) Kondo, S. et al. (Ed.), Phase 1 Code Assessment of SIMMER-III, A Computer Program for LMFR Core Disruptive Accident Analysis, JAEA-Research 2019-009, 2020, 382p.

12) Kondo, S. et al., Phase 2 Code Assessment of SIMMER-III, A Computer Program for LMFR Core Disruptive Accident Analysis, JNC TN9400 2000-105, 2000, 777p.

13) Kamiyama, K., Brear, D. J., et al., Establishment of Freezing Model for Reactor Safety Analysis, J. Nucl. Sci. and Technol., Vol. 43, No. 10, 2006, pp. 1206–1217.

14) Kamiyama, K., Konishi K., et al., Experimental studies on the upward fuel discharge for elimination of severe recriticality during core-disruptive accidents in sodium-cooled fast reactors, J. Nucl. Sci. and Technol., Vol. 51, No. 9, 2014, pp. 1114–1124.

15) Toyooka, J. et al., SIMMER-III Analysis of EAGLE-1 In-Pile Tests Focusing on Heat Transfer from Molten Core Material to Steel-Wall Structure, Proceedings of NTHAS7: The Seventh Korea-Japan Symposium on Nuclear Thermal Hydraulics and Safety, Chuncheon, Korea, 2010, N7P0058.

16) Toyooka, J. et al., Improvements to the SIMMER Code Model for Steel Wall Failure Based on EAGLE-1

Test Results, Proceedings of NTHAS10: The Tenth Korea-Japan Symposium on Nuclear Thermal Hydraulics and Safety, Kyoto, Japan, 2016, N10P1116.

Nomenclature

Symbols

D_h	Hydraulic diameter	
E_r	Entrainment fraction	
E_u	Equilibrium entrainment fraction	
h, H	Heat transfer coefficient (HTC)	
F	Multiplication factor for liquid film-structure HTC	
g	Gravitational acceleration	
Gr	Grashof number	$\mathrm{Gr}_j = \frac{8g\beta_i R_i^3}{\nu_i^2}\Delta T_{int,i}$
K	Thermal conductivity	
Pe	Peclet number of *CP* fluid *j*	$\mathrm{Pe}_j = \mathrm{Re}_j\mathrm{Pr}_j = \frac{2R_jV_{ij}}{\alpha_i}$
Pe*	Modified Peclet number of the *DP* fluid *i*	$\mathrm{Pe}_i^* = \frac{2R_iV_{ij}}{\alpha_i(1+\kappa)}$
Pr	Prandtl number	
R_i	Radius of fluid (particle) component *i*	
Re	Reynolds number:	
	DP (particle) *Re*	$\mathrm{Re}_i = \frac{\rho_i V_{ij} 2R_i}{\mu_i}$
	CP to particles Re	$\mathrm{Re}_j = \frac{\rho_i V_{ij} 2R_j}{\mu_i}$
	CP to structure *Re*	$\mathrm{Re}_{D_h} = \frac{\rho_i V_i D_h}{\mu_i}$
T	Temperature	
V_i	Velocity of CP liquid *i*	
V_{ij}	Velocity of CP liquid *i* relative to the particle *j*	
W	Liquid film thickness	

Greek symbols

α	Void fraction; volume fraction; thermal diffusivity	
β, χ, γ	Weighting factors defined by Eqs. (21), (22) and (28), respectively	
β	Thermal expansion coefficient	
κ	Viscosity ratio	$\kappa = \frac{\mu_{dp}}{\mu_{cp}}$

μ	Viscosity
ν	Kinematic viscosity
ρ	Density
τ_{ij}^{c}	Contact timescale for droplet components *i* and *j* in dispersed flow

Subscripts

i	Energy component for which the HTC is being calculated
j	Energy component being interacted with
cp	Continuous phase (external fluid)
dp	Dispersed phase (particle)
ic	Internal circulation
os	Oscillating particle
int	Interface

Table 1. SIMMER-III/SIMMER-IV fluid-dynamics structure-field components.

Density components (MCSR)		**Energy components (MCSRE)**	
SIMMER-III/SIMMER-IV*		**SIMMER-III/SIMMER-IV***	
*s*1	Fertile pin fuel surface node	*S*1	Pin fuel surface node
*s*2	Fissile pin fuel surface node		
*s*3	Left fertile crust fuel	*S*2	Left crust fuel
*s*4	Left fissile crust fuel		
*s*5	Right fertile crust fuel	*S*3	Right crust fuel
*s*6	Right fissile crust fuel		
--/*s*7	Front fertile crust fuel*	--/*S*4	Front crust fuel*
--/*s*8	Front fissile crust fuel*		
--/*s*9	Back fertile crust fuel*	--/*S*5	Back crust fuel*
--/*s*10	Back fissile crust fuel*		
*s*7/s11	Cladding	*S*4/*S*6	Cladding
*s*8/*s*12	Left can wall surface node	*S*5/*S*7	Left can wall Surface node
*s*9/*s*13	Left can wall interior node	*S*6/*S*8	Left can wall Interior node
*s*10/*s*14	Right can wall surface node	*S*7/*S*9	Right can wall Surface node
*s*11/*s*15	Right can wall interior node	*S*8/*S*10	Right can wall Interior node
--/*s*16	Front can wall surface node*	--/*S*11	Front can wall surface node*
--/*s*17	Front can wall interior node*	--/*S*12	Front can wall interior node*
--/*s*18	Back can wall surface node*	--/*S*13	Back can wall surface node*
--/*s*19	Back can wall interior node*	--/*S*14	Back can wall interior node*
*s*12/*s*20	Control	*S*9/*S*15	Control

Table 2. SIMMER-III/SIMMER-IV fluid-dynamics liquid- and vapor-field components.

Density components "*m*" (MCLR)		**Energy components "*M*" (MCLRE)**		**Velocity fields "*q*"**	
				default	**recommended**
*l*1	Liquid fertile fuel	*L*1	Liquid fuel	*q*1	*q*1
*l*2	Liquid fissile fuel			*q*1	*q*1
*l*3	Liquid steel	*L*2	Liquid steel	*q*2	*q*2
*l*4	Liquid sodium	*L*3	Liquid sodium	*q*2	*q*3
*l*5	Fertile fuel particles	*L*4	Fuel particles	*q*1	*q*1
*l*6	Fissile fuel particles			*q*1	*q*1
*l*7	Steel particles	*L*5	Steel particles	*q*1	*q*2
*l*8	Control particles	*L*6	Control particles	*q*2	*q*4
*l*9	Fertile fuel chunks	*L*7	Fuel chunks	*q*2	*q*5
*l*10	Fissile fuel chunks			*q*2	*q*5
*l*11	Fission gas in liquid fuel			*q*1	*q*1
*l*12	Fission gas in fuel particles			*q*1	*q1*
*l*13	Fission gas in fuel chunks			*q*2	*q*5
(MCGR)		**(material component) ***			
*g*1	Fertile fuel vapor	*G*1	Fuel vapor	*q*3	*q*6
*g*2	Fissile fuel vapor			*q*3	*q*6
*g*3	Steel vapor	*G*2	Steel vapor	*q*3	*q*6
*g*4	Sodium vapor	*G*3	Sodium vapor	*q*3	*q*6
*g*5	Fission gas	*G*4	Fission gas	*q*3	*q*6

***** *All vapor components, behaving as a vapor mixture and having the same temperature, are treated as a single energy component* "*G*" *and assigned to the same velocity field.*

Table 3. HTC input variables and Nusselt number correlations.

Variable	Gas/vapor	Liq. Fuel	Liq. Steel	Liq. Na	Fuel Particles/Steel Particles/Control/Fuel Chunks
Conduction in a rigid particle: Nu = *a*					
a	HCDP(8)	HCDP(1)	HCDP(2)	HCDP(3)	HCDP(4)/HCDP(5)/HCDP(6)/HCDP(7)
Conduction in fluid around a particle: Nu = *b*					
b	HCDGP	HCDLP(1)	HCDLP(2)	HCDLP(3)	-
Conduction from bubbly flow liquid or gas in dispersed flow to structure: Nu = *c*					
c	HCDGS	HCDLBS(1)	HCDLBS(2)	HCDLBS(3)	-
Conduction from annular flow liquid film to structure: Nu = *d*					
d	-	HCDLAS(1)	HCDLAS(2)	HCDLAS(3)	-
Forced convection from CP fluid to rigid particles: Nu = $e_1\mathrm{Re}_D^{e_2}\mathrm{Pr}^{e_3}\left(1+e_4\mathrm{Re}_D^{e_5}\right)$					
e_1	HFCGP(l)	HFCLP(1,1)	HFCLP(1,2)	HFCLP(1,3)	-
e_2	HFCGP(2)	HFCLP(2,1)	HFCLP(2,2)	HFCLP(2,3)	-
e_3	HFCGP(3)	HFCLP(3,1)	HFCLP(3,2)	HFCLP(3,3)	-
e_4	HFCGP(4)	HFCLP(4,1)	HFCLP(4,2)	HFCLP(4,3)	-
e_5	HFCGP(S)	HFCLP(5,1)	HFCLP(5,2)	HFCLP(5,3)	-
Natural convection from CP fluid to rigid particles: Nu = $f_1\left(\mathrm{Gr}_D\mathrm{Pr}^{f_3}\right)^{f_2}$					
f_2	HNCGP(l)	HNCLP(1,1)	HNCLP(1,2)	HNCLP(1,3)	-
f_2	HNCGP(2)	HNCLP(2,1)	HNCLP(2,2)	HNCLP(2,3)	-
f_3	HNCGP(3)	HNCLP(3,1)	HNCLP(3,2)	HNCLP(3,3)	-
Forced convection from CP fluid to structure: Nu = $g_1\mathrm{Re}_{D_h}^{g_2}\mathrm{Pr}^{g_3}$					
g_1	HFCGS(1)	HFCLS(1,1)	HFCLS(1,2)	HFCLS(1,3)	-
g_2	HFCGS(2)	HFCLS(2,1)	HFCLS(2,2)	HFCLS(2,3)	-
g_3	HFCGS(3)	HFCLS(3,1)	HFCLS(3,2)	HFCLS(3,3)	-
Conduction from multiphase, multicomponent mixture, $K_{mix}^{h_2}=\sum_{i=1}^{8}a_iK_i^{h_2}$, to structure: Nu = h_1					
h_1: HCDMXS		h_2: HKEXP			
Convection in CP liquid to circulating particle (Re_D>HREIC): Nu = $i_1\mathrm{Pr}^{i_2}\left[1-\left(i_3+i_4\kappa^{i_5}\right)/\mathrm{Re}_D^{1/2}\right]^{i_6}$					
i_1	-	HICLCP(1,1)	HICLCP(1,2)	HICLCP(1,3)	-
i_2	-	HICLCP(2,1)	HICLCP(2,2)	HICLCP(2,3)	-
i_3	-	HICLCP(3,1)	HICLCP(3,2)	HICLCP(3,3)	-
i_4	-	HICLCP(4,1)	HICLCP(4,2)	HICLCP(4,3)	-
i_5	-	HICLCP(5,1)	HICLCP(5,2)	HICLCP(5,3)	-
i_6	-	HICLCP(6,1)	HICLCP(6,2)	HICLCP(6,3)	-
Circulating fluid particle (Re_D >HREIC): Nu → Nu×*F*, $F=1+j_1\left[1+\tanh\left(j_2\ln\left(\mathrm{Pe}_{dp}^*/j_3\right)\right)\right]$					
j_1	-	HICLDP(1,1)	HICLDP(1,2)	HICLDP(1,3)	-
j_2	-	HICLDP(2,1)	HICLDP(2,2)	HICLDP(2,3)	-
j_3	-	HICLDP(3,1)	HICLDP(3,2)	HICLDP(3,3)	-
Oscillating fluid particle internal Nu (Re>HREOS):1 Nu → Nu×k					
k	HOSGBU	HOSLDP(1,1)	HOSLDP(1,2)	HOSLDP(1,3)	-

Table 4. HTC input variables: recommended and default data.

Variable	Gas/vapor	Liq. Fuel	Liq. Steel	Liq. Na	Fuel Particles/Steel Particles/Control/Fuel Chunks
Conduction in a rigid particle: Nu = a					
a	10	10	10	10	10/10/10/10
Conduction in fluid around a particle: Nu = b					
b	2	2	2	2	-
Conduction from bubbly flow liquid or gas in dispersed flow to structure: Nu = c					
c	5	5	5	5	-
Conduction from annular flow liquid film to structure: Nu = d					
d	-	2	2	2	-
Forced convection from CP fluid to rigid particles: Nu = $e_{i1}\mathrm{Re}_j^{e_{i2}}\mathrm{Pr}_i^{e_{i3}}\left(1+e_{i4}\mathrm{Re}_j^{e_{i5}}\right)$					
e_1	0.542	0.542	0.646	0.68	-
e_2	0.5	0.5	0.5	0.5	-
e_3	0.45	0.45	0.5	0.5	-
e_4	0.012	0.012	0.008	0.0	-
e_5	0.333	0.333	0.333	0.0	-
Natural convection from CP fluid to rigid particles: Nu = $f_{i1}\left(\mathrm{Gr}_j\mathrm{Pr}^{f_{i3}}\right)^{f_{i2}}$					
f_2	0.474	0.474	0.53	0.62	-
f_2	0.25	0.25	0.25	0.25	-
f_3	1.44	1.44	1.74	1.91	-
Forced convection from CP fluid to structure: Nu = $g_{i1}\mathrm{Re}_{D_h}^{g_{i2}}\mathrm{Pr}_i^{g_{i3}}$					
g_1	0.023	0.023	0.025	0.025	-
g_2	0.8	0.8	0.8	0.8	-
g_3	0.3	0.3	0.8	0.8	-
Conduction from multiphase, multicomponent mixture, $K_{mix}^{h_2}=\sum_{i=1}^{8}a_iK_i^{h_2}$, to structure: Nu = h_1					
h_1: 5.0		h_2: -0.2			
Convection in CP liquid to circulating particle (Re_D>50): Nu = $i_1\mathrm{Pr}^{i_2}\left[1-\left(i_3+i_4\kappa^{i_5}\right)/\mathrm{Re}_D^{1/2}\right]^{i_6}$					
i_1	-	1.13	1.13	1.13	-
i_2	-	0.5	0.5	0.5	-
i_3	-	2.89	2.89	2.89	-
i_4	-	2.15	2.15	2.15	-
i_5	-	0.64	0.64	0.64	-
i_6	-	0.5	0.5	0.5	-
Circulating fluid particle (Re_D >50): Nu → Nu×F, F=$1+j_1\left[1+\tanh\left(j_2\ln\left(\mathrm{Pe}_{dp}^*/j_3\right)\right)\right]$					
j_1	-	0.842	0.842	0.842	-
j_2	-	1.025	1.025	1.025	-
j_3	-	200	200	200	-
Oscillating fluid particle internal Nu (Re 0>300): Nu → Nu×k					
k	2.7	2.7	2.7	2.7	-

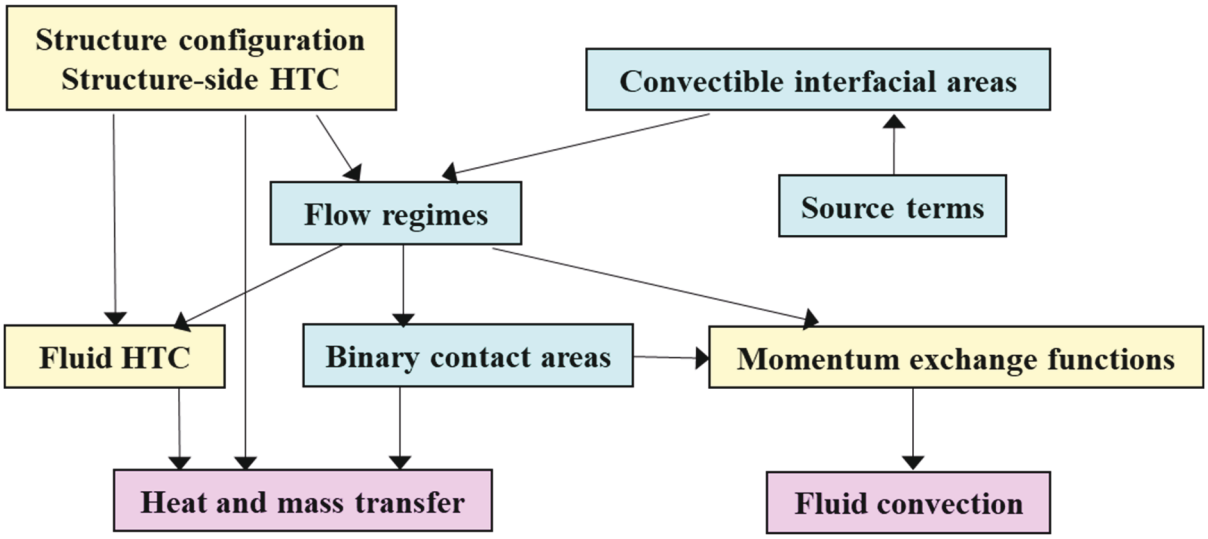

Fig. 1. SIMMER-III/SIMMER-IV Step 1 calculational flow.

	Energy component	Energy component which is being interacted with: Gas/ Vapor G	Liquid Fuel L1	Liquid Steel L2	Liquid Sodium L3	Fuel Particle L4	Steel Particle L5	Control Particle L6	Fuel Chunk L7	Fuel pin Structure K1	Left Structure K2	Right Structure K3	Mass transfer paths M/F	Mass transfer paths V/C
HTC	Gas/ Vapor G		V/C HGLM(1) I1{1}	V/C HGLM(2) I2{2}	V/C HGLM(3) I3{3}	V/C HGLM(4) I4{3}	V/C HGLM(5) I5{3}	V/C HGLM(6) I6{3}	V/C HGLM(7) I7{3}	V/C HGS I29{3}	V/C HGS I37{3}	V/C HGS I45{3}		27
HTC	Liquid Fuel L1	V/C HLMG(1) I1{1}		V/C HRT(1) I8{-}	V/C HRT(2) I9{-}	M/F HRT(3) I10{1}	M/F HRT(4) I11{1}	M/F HRT(5)	M/F HRT(6) I13{1}	M/F HRS(1) I30{1}	M/F HRS(8) I38{1}	M/F HRS(10) I46{1}	6	1
HTC	Liquid Steel L2	V/C HLMG(2) I2{1}	M/F HRT(7) I8{1}		V/C HRT(8) I14{-}	M/F HRT(9)	M/F HRT(10) I16{1}	M/F HRT(11)	M/F HRT(12)	M/F HRS(2) I31{1}	M/F HRS(9) I39{1}	M/F HRS(11) I47{1}	4	2
HTC	Liquid Sodium L3	V/C HLMG(3) I3{1}	M/F HRT(13) I9{1}	M/F HRT(14) I14{1}		M/F HRT(15)	M/F HRT(16)	M/F HRT(17)	M/F HRT(18)	M/F HRS(3)	M/F HRS(3)	M/F HRS(3)		3
HTC	Fuel Particle L4	V/C HPT(1)	M/F HPT(1) I10{1}	M/F HPT(1)	M/F HPT(1)		M/F HPT(1)	M/F HPT(1)	M/F HPT(1)	M/F HRS(4)	M/F HRS(4)	M/F HRS(4)	1	
HTC	Steel Particle L5	V/C HPT(2)	M/F HPT(2) I11{1}	M/F HPT(2) I16{1}	M/F HPT(2)	M/F HPT(2)		M/F HPT(2)	M/F HPT(2)	M/F HRS(5)	M/F HRS(5)	M/F HRS(5)	2	
HTC	Control Particle L6	V/C HPT(3)	M/F HPT(3)	M/F HPT(3)	M/F HPT(3)	M/F HPT(3)	M/F HPT(3)		M/F HPT(3)	M/F HRS(6)	M/F HRS(6)	M/F HRS(6)		
HTC	Fuel Chunk L7	V/C HPT(4)	M/F HPT(4) I13{1}	M/F HPT(4)	M/F HPT(4)	M/F HPT(4)	M/F HPT(4)	M/F HPT(4)		M/F HRS(7)	M/F HRS(7)	M/F HRS(7)	1	
STRCON	Fuel Pin Structure K1	V/C I29{-}	M/F I30{1}	M/F I31{1}	M/F	M/F	M/F	M/F	M/F	*Heat and mass transfer calculated in V/C or M/F routine.*			2	
STRCON	Left Structure K2	V/C I37{-}	M/F I38{2}	M/F I39{1}	M/F	M/F	M/F	M/F	M/F	*HTC(n) is an array name and (the number of HTCs).*			3	
STRCON	Right Structure K3	V/C I45{-}	M/F I46{2}	M/F I47{1}	M/F	M/F	M/F	M/F	M/F	*Interface ID and {the number of mass transfer paths}.*			3	
										Total number of paths:			**22**	**33**

Fig. 2. Role of HTCs in SIMMER-III heat and mass transfer.

	Energy component	Energy component which is being interacted with:													Mass transfer paths	
		Gas/ Vapor G	Liquid Fuel L1	Liquid Steel L2	Liquid Sodium L3	Fuel Particle L4	Steel Particle L5	Control Particle L6	Fuel Chunk L7	Fuel pin Structure K1	Left Structure K2	Right Structure K3	Front Structure K4	Back Structure K5	M/F	V/C
HTC	Gas/ Vapor G		V/C HGLM(1) I1{1}	V/C HGLM(2) I2{2}	V/C HGLM(3) I3{3}	V/C HGLM(4) I4{3}	V/C HGLM(5) I5{3}	V/C HGLM(6) I6{3}	V/C HGLM(7) I7{3}	V/C HGS I29{3}	V/C HGS I37{3}	V/C HGS I45{3}	V/C HGS I53{3}	V/C HGS I61{3}		33
	Liquid Fuel L1	V/C HLMG(1) I1{1}		V/C HRT(1) I8{-}	V/C HRT(2) I9{-}	M/F HRT(3) I10{1}	M/F HRT(4) I11{1}	M/F HRT(5)	M/F HRT(6) I13{1}	M/F HRS(1) I30{1}	M/F HRS(8) I38{1}	M/F HRS(10) I46{1}	M/F HRS(8) I54{1}	M/F HRS(10) I62{1}	8	1
	Liquid Steel L2	V/C HLMG(2) I2{1}	M/F HRT(7) I8{1}		V/C HRT(8) I14{-}	M/F HRT(9)	M/F HRT(10) I16{1}	M/F HRT(11)	M/F HRT(12)	M/F HRS(2) I31{1}	M/F HRS(9) I39{1}	M/F HRS(11) I47{1}	M/F HRS(9) I55{1}	M/F HRS(11) I63{1}	6	2
	Liquid Sodium L3	V/C HLMG(3) I3{1}	M/F HRT(13) I9{1}	M/F HRT(14) I14{1}		M/F HRT(15)	M/F HRT(16)	M/F HRT(17)	M/F HRT(18)	M/F HRS(3)	M/F HRS(3)	M/F HRS(3)	M/F HRS(3)	M/F HRS(3)		3
	Fuel Particle L4	V/C HPT(1)	M/F HPT(1) I10{1}	M/F HPT(1)	M/F HPT(1)		M/F HPT(1)	M/F HPT(1)	M/F HPT(1)	M/F HRS(4)	M/F HRS(4)	M/F HRS(4)	M/F HRS(4)	M/F HRS(4)	1	
	Steel Particle L5	V/C HPT(2)	M/F HPT(2) I11{1}	M/F HPT(2) I16{1}	M/F HPT(2)	M/F HPT(2)		M/F HPT(2)	M/F HPT(2)	M/F HRS(5)	M/F HRS(5)	M/F HRS(5)	M/F HRS(5)	M/F HRS(5)	2	
	Control Particle L6	V/C HPT(3)	M/F HPT(3)	M/F HPT(3)	M/F HPT(3)	M/F HPT(3)	M/F HPT(3)		M/F HPT(3)	M/F HRS(6)	M/F HRS(6)	M/F HRS(6)	M/F HRS(6)	M/F HRS(6)		
	Fuel Chunk L7	V/C HPT(4)	M/F HPT(4) I13{1}	M/F HPT(4)	M/F HPT(4)	M/F HPT(4)	M/F HPT(4)	M/F HPT(4)		M/F HRS(7)	M/F HRS(7)	M/F HRS(7)	M/F HRS(7)	M/F HRS(7)	1	
STRCON	Fuel Pin Structure K1	V/C I29{-}	M/F I30{1}	M/F I31{1}	M/F	M/F	M/F	M/F	M/F						2	
	Left Structure K2	V/C I37{-}	M/F I38{2}	M/F I39{1}	M/F	M/F	M/F	M/F	M/F						3	
	Right Structure K3	V/C I45{-}	M/F I46{2}	M/F I47{1}	M/F	M/F	M/F	M/F	M/F						3	
	Front Structure K4	V/C I53{-}	M/F I38{2}	M/F I39{1}	M/F	M/F	M/F	M/F	M/F						3	
	Back Structure K5	V/C I61{-}	M/F I46{2}	M/F I47{1}	M/F	M/F	M/F	M/F	M/F						3	
														Total number of paths:	**32**	**39**

Heat and mass transfer calculated in V/C or M/F routine.

HTC(n) is an array name and (the number of HTCs).

Interface ID and {the number of mass transfer paths}.

Fig. 3. Role of HTCs in SIMMER-IV heat and mass transfer.

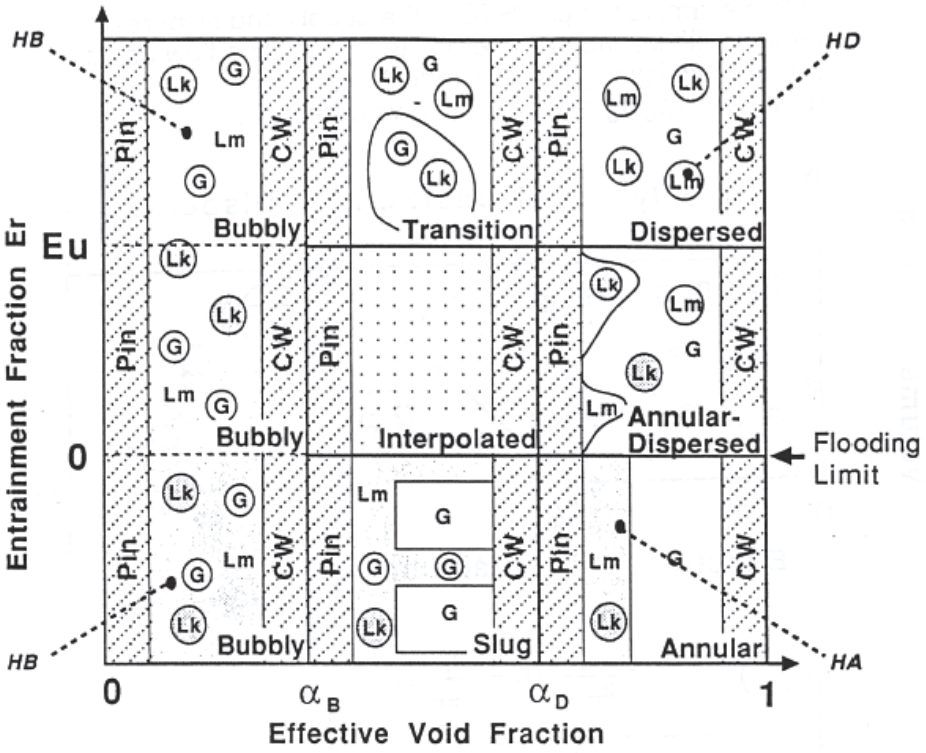

Heat transfer coefficients in well-defined geometries:

$H_B\ (HB)$ – Bubbly flow regime HTC

$H_A\ (HA)$ – Annular flow regime HTC

$H_D\ (HD)$ – Dispersed flow regime HTC

Interpolation along the x-axis (slug and transition flow):

$$\log H_{tran} = \beta \log H_B + (1-\beta) \log H_D$$
$$\log H_{slug} = \beta \log H_B + (1-\beta) \log H_A \qquad \beta = \left(\frac{\alpha_D - \alpha}{\alpha_D - \alpha_S}\right)$$

Interpolation along the y-axis (annular dispersed flow):

$$log\ H_{anndsp} = \chi\ log\ H_A + (1-\chi)\ log\ H_D \qquad \chi = 1 - \frac{E_r}{E_u}$$

Interpolated flow regime obtained by interpolation between slug and transition flows

Fig. 4. Flow regime map used in HTC interpolation.

Appendix A: Internal Heat Transfer in Rigid Particles

A.1. Introduction

This Appendix attempts to justify the heat transfer coefficient (HTC) calculation inside a rigid particle. The heat transfer mechanism is molecular conduction, and the geometry of the particle is assumed to be spherical (or else the particle can be represented by an equivalent sphere). In this appendix, a particle refers not just to solid particles, but also to non-circulating, non-oscillating droplets and bubbles.

This appendix is subdivided as follows. The conduction equation used in the SIMMER-III formulation is described. Although the heat transfer equation is easily stated, a general solution cannot be obtained for two reasons. Firstly, heat transfer is generally time-dependent, due to the finite volume of the particle, whereas a steady-state HTC is required for SIMMER-III. Secondly, simplifying assumptions must be made about the boundary conditions, since these are not usually known in advance for the conditions in which SIMMER-III is applied.

The SIMMER-III approach is then applied to two problems: steady-state conduction from a power-producing sphere and a basic transient conduction problem. By comparing the SIMMER-III approach with analytical solutions, a suitable constant value of Nusselt number is recommended. A method for evaluating particle HTCs in the dispersed flow regime is then described.

In addition to justifying the particle internal HTC, the SIMMER-III formulation for cases of finite internal and external thermal resistances is compared with analytical solutions. Finally, recommendations are made for user-input parameters to model internal particle heat transfer.

A.2. Conduction Equation and SIMMER-III Constraints

The particle is assumed to have temperature-independent physical properties and, for simplicity, the internal power generation is assumed to be uniform. The two basic equations which describe conduction in spherical geometry are:

$$q(r,t) = -k\frac{\partial T(r,t)}{\partial r}\text{ , and} \tag{A-1}$$

$$\frac{\partial T(r,t)}{\partial t} = \frac{\alpha}{r^2}\frac{\partial}{\partial r}\left[r^2\frac{\partial T(r,t)}{\partial r}\right] + \frac{Q^*(t)}{\rho c}\text{ .} \tag{A-2}$$

where Q^* is uniform power generation per unit volume. Equation (A-1) is Fourier's law; Eq. (A-2) is Fourier's law plus the conservation of energy. To obtain a solution to Eq. (A-2) the boundary conditions must be specified (as a function of time) and the spatial distribution of temperature in the particle must be known.

In modeling particles with SIMMER-III the following constraints are imposed:

- Only the mass-averaged particle temperature is known; the temperature distribution inside the particle is not modeled.
- The time-dependent behavior of the boundary conditions is unknown. Only instantaneous average temperatures of particle and surrounding fluid are known.

- The particle Nusselt number is constant.

Equations (A-1) and (A-2) are in a more suitable format for SIMMER-III if they are integrated over the volume of the particle and the Nusselt number is introduced:

$$q_{r=R}(t) = \frac{k\mathrm{Nu}}{D}\left(\hat{T}_p(t) - T_i(t)\right), \text{ and} \tag{A-3}$$

$$\frac{d\hat{T}_p(t)}{dt} + \frac{3\alpha\mathrm{Nu}\hat{T}_p(t)}{2R^2} = \frac{3\alpha\mathrm{Nu}T_i(t)}{2R^2} + \frac{\alpha Q^*(t)}{k}, \tag{A-4}$$

where $\hat{T}_p$ is the average particle temperature. Equation (A-3) describes the heat flux out of the particle; Eq. (A-4) describes the temperature history of the particle. To solve Eqs. (A-3) and (A-4) as a function of *Nu* it is necessary to specify the time-dependent interface temperature T_i and power generation Q^*. The problem is to recommend a suitable value of Nu for the various application areas of SIMMER-III. This is done below by postulating some idealized scenarios for which analytical solutions are available, and finding the most appropriate value of *Nu* for each scenario.

(1) A steady-state conduction problem

Steady-state heat transfer from a particle can be achieved if the internal power production is constant and the rate of heat removal through the surface of the particle is equal to the power production in the particle. This can be the case for a particle heated by nuclear heating.

The analytical solution is obtained from Eq. (A-2). First the equation is made independent of time:

$$\frac{1}{r^2}\frac{d}{dr}\left(r^2\frac{dT(r)}{dr}\right) + \frac{Q^*}{k} = 0\,. \tag{A-5}$$

Equation (A-5) is easily integrated to obtain the steady-state quadratic temperature distribution:

$$T(r) = T_i + \frac{Q^*}{6k}(\mathrm{R}^2 - \mathrm{r}^2)\,. \tag{A-6}$$

Thus the average particle temperature may be evaluated:

$$\hat{\theta}_p = \frac{\int_0^R T(r)4\pi r^2 dr}{\frac{4}{3}\pi r^3} - T_i = \frac{Q^* R^2}{15k}\,. \tag{A-7}$$

The solution in the SIMMER-III formulation can be obtained from either Eq. (A-3) or (A-4):

$$Nu = \frac{2R^2 Q^*}{3k\hat{Q}_p}\,. \tag{A-8}$$

The SIMMER-III formulation can be made to reproduce the analytical result by substituting the analytical temperature difference Eq. (A-7) into Eq. (A-8):

$$\mathrm{Nu} = 10\,. \tag{A-9}$$

Thus the SIMMER-III formulation can exactly reproduce the steady-state heat transfer from a power-producing particle if the Nusselt number is set to 10. This value corresponds to heat transfer from the mass centroid of the particle to its surface. The above approach was used to justify the value of *Nu* used by the AFDM code. However, the scenario is not typical of SIMMER-III calculations, where transient temperature variations can be anticipated.

(2) A basic transient: step change in interface temperature

The most basic transient conduction problem for which an analytical solution exists is heat conduction within a sphere which is initially at uniform temperature when a constant temperature boundary condition is imposed. This might be the case for a particle or droplet which experiences a sudden change in ambient temperature in a fluid with a low resistance to heat transfer. The particle takes a certain time to approach equilibrium conditions, which can be evaluated both analytically and using the SIMMER-III formulation.

The analytical solution for an initially uniform temperature sphere with constant surface temperature and heat generation is in the text book[1)] as:

$$\theta(r,t) = \frac{2R\theta_0}{\pi r}\sum_{n=1}^{\infty}\left[\frac{(-1)^{n+1}}{n}\sin\left(\frac{n\pi r}{R}\right)\exp\left(\frac{-n^2 t}{\tau}\right)\right] + \frac{Q^* r^2}{6k}. \tag{A-10}$$

where the thermal time constant of the particle is:

$$\tau = \frac{R^2}{\pi^2 \alpha}. \tag{A-11}$$

The thermal time constant of a particle is an indication of the timescale over which the particle attains thermal equilibrium with the surrounding fluid.

The heat generation term in Eq. (A-10) gives the steady-state solution described above. Since it is the transient heat transfer which is of most interest, the power generation term is ignored. Useful solutions which are readily obtained from Eq. (A-10) are the average particle temperature, the heat flux out of the particle and the fractional approach to equilibrium:

$$\hat{\theta}_p(t) = \frac{6\theta_0}{\pi^2}\sum_{n=1}^{\infty}\frac{1}{n^2}\exp\left(\frac{-n^2 t}{\tau}\right), \tag{A-12a}$$

$$q_R(t) = \frac{2k\theta_0}{R}\sum_{n=1}^{\infty}\exp\left(\frac{-n^2 t}{\tau}\right), \text{and} \tag{A-12b}$$

$$F(t) = 1 - \frac{6}{\pi^2}\sum_{n=1}^{\infty}\frac{1}{n^2}\exp\left(\frac{-n^2 t}{\tau}\right). \tag{A-12c}$$

From the first two expressions, it can be seen that the analytical expression implies a transient Nusselt number:

$$Nu(t) = \frac{2R}{k}\frac{q_R}{\hat{\theta}_p} = \frac{2\pi^2}{3}\sum_{n=1}^{\infty}\exp\left(\frac{-n^2 t}{\tau}\right)\Bigg/\sum_{n=1}^{\infty}\frac{1}{n^2}\exp\left(\frac{-n^2 t}{\tau}\right). \quad \text{(A-13)}$$

The instantaneous Nu approaches an asymptotic value at long times (see also Ref. 2)):

$$\mathrm{Nu} = \frac{2\pi^2}{3} = 6.58 \ \text{ as } \ t \to \infty\,. \quad \text{(A-14)}$$

Another useful quantity is the time-averaged Nusselt number:

$$\widehat{\mathrm{Nu}}(T) = \frac{1}{T}\int_0^T \mathrm{Nu}(t)dt = -\frac{2\pi^2}{3}\frac{\tau}{T}\ln\left[\frac{6}{\pi^2}\sum_{n=1}^{\infty}\frac{1}{n^2}\exp\left(\frac{-n^2 T}{\tau}\right)\right]. \quad \text{(A-15)}$$

Although the time-averaged Nu approaches the steady-state value at long times, at times shorter than the time constant of the particle it is larger than the instantaneous Nu. Equations (A-13) and (A-15) indicate that the SIMMER-III formulation, which is constrained to a constant value of *Nu*, cannot reproduce the transient heat loss from a particle exactly. Over long timescales the most suitable value of *Nu* is 6.58. However, for heat transfer on the timescale of the particle a higher value of Nu is warranted.

The SIMMER-III formulation imposes a constant Nusselt number and so the solution is different from the analytical solution described above. The normalized heat loss from a particle using the SIMMER-III formulation can be obtained from Eqs. (A-3) and (A-4):

$$\hat{\theta}_p(t) = \theta_0 \exp\left(\frac{-3\mathrm{Nu}t}{2\pi^2\tau}\right), \text{and} \quad \text{(A-16a)}$$

$$F(t) = \left[1 - \exp\left(\frac{-3\mathrm{Nu}t}{2\pi^2\tau}\right)\right]. \quad \text{(A-16b)}$$

To identify a suitable value of Nu in the SIMMER-III formulation, the normalized heat loss calculated by SIMMER-III (Eqs. (A-16a) and (A-16b)) is compared with the analytic solution (Eqs. (A-12a), (A-12b) and (A-12c)). The first point to note is that no single value of *Nu* reproduces the analytical solution over all timescales. The second point is that most heat loss occurs within the thermal time constant of the particle, so that the steady-state value of Nu is achieved only when thermal equilibrium has almost been achieved. Thus, a larger value of Nu than 6.58 reproduces the heat loss from the particle better. The steady-state conduction value obtained above, Nu = 10, is a reasonable approximation to the analytical solution.

The above case of a uniform temperature sphere suddenly placed in a constant temperature bath is ideal, but it does provide an example of the transient behavior of particles and droplets in SIMMER-III calculations. Alternative scenarios can be evaluated, for example the case of a sphere placed in an infinite medium, which involves a time-varying interface temperature. However, the solution to this problem is considerably more complicated and does not give more information than the example discussed.

(3) Particle-particle heat transfer in dispersed flow

In the dispersed flow regime, heat transfer between particles and droplets by conduction is possible via collisions. In fact, only heat transfer involving liquid droplets will be considered, since the contact areas during particle/particle collisions and particle/structure collisions are considered to be negligible.

In many cases the contact times between droplets are less than the thermal time constants of the droplets, in which case the heat transferred during the collision is larger than would be expected from considerations of a long-time contact of a particle in a continuous fluid. This suggests an alternative approach: estimate the average contact time and to use that time to optimize the value of Nu. The optimization is performed using the above equations for transient heat transfer out of an initially uniform temperature sphere. Equation (A-15) gives:

$$\frac{1}{\mathrm{Nu}} = \frac{-2\pi^2 r}{3\tau_{con}} \ln\left[\frac{6}{\pi^2}\sum_{n=1}^{\infty}\frac{1}{n^2}\exp\left(\frac{-n^2\tau_{con}}{\tau}\right)\right], \tag{A-17}$$

where τ_{con} is the average contact time and is calculated to be consistent with the calculation of the binary contact area between the two components. This is because the interfacial area calculation for discontinuous components in SIMMER-III is based on the SIMMER-II approach[3]:

$$\hat{a}_{ij} = A_{ij}^{c} Z_{ij}^{c} \tau_{ij}^{c} . \tag{A-18}$$

Thus, the contact time τ_{con} is equated to the contact time τ_{ij}^{c} for dispersed components *i* and *j*:

$$\tau_{ij}^{c} = \frac{2(R_i + R_j)}{\Delta V}. \tag{A-19}$$

A disadvantage of this method for calculating Nu is that the infinite series in Eq. (A-17) must be approximated.

(4) Combined internal and external heat transfer

The Nusselt numbers derived above apply to a sphere for which the external resistance is assumed to be negligible. It is worthwhile comparing the SIMMER-III formulation for a finite, steady-state external resistance with analytical solutions. In SIMMER-III heat transfer is calculated via an interface temperature, which can be considered to be the particle surface temperature when there is no phase change. The rate of heat transfer between the particle and the bulk fluid is then:

$$q = \frac{1}{D}\frac{(T_{dp} - T_{cp})}{\left(\frac{1}{k_{dp}\mathrm{Nu}_{dp}} + \frac{1}{k_{cp}\mathrm{Nu}_{cp}}\right)} = \frac{k_{dp}}{D}\frac{(T_{dp} - T_{cp})}{\left(\frac{1}{\mathrm{Nu}_{dp}} + \frac{1}{2\mathrm{Bi}}\right)}, \tag{A-20}$$

where the suffices "*dp*" and "*cp*" are used to distinguish properties in the dispersed and continuous phases, respectively, and the Biot number is defined by:

$$\mathrm{Bi} = \frac{k_{cp} R}{k_{dp}}. \tag{A-21}$$

The fractional approach to equilibrium for a sphere at initially uniform temperature is still given by Eqs. (A-16a) and (A-16b), but the particle Nusselt number in Eqs. (A-16a) and (A-16b) must be replaced as follows:

$$\mathrm{Nu} \rightarrow \frac{1}{\left(\frac{1}{\mathrm{Nu}_{dp}} + \frac{1}{2\mathrm{Bi}}\right)}. \tag{A-22}$$

When the internal resistance is negligible compared to the external resistance, Nu_{dp}, is large, and the Biot number determines the time for the particle to achieve equilibrium. From Eqs. (A-20), (A-3), (A-16a) and (A-16b) the fractional approach to equilibrium is:

$$F(t) = \left[1 - \exp\left(\frac{-3\mathrm{Bi}t}{\pi^2\tau}\right)\right], \tag{A-23}$$

which is identical to one recommended in Ref. 2) for the case of negligible internal resistance.

For the case when the internal and external resistances are comparable, graphical solutions for the fractional approach to equilibrium are presented in Ref. 2). The SIMMER-III formulation qualitatively reproduces the behavior of Eqs. (A-16a) and (A-16b), with the Nusselt number given by Eq. (A-22). Thus, the SIMMER-III framework for calculating heat transfer with no phase change between particles and a surrounding fluid is satisfactory, at least when the external heat transfer is steady-state.

(5) Heat transfer in rigid spheres in other codes

The SIMMER-III formulation is essentially derived from SIMMER-II[3] and AFDM[4]. Both of these codes use a constant value of *Nu* to model heat transfer from particles and droplets, with *N*u=10.

A.3. Recommendations for SIMMER-III

The form of the HTC for heat transfer inside a rigid particle in SIMMER-III is:

$$h = \frac{k}{D}\mathrm{Nu}\,, \tag{A-24}$$

where Nu is a user-input parameter; the recommended value of Nu is:

$$\mathrm{Nu} = 10\,. \tag{A-25}$$

The method described above for heat transfer between droplets in the dispersed phase is available as an option in SIMMER-III.

References for Appendix A

1) Carslaw, H.S., Jaeger, J.C., Conduction of Heat in Solids, 2nd edition, Oxford University Press, 1959, 510p.

2) Clift, R., Grace, J.R. et al., Bubbles, Drops, and Particles, Academic Press, 1978, 380p.

3) Bohl, W. R. et al., SIMMER-II: A Computer Program for LMFBR Disrupted Core Analysis, LA-11415-MS, Los Alamos National Laboratory, 1990.

4) Berthier, J. et al., AFDM: An Advanced Fluid Dynamics Model, Volume III: Heat Transfer and Momentum Exchange Coefficients, LA-11692-MS, Vol. III, Los Alamos National Laboratory, 1990.

Nomenclature for Appendix A

$\hat{a}_{i,j}$	Instantaneous binary area for dispersed components i, j	
$A_{i,j}^{c}$	Contact area for each droplet-droplet collision	
Bi	Biot number	$\mathrm{Bi} = \frac{k_{cp}R}{k_{dp}}$
c	Specific heat capacity of particle	
D	Diameter of the particle	
F	Fractional approach to equilibrium	
h	Heat transfer coefficient (HTC)	$h = \frac{k}{D}\mathrm{Nu}$
k	Thermal conductivity of the particle	
Nu	Nusselt number	
q	Heat flux	
Q^*	Uniform power generation per unit volume	
r	Coordinate in the radial direction	
R	Particle radius: $R = D/2$	
t	Time	
τ	Thermal time constant of a particle, defined by Eq. (A-11)	
T	Temperature	
T_i	Interface temperature	
$\hat{T}_p$	Average particle temperature	
$\Delta T_{i,j}$	Velocity difference between the two components *i* and	
$Z_{i,j}$	Number of collisions per unit time	

Greek symbols

α	Thermal diffusivity of particles	$\alpha = \frac{k}{\rho c}$
ρ	Density of particle	
τ	Thermal time constant of a particle, defined by Eq. (A-11)	
τ_{con}	Average time constant	
τ_{ij}^{c}	Duration of contact for each droplet-droplet collision	
θ	Temperature relative to the interface	$\theta(r,t) = T(r,t) - T_i.$
θ_0	Initial particle temperature	
$\hat{\theta}_p$	Average relative particle temperature	$\hat{\theta}_p = \hat{T}_p - T_i.$

Subscripts

cp	Continuous Phase (i.e. the surrounding fluid)
dp	Dispersed Phase (i.e. the particle)
i	Interface (surface of particle)
i,j	Denotes droplets *i* and *j* in the dispersed phase
p	Particle
r=R	Evaluated at the surface of the particle
0	Initial value

Appendix B: External Heat Transfer from Rigid Spheres by Forced Convection

B.1. Introduction

This appendix summarizes the approach used to evaluate forced convection heat transfer between a rigid sphere and a fluid (liquid or gas). A fluid-side (external) total Nusselt number is required in order to calculate heat transfer from particles and non-circulating droplets to continuous vapor or liquid in SIMMER-III. A number of heat transfer correlations are collated in this appendix even though many are suitable for restricted ranges of Reynolds number and Prandtl number, so that the code user can choose a correlation appropriate to the conditions being modeled.

Although particles, droplets and bubbles are not always spherical, and the shape regime of the particle influences heat transfer, this effect is too complicated to take into account in SIMMER-III. The surface roughness of particles is also ignored and rotation of spheres is neglected. Correlations and criteria for internal circulation for a fluid sphere are discussed in Appendix D, as is natural convection.

SIMMER-III is intended to be applied to a wide range of flow conditions, and so the forced convection HTC needs to be appropriate for several orders of magnitude of Reynolds number. To get a feel for some typical conditions: a 5 mm diameter particle in liquid fuel flowing with differential velocity 1 m/s has a Reynolds number of 10^4, whilst the same particle in fission gas with temperature 1200 K and flowing at 10 m/s has a Reynolds number of 10^3. A successful correlation must also take account of the wide range in fluid Prandtl number to which the code will be applied: from a Prandtl number of about 7 (for water) to 0.005 (liquid sodium).

This Appendix is subdivided as follows. Two sections describe the flow dynamics and how local heat transfer varies around a sphere. Theoretical heat transfer correlations based on these observations are then reviewed. A section examines total heat transfer correlations for spheres in the light of experimental results. Since experimental results are sparse for liquid metals, the following section examines the data and correlations available for single cylinders in cross-flow. Secondary effects are then reviewed, e.g. the influence of turbulence and multi-particle flow. Finally, formulae to calculate HTCs in SIMMER-III are recommended. Nomenclature is defined after References.

B.2. Flow Dynamics around a Single Rigid Sphere

It is worthwhile briefly reviewing the behavior of the flow field as a function of Reynolds number since the flow dynamics has an impact on theoretical considerations of heat transfer from a sphere. More detailed descriptions are available in Refs. 1) and 2).

- ***Creeping flow*** (Re < 1). There is no wake at the rear of the particle; the flow field is axi-symmetric around the particle.
- ***Unseparated flow*** (1 < Re < 20). There is no wake at the rear of the particle but the flow field is increasingly asymmetric with increasing Reynolds number.
- ***Onset of separation*** (Re = 20). A re-circulating wake forms, initially at the rear stagnation point.

- ***Steady wake region*** (20 < Re < 130). The separation point moves forward over the sphere; the wake widens and lengthens but remains attached to the sphere. The dominant contribution to the profile drag is still skin friction.
- ***Onset of wake instability*** (130 < Re < 400). Vortex shedding starts; the separation point continues to move forward over the sphere. For Re >150 form (pressure) drag becomes more important than skin drag.
- ***High sub-critical Reynolds number*** (400 < Re < 3.5×10^5). Flow is unsteady and asymmetric due to the wake instability and vortex shedding. A laminar boundary layer may be considered to cover the front part of the sphere. The separation point continues to move forward, crossing the equator at Re ~ 5000 and reaching a limit of about 800. Some authors consider that a fully turbulent boundary layer immediately reattaches to the sphere, behind which is the wake region. Form (pressure) drag dominates over skin friction, so the drag coefficient is virtually insensitive to Re.
- ***Critical transition and supercritical flow*** (Re > 3.5×10^5). As the Reynolds number increases above about 2×10^5 the boundary layer becomes turbulent before detaching from the surface, with the result that the separation point rapidly moves downstream and the wake becomes smaller. The form drag drops sharply at the critical transition.

B.3. Local Heat Transfer Behavior around a Sphere

The total Nusselt number is composed of the variation of local Nusselt number around a sphere. Local Nusselt numbers are deduced from experiments and numerical analysis (the Nusselt number can be equated with Sherwood number due to the equivalence of heat and mass transfer for spheres). The Nusselt numbers are evaluated at a constant Schmidt (Prandtl) number which corresponds to heat transfer to air.

Up to flow separation (Re = 20) the local Nusselt number decreases monotonically from front to rear. Once separation occurs, there is a minimum in the Nusselt number which is associated with, but slightly aft of, the separation point. The increased heat transfer at the rear of the sphere is caused by the action of the recirculating wake.

At higher Reynolds number (Re > 3000) the forward portion of the sphere approaches (laminar) boundary layer flow, with the local heat transfer reaching a minimum at the flow separation point (where the surface velocity approaches zero). The heat transfer behavior behind the separation point is more complicated, reflecting the complex flow behavior. It seems that there is a sudden increase in heat transfer associated with the reattachment of a turbulent boundary layer to the sphere. There is then a second minimum in the Nusselt number due to the final separation of the boundary layer followed by heat transfer increasing smoothly in the wake region. Heat transfer behind the separation point increases more rapidly with Reynolds number than at the front.

The dependence of local Nusselt number has been quantified in some detail by Hayward and Pei[2)] for Reynolds numbers between 2600 and 6100. They consider that heat transfer around a sphere should be divided into three regions: a laminar boundary layer covering the front of the sphere, a turbulent boundary

layer and a turbulent wake. The laminar boundary layer and wake cover most of the sphere. In the laminar boundary layer the local heat transfer is approximately $\mathrm{Nu}_{local} \propto \mathrm{Re}^{0.5}$, although the exponent was found to be slightly higher than 0.5 and this is attributed to the effect of freestream turbulence. The wake region can be approximated by $\mathrm{Nu}_{local} \propto \mathrm{Re}^{0.8}$.

B.4. Theoretical Treatments of Total Heat Transfer for a Sphere

Analytical solutions for flow around, and heat transfer from, rigid spheres are limited to very low Reynolds number. Numerical solutions can make predictions only for steady, axisymmetric flow, at intermediate Reynolds number. At higher Reynolds number it is necessary to rely on heat transfer correlations based on experimental results and boundary layer theory.

The steady-state conduction solution for a sphere surrounded by an infinite stagnant fluid is (Refs. 1), 3), etc.):

$$\mathrm{Nu} = 2\,, \tag{B-1}$$

which is effectively the minimum HTC (though at low fluid velocities natural convection would effect higher heat transfer rates and dominate both pure conduction and forced convection).

For creeping flow, $\mathrm{Nu} \to \mathrm{Pe}^{1/3}$ and Clift et al.[1] recommends the following equation based on analytical and numerical solutions:

$$\mathrm{Nu} = 1 + (1 + \mathrm{Pe})^{1/3}\,, \tag{B-2}$$

Although the creeping flow regime covers a limited range of Reynolds number, it is an important regime for very small particles. Numerical results in the range $1 \leq \mathrm{Re} \leq 400$ and $0.25 \leq \mathrm{Pr} \leq 100$ can be correlated by the following expression:

$$\mathrm{Nu} = 1 + (1 + \mathrm{Pe})^{1/3}\mathrm{Re}^{0.08}. \tag{B-3}$$

At higher Reynolds numbers, boundary layer theory predicts that in the laminar boundary layer region, which covers the front half of the sphere, the local Nusselt number has the following dependency on Reynolds number: $\mathrm{Nu}_{local} \propto \mathrm{Re}^{0.5}$. However, a different dependency is predicted for the turbulent boundary layer (at the rear of the sphere): $\mathrm{Nu}_{local} \propto \mathrm{Re}^{0.8}$. These dependencies, and the data from Ref. 2) described above, suggest that a heat transfer correlation which is fitted to experimental data at higher Reynolds numbers should have two terms, corresponding to the laminar and turbulent boundary layers respectively. Note that some authors consider the dependency to be $\propto \mathrm{Re}^{2/3}$ or $\propto \mathrm{Re}$ in the wake region, e.g. by Churchill[4].

The Reynolds-Colburn analogy for relating heat transfer to (total) drag cannot be applied in the case of a sphere. This is due to the complex superposition of skin friction and form drag, and the heat transfer behavior in the wake. It is clear that the behavior of the Nusselt number does not follow the drag coefficient curve. In fact the Nusselt number behavior is remarkably smooth, at least up to the critical transition.

Much of the above reasoning applies to liquids and gases with Prandtl numbers of about 0.7 and upwards. For liquid metals, with Prandtl number of the order 0.01, Nusselt numbers are generally correlated with the Peclet number (e.g. by Holman[5]). The following analytical solution is recommended by Dwyer.[6]

It was obtained by Hsu[7] by assuming potential flow around a sphere, which is applicable in the limit $\mathrm{Re} \to \infty$ and assumes slip at the surface of the sphere:

$$\mathrm{Nu} = 1.13\mathrm{Pe}^{1/2}\,, \tag{B-4}$$

where the constant 1.13 in Eq. (B-4) is appropriate for uniform wall temperature (the constant for uniform heat flux condition is 1.29).

B.5. Heat Transfer Correlations for Rigid Spheres

A number of heat transfer correlations are listed in Table B-1. The heat transfer correlations have been fitted to both heat and mass transfer data involving liquids as well as gases, many for restricted ranges of Reynolds number. Virtually all of the correlations are restricted to fluids with Prandtl number of order unity and higher. The Reynolds and Prandtl numbers in some of the correlations should be calculated using film or wall temperatures (for example Whitaker's[3] and Vliet's[8] correlations, should be explicitly corrected for the wall temperature). However, in SIMMER-III it is too costly and inconvenient to evaluate properties at the wall temperatures, and so bulk temperatures only are used to evaluate the correlations. The correlation by Torii and Yoshida[9] should be a function of turbulence intensity, but has been evaluated for zero intensity.

Most data for spheres have been obtained for heat and mass transfer to air. Mass transfer experiments measure, for example, the evaporation of droplets in an airstream. The results can be directly applied to heat transfer because of the equivalence of the Nusselt and Sherwood numbers, and in fact the spread of results obtained by either heat or mass transfer seems to be less than the spread of results between different authors. For example, Achenbach's data[10] was obtained by a combination of mass transfer at lower Reynolds number, and heat transfer at higher Re. A further point to note is that the physical properties of air are not as sensitive to temperature differences as water.

In Ref. 1) it is remarked that reliable data is limited because the influences of the support and guard heater were not appreciated in earlier experiments. Clift et al. compiled experimental results in which the turbulence intensity is believed to be less than 3% and effects such as natural convection and conduction through the support are either negligible or corrected for. Additional data by Achenbach[10] is not only compatible with this data, the results also extend the database beyond the critical transition. The correlation fits the data well up to the critical transition, with a maximum error of ~10%. These correlations have been used to calculate Nusselt numbers for heat transfer to air over a wide range of Reynolds number, despite the restrictions of the data on which they are based. Apart from Clift's correlation, the formulae recommended by Achenbach and Whitaker also fit the air data very well over the whole range of Reynolds number up to the critical transition. All three correlations have the dependency $\mathrm{Nu} \propto \mathrm{Re}^{1/2}$ at intermediate Reynolds number and $\mathrm{Nu} \propto \mathrm{Re}^{0.7}$ or $\mathrm{Nu} \propto \mathrm{Re}^{0.8}$ at higher Re. The simpler correlations of McAdams[11] and Torii[9] ($\mathrm{Nu} \propto \mathrm{Re}^{0.6}$) and Vliet[8] ($\mathrm{Nu} \propto \mathrm{Re}^{0.54}$) also fit the data quite well, although they underpredict the data at low Re.

Note that at very low Reynolds number ($\mathrm{Re} \to 1$) virtually none of the above correlations tends to the analytical formula predicted for creeping flow. It seems that a simple addition of steady-state conduction (for no flow) and laminar boundary theory (valid for Re greater than about 50) is sufficient to represent the

creeping flow regime. This is in agreement with Churchill's conclusions for combining forced and free convection[4]. At the critical transition the data shows a step change in Nu as a function of Re, and then resumes a steady increase with a steeper gradient. Thus, at very high Reynolds numbers, i.e. for supercritical flow, the above correlations underestimate heat transfer. Note that Whitaker's and Clift's correlations have a limiting dependency $\mathrm{Nu} \propto \mathrm{Re}^{0.7}$, but these correlations were constructed before Achenbach's more extensive data became available. Achenbach's data suggests a steeper limiting dependency of $\mathrm{Nu} \propto \mathrm{Re}^{0.8}$, which is in agreement with the measurements of local Nusselt number made by Hayward and Pei[2].

Lee and Ryley have measured the evaporation of single water droplets into both air and superheated steam for the Reynolds number range 64 to 250.[12] In the case of air the measured Nusselt numbers conformed to the correlation from Ranz.[13), 14)] For evaporation into steam, the measured Nusselt numbers are also compatible with air data, once allowance has been made for the higher Prandtl number of steam (Pr = 1).

Heat transfer from rigid spheres to water and oil has been analyzed by Vliet and Leppert.[8)] The authors note that the variation in physical properties of liquids is not insignificant and so plot, and correlate, their results using a Sieder and Tate correction factor[5)] of $(\mu/\mu_w)^{0.25}$. The high Re water data was obtained for both high and low temperature differences between the wall and the water, and without the Sieder and Tate correction factor the data divides into 2 distinct groups. The correlations fit the liquid data adequately, to within 20 to 30% better accuracy can be achieved using the Sieder and Tate correction factor, or by using the film temperature. Most of the above data has been obtained for heat transfer from isothermal spheres. Heat transfer correlations for uniformly heated spheres are about 10% higher than for isothermal spheres.[15)]

The most convenient correlation, which agrees well with the above data for both gases and liquids over a wide range of Reynolds number, is the one recommended by Whitaker.[3)] The equation needs to be adapted slightly for SIMMER-III by removing the dependence on wall properties:

$$\mathrm{Nu} = 2 + 0.4\mathrm{Re}^{1/2}\mathrm{Pr}^{0.4}(1 + 0.15\mathrm{Re}^{1/6}) , \qquad \text{(B-5)}$$

which correctly tends to the steady-state conduction value at low Reynolds number. At intermediate *Re* heat transfer through the laminar boundary layer dominates. At high Re the second term in the brackets on the RHS becomes significant, and the Nusselt number dependence becomes $\mathrm{Nu} \propto \mathrm{Re}^{2/3}$ as heat transfer in the wake region becomes dominant. Equation (B-5) is the formula which was used to calculate heat transfer from solid particles, droplets and bubbles in early versions of SIMMER-III.

Whitaker's correlation is suitable for gases and liquids with Prandtl number of order unity and higher, but is inappropriate for liquid metals. The only data which seems to be available for liquid metals are measurements made by Witte for heat transfer from a sphere propelled through liquid sodium.[16)] All of these formulae predict Nusselt numbers which are considerably higher than the experimental data, by a factor of 2 to 3. The situation for liquid metals is therefore extremely unsatisfactory. A correlation given by Ref. 16) is available for liquid sodium, but it is based on data for the very restrictive range of Reynolds number. Furthermore, there is no additional corroborative data, and no information at all for heat transfer to liquids with Prandtl numbers between 0.01 and 0.1, which is required for liquid steel. Therefore, it was decided to investigate heat transfer and correlations for cylinders in crossflow in the next section.

B.6. Prandtl Number-Dependence for a Cylinder in Crossflow

Fluid flow around, and heat transfer from, a circular cylinder in crossflow exhibits most of the characteristics described above for spheres. In fact, the fluid dynamics is so similar that Whitaker recommends that his correlation, derived for a sphere, can also be applied to a cylinder in crossflow. Heat transfer from cylinders seems to have been investigated more thoroughly than spheres; there is not only experimental data for gases and liquids with Pr ~ 1, but also from more than author for liquid sodium, and for liquid mercury. This range of data has enabled a Prandtl-number dependence of heat transfer to be proposed.

A comprehensive correlating equation for a cylinder in cross-flow has been proposed by Churchill and Bernstein.[17] The correlation is said to be valid for liquid metals. Heat transfer through the laminar boundary layer and in the wake region is treated separately. By analyzing laminar boundary layer heat transfer for forced convection to a flat plate, and free and forced convection to a cylinder, Churchill and Bernstein recommend the following dependence for Nusselt number:

$$\mathrm{Nu} \propto \frac{\mathrm{Re}^{1/2}\mathrm{Pr}^{1/3}}{\left[1+\left(\frac{0.4}{\mathrm{Pr}}\right)^{2/3}\right]^{1/4}}. \tag{B-6}$$

The constant "0.4" in Eq. (B-6) is said to be "quite uncertain". For the wake region Churchill and Bernstein use experimental data to argue a limiting dependence of $\mathrm{Nu} \propto \mathrm{Re}$, and they postulate that the Pr-dependence is the same as for the laminar-boundary layer regime. If the resulting correlations for the two regions are added linearly, and calibrated with experimental data, the following formula is obtained:

$$\mathrm{Nu} = 0.3 + \frac{0.62\mathrm{Re}^{1/2}\mathrm{Pr}^{1/3}}{\left[1+\left(\frac{0.4}{\mathrm{Pr}}\right)^{2/3}\right]^{1/4}}\left[1+\left(\frac{\mathrm{Re}}{281770}\right)^{1/2}\right]. \tag{B-7}$$

In fact, Churchill and Bernstein suggest that a better fit to data is obtained by adding the heat transfer correlations for the laminar boundary layer and wake regions non-linearly:

$$\mathrm{Nu} = 0.3 + \frac{0.62\,\mathrm{Re}^{1/2}\,\mathrm{Pr}^{1/3}}{\left[1+\left(\frac{0.4}{\mathrm{Pr}}\right)^{2/3}\right]^{1/4}}\left[1+\left(\frac{\mathrm{Re}}{282000}\right)^{5/8}\right]^{4/5}. \tag{B-8}$$

Churchill and Bernstein have calibrated and compared Eqs. (B-7) and (B-8) against a variety of (selected) experimental data, including heat transfer from cylinders to liquid mercury (Pr = 0.0225) and liquid sodium (Pr = 0.0058 and 0.0073). Either of Eq. (B-7) or (B-8) fits the selected data satisfactorily. However, note that the mercury data covers only extremely low values of Re, and the sodium data extends only up to $Re = 10^4$, which is in fact insufficient to test the Pr-dependence of heat transfer in the wake.

At intermediate Reynolds number, Eq. (B-7) translates into the following simple formulae for air and liquid sodium, respectively:

$$\mathrm{Nu} \cong 0.54\mathrm{Re}^{1/2}\mathrm{Pr}^{1/3}\left[1+\left(\frac{\mathrm{Re}}{281770}\right)^{1/2}\right] \text{ for air, and}$$

$$\mathrm{Nu} \cong 0.71\mathrm{Pe}^{1/2}\left[1+\left(\frac{\mathrm{Re}}{281770}\right)^{1/2}\right] \text{ for liquid sodium.} \quad \text{(B-9)}$$

With respect to air, Eq. (B-9) is very similar to Whitaker's correlation. In fact, it differs from Whitaker's correlation in only two respects: the proportion of heat transferred through the laminar boundary layer is higher at low Re, and as $\mathrm{Re} \to \infty$, $\mathrm{Nu} \propto \mathrm{Re}$. With respect to sodium, Eq. (B-9) seems to have the correct dependence on Peclet number if the wake heat transfer is ignored. Sodium data for cylinders has been obtained by Ishiguro et al.[18] and Andreevskii.[19] The data can be correlated by the equation:

$$\mathrm{Nu} = 0.3 + a\mathrm{Pe}^{1/2}, \quad \text{(B-10)}$$

where the constant a lies in the range 0.62 to 0.75. The data is about 30% beneath the potential flow theoretical solution. Equation (B-9) is in good agreement with Eq. (B-10) if one considers only heat transfer through the laminar boundary layer. However, the wake heat transfer is predicted to increase the Nusselt number noticeably at higher Reynolds number, with the result that the Nusselt numbers predicted by Eqs. (B-9) and (B-10) differ by about 40% at Re = 20,000.

When validating their correlation, Churchill and Bernstein seem to have ignored the local heat transfer data for a cylinder in a sodium crossflow. The sodium data obtained by both Andreevskii and Ishiguro are consistent in that heat transfer is highest at the front stagnation point and decreases monotonically to the rear stagnation point, even at relatively high Re. This is in direct contrast to the air data which is strongly influenced by the fluid flow behavior. The implication is that there is no increase in heat transfer in the wake region of a cylinder during liquid sodium flow for the highest Reynolds numbers measured.

It seems that Churchill and Bernstein's assumption that the Pr-dependence of heat transfer in the wake is the same as that for a laminar boundary layer is not correct. To be consistent with Andreevskii's and Ishiguro's data, Churchill and Bernstein's correlation must be adapted to ensure no (or low) wake heat transfer for low Prandtl number fluids.

It was noted above that for normal liquids (i.e. Pr > 0.7) heat transfer from both spheres and cylinders could be correlated using the same empirical correlations. Furthermore, both boundary layer theory and potential flow theory predict similar correlations with similar multiplicative constants. However, the sodium heat transfer data obtained for a sphere by Witte[16] is clearly far below the data obtained for a cylinder. Comparing Witte's correlation with Eq. (B-9) or (B-10), the sphere data is almost half that of the cylinder. Furthermore, Witte reports that "cooling rates at the front and back of the sphere are not greatly different", which is in complete contrast to Andreevskii and Ishiguro's data for cylinders, yet Witte recorded lower heat transfer rates. This casts some doubt on the reliability of the sodium heat transfer data for spheres.

B.7. Recommended Correlation for Spheres

To formulate a comprehensive correlation for forced convection heat transfer from spheres, the approach used by Churchill and Bernstein is adopted. The total Nusselt number is obtained by adding heat

transfer through the laminar boundary layer and wake regions. Heat transfer through the laminar boundary layer has the same form as Eq. (B-6). For the wake, it is assumed that the Nusselt number dependence as $\mathrm{Re} \to \infty$ is $\mathrm{Nu} \propto \mathrm{Re}^{5/6}$, which is consistent with both Hayward's data and Achenbach's data for subcritical flow. For high Pr fluids it is assumed that $\mathrm{Nu} \propto \mathrm{Re}^{5/6}\mathrm{Pr}^{1/3}$ as $\mathrm{Re} \to \infty$ (this is the same dependency as the correlations recommended by Churchill and Bernstein and Whitaker). However, for very low Pr fluids it is assumed that $\mathrm{Nu} \propto \mathrm{Pe}^{5/6}$ as $\mathrm{Re} \to \infty$. This ensures that the Nusselt number is dependent only on Peclet number for low Pr fluids, and helps to reduce heat transfer in the wake. The proposed correlation has the following form:

$$\mathrm{Nu} = 2 + \frac{a\mathrm{Re}^{1/2}\mathrm{Pr}^{1/3}}{\left[1+\left(\frac{0.4}{\mathrm{Pr}}\right)^{2/3}\right]^{1/4}} + \frac{b\mathrm{Re}^{5/6}\mathrm{Pr}^{1/3}}{\left[1+\left(\frac{0.4}{\mathrm{Pr}}\right)^{2/3}\right]^{3/4}}, \tag{B-11}$$

where *a* and *b* are constants which allow the correlation to be fitted to data. If Eq. (B-11) is fitted to air data, the following correlation is obtained:

$$\mathrm{Nu} = 2 + \frac{0.593\mathrm{Re}^{1/2}\mathrm{Pr}^{1/3}}{\left[1+\left(\frac{0.4}{\mathrm{Pr}}\right)^{2/3}\right]^{1/4}} \left\{1 + \left[\frac{\left(\frac{\mathrm{Re}}{244140}\right)^{2/3}}{1+\left(\frac{0.4}{\mathrm{Pr}}\right)^{2/3}}\right]^{1/2}\right\}. \tag{B-12}$$

Equation (B-12) is the proposed heat transfer correlation for spheres for all Prandtl numbers and Reynolds numbers up to the critical transition. It is also very similar to Churchill and Bernstein's correlation for a single cylinder in cross-flow, and so can also be used for this configuration. Equation (B-12) reduces to the following formulae for air and sodium:

$$\mathrm{Nu} \cong 0.542Re^{1/2}\mathrm{Pr}^{0.45}\left[1+\left(\frac{\mathrm{Re}}{296300}\right)^{1/3}\right] \text{ for air, and} \tag{B-13a}$$

$$\mathrm{Nu} \cong 0.68\mathrm{Pe}^{1/2} \text{ for liquid sodium, up to } \mathrm{Re} \approx 20000\,. \tag{B-13b}$$

Equations (B-13a) and (B-13b) are similar to Whitaker's correlation, based mainly on air and water, and the expression for sodium is consistent with the experimental data obtained for cylinders in cross-flow. However, the expression is about 80% higher than Witte's data for heat transfer to sodium. Equation (B-12) is compared with air, steam, water, oil and sodium data for spheres and reproduces the data well for all Reynolds numbers up to the critical transition, with the exception of Witte's sodium data (some of the water data is augmented by natural convection).

It is useful to see how a simpler expression of the form $\mathrm{Nu} = 2 + a\mathrm{Re}^{\mathrm{b}}\mathrm{Pr}^{\mathrm{c}}$ can be used in place of the more complicated correlation Eq. (B-12) for restricted ranges of Re and Pr. The values of the exponents for Re and Pr are calculated as follows:

$$b = \frac{\mathrm{Re}}{(\mathrm{Nu}-2)}\left(\frac{\partial \mathrm{Nu}}{\partial \mathrm{Re}}\right)_{\mathrm{Pr}} = \frac{1}{2}\left\{1+\frac{2}{3}\left[1+\frac{\left[1+\left(\frac{0.4}{\mathrm{Pr}}\right)^{2/3}\right]^{1/2}}{\left(\frac{\mathrm{Re}}{244140}\right)^{1/3}}\right]^{-1}\right\}, \text{and} \tag{B-14a}$$

$$\begin{aligned} c = \frac{\mathrm{Pr}}{(\mathrm{Nu}-2)}\left(\frac{\partial \mathrm{Nu}}{\partial \mathrm{Pr}}\right)_{\mathrm{Re}} \\ = \frac{1}{3}\left\{1+\frac{1}{2}\left[1+\left(\frac{\mathrm{Pr}}{0.4}\right)^{2/3}\right]^{-1}\right. \\ \left.+\left[1+\left(\frac{\mathrm{Pr}}{0.4}\right)^{2/3}\right]^{-1}\left[1+\frac{\left[1+\left(\frac{0.4}{\mathrm{Pr}}\right)^{2/3}\right]^{1/2}}{\left(\frac{\mathrm{Re}}{244140}\right)^{1/3}}\right]^{-1}\right\}. \end{aligned} \tag{B-14b}$$

The Re exponent varies from 0.5 for low Re (laminar) heat transfer to 0.8 at high Re (turbulent) heat transfer, as expected. The behavior of the Pr exponent will be used to recommend correlations for SIMMER-III.

In summary, the situation for predicting heat transfer from a single cylinder or sphere to a liquid metal is not entirely satisfactory due to a lack of reliable data and inconsistencies between data obtained by different workers. Consequently, the Prandtl number-dependence of heat transfer is particularly uncertain (the forced convection Nusselt number for liquid metals has an uncertainty of about 100%). Given the experimental data described above Eq. (B-12) is the best correlation which uses physical properties evaluated at the bulk temperature, and which can be applied to liquid metals.

B.8. Secondary Effects

The expressions derived above for heat transfer from a single sphere give the minimum heat transfer rate. Natural convection augments forced convection heat transfer at low relative velocities, and is described in Appendix D. Other factors which influence the heat transfer are listed below, and an attempt is made to quantify their effects.

(1) Variation in material properties

The effect of the variation of physical properties of the fluid between the surface of the sphere and bulk fluid is discussed in Ref. 17) with respect to cylinders. The authors conclude that the dependence of heat transfer on the variation of physical properties is undefined, and recommend using the film temperature to evaluate the properties. This is not an option for SIMMER-III, where physical properties are evaluated at the liquid bulk temperature. For spheres the water data described above indicates that the influence of the variation of physical properties is appreciable.

Heat transfer correlations evaluated at the free-stream temperature are often corrected by a term $(\mu_w/\mu_b)^n$ where n ~ 0.14 to 0.25. The viscosities of water, liquid steel and liquid sodium in particular can

potentially differ by an order of magnitude for a large temperature difference between the wall and the bulk fluid. This difference translates to a maximum enhancement of heat transfer by ~ 60%, which is not insignificant.

(2) Freestream turbulence and large single spheres

Experimental results for heat transfer from spheres are known to be sensitive to the presence of freestream turbulence, and experiments performed particularly since the late 1960s have taken care to ensure that the sphere support and tunnel blockage do not introduce excessive unwanted turbulence. The correlations for heat transfer from spheres discussed above were derived for low levels of turbulence intensity. It is therefore useful to try to quantify the influence of more realistic levels of turbulence.

The effect of turbulence depends to some extent on the scale of the turbulent fluctuations with respect to the particle size. For small particles, the turbulent fluctuations are larger than the particle, and the particles typically have a fluctuating motion which follows the turbulent fluid motion. Since the particles follow the fluid flow, it is most appropriate to treat them as if the particles and the fluid are in the same flow field (see below). For particles which are larger than the scale of turbulence, or which are fixed with respect to the fluid flow, the effect of the turbulence is to modify the flow field and local heat transfer around the particle. This subsection briefly reviews the data for how turbulence influences heat transfer from large particles.

Freestream turbulence is usually characterized by its relative intensity: $\mathrm{Tu} = V_{rms}/V$ where V_{rms} is the r.m.s. fluctuating velocity of the fluid and V is the mean velocity of the fluid relative to the particle. Turbulence seems to have two important effects. Firstly, the penetration of eddies in the laminar boundary layer results in a linear increase in Nusselt number with Tu.[2] Secondly turbulence precipitates the critical transition.[1] The Reynolds number at which the critical transition occurs, denoted Re_c is then a function of Tu. The dependence of Re_c on Tu according to Clift and Torii is clearly sensitive to the turbulence intensity but different workers differ as to how sensitive it is to Tu. For a sphere subjected to a constant mean flow velocity, a critical turbulence intensity Tu_c can be defined which also marks the transition to supercritical flow.

In subcritical flow heat transfer from the front portion of a sphere is increased only slightly; although larger increases are experienced over the rear portion. When the turbulence intensity is sufficiently high for the flow to be supercritical heat transfer from the front of the sphere increases more sharply and heat transfer in the wake becomes even more complex. If the effect of turbulence on heat transfer is to be modeled a distinction between sub- and super-critical flow needs to be made.

The augmentation of the total Nusselt number by turbulence has been estimated for relatively low levels of turbulence. Clift et al.[1] consider that a correlation can be established only for $\mathrm{Tu} \ll \mathrm{Tu}_c$; the Nusselt number can be considered to be a linear function of Tu up to Tu_c and the Nusselt number at the critical transition is given by:

$$\frac{\mathrm{Nu}_c}{\mathrm{Nu}_{nt}} = 1 + \left(\frac{\mathrm{Re}}{664330}\right)^{0.57}, \tag{B-15}$$

where Nu_{nt} is Nusselt number for zero turbulence intensity. The following dependence of Nusselt number on turbulence is recommended by Torii:

$$\mathrm{Nu} = 2 + (57.3 + 64.3\mathrm{Tu})\left(\frac{\mathrm{Re}}{8000}\right)^{m} \mathrm{Pr}^{n}\text{, where} \tag{B-16}$$

$m = 0.59 + 1.41Tu^{0.8}$, $n = 0.4 + 1.25\mathrm{Tu}$,

$1.6 \times 10^4 \leq \mathrm{Re} \leq 1.4 \times 10^5$, $0.7 \leq \mathrm{Pr} \leq 2.6$, and $\mathrm{Tu} \leq 0.08$.

The enhancement of Nusselt number predicted by Eqs. (B-15) and (B-16) for turbulence intensities in air is found to be up to 10%. The two recommendations are not consistent, but it seems that for low Reynolds number, up to about Re = 10,000, the influence of free-stream turbulence is small. Even for high Re, turbulence increases the Nusselt number by a maximum of ~ 30% before the critical transition.

Explicitly modeling the effect of freestream turbulence is difficult for two reasons. Firstly, quantitative data on the influence of turbulence is patchy (especially beyond the critical transition) and not entirely consistent. Secondly, the particles modeled by SIMMER-III are not fixed, which means they move to some extent with the fluid flow (depending on the inertia of the particles and the scale of turbulence). Moreover, the effect of free-stream turbulence in liquid metals is unlikely to be as important as air, due to the large molecular thermal conductivity of metals.

(3) Presence of wall

Wall effects are discussed in Ref. 1). The presence of a wall seems to have minimal effect on heat transfer unless the sphere diameter approaches the size of the hydraulic diameter (when the sphere diameter is half the hydraulic diameter the difference in velocities required to produce the same Nusselt number is 20%). Wall effects can therefore be ignored.

(4) Effect of more than one sphere in the flow field

SIMMER-III is typically applied to situations where there is more than one sphere or particle in the flow. The influence of other particles on overall drag is known to be important and is treated in the SIMMER-III momentum exchange formulation by using Ishii's drag similarity hypothesis. However, heat transfer from spheres does not respond the same way as drag to the flow behavior, so it needs to be treated separately.

An insight into how single and multi-particle systems differ is obtained by investigating heat transfer around a pair of equi-sized spheres in axi-symmetric flow. For low Reynolds number (creeping) flow there are mathematical models Aminzadeh et al. which predict the heat transfer behavior.[20] These show that for spheres less than about 4 sphere diameters apart, the overall Nusselt number for both spheres is less than that for a single sphere. This is because the proximity of the two spheres causes a region of stagnant fluid to accumulate between the spheres. The Nusselt numbers for both spheres also drop below the minimum value of two for an isolated sphere at low Re. Overall Nusselt numbers are depressed to at most two-thirds of the corresponding single-sphere value. Aminzadeh et al. note that experiments indicate this effect for Reynolds numbers up to about 50. In Ref. 21), similar effects occur in experiments performed up to Re = 1700.

At higher Reynolds number flow there is no adequate mathematical model, and it is necessary to rely on experimental results. Pei and Hayward[22] have made detailed measurements of the flow behavior and local heat transfer around a pair of spheres as a function of their separation at Re = 9000. There are three types of behavior depending on separation of the spheres:

- ***Spheres are far apart*** *(greater than about 3 sphere diameters)*. Heat transfer from the leading sphere is very similar to a single sphere, although the wake heat transfer is somewhat reduced. The flow around the trailing sphere is affected by the blockage of the main flow, resulting in shifting of the laminar separation point to the rear of the sphere. Although the heat transfer from the rear of the sphere is reduced, heat transfer close to the equator is increased and the overall Nusselt number is almost unaffected.
- ***Spheres are near*** *(between about 1.1 and 3 diameters)*. A single vortex is formed between the spheres, so that the external flow behaves as if the 2 spheres are a single body. The vortex enhances heat transfer in the wake region of the leading sphere, helped by a rapid exchange of fluid between the vortex and the external flow. Heat transfer from the trailing sphere is more complex: although the heat transfer at the very front is depressed, the laminar boundary separation point moves to the rear of the sphere which results in a net increase in heat transfer across the laminar boundary layer.
- ***Spheres are very close*** *(less than 1.12 diameters)*. A second vortex is formed inside the first vortex. ***Heat*** transfer in the wake of the leading sphere is very much enhanced. Heat transfer through the front of the trailing sphere is depressed, though the laminar separation is now about 120^{o}.

In summary, heat transfer from spheres greater than about two diameters apart can be treated independently with good accuracy. For closer spheres the overall heat transfer either decreases or increases, depending on the Reynolds number. The above results indicate that the overall heat transfer from two spheres can be estimated to within 50% for all separation distances by simply adding heat transfer from each sphere independently.

In equi-spaced multi-particle systems a separation distance of 2 diameters corresponds to a particle volume fraction of only 5 to 10%. Furthermore, clustering of particles occurs due to drag, which would introduce inhomogeneity in reality, if not in SIMMER-III. It is impossible to predict the overall heat transfer behavior of particle clusters from the behavior of single and pairs of particles, but the above result for a pair of spheres suggests that adding the heat transfer from each sphere independently is a reasonable first approximation.

B.9. Influence of Turbulent Flow on Small Particles

In SIMMER-III fuel and steel particles are, by default, in the same velocity field as liquid fuel, whilst control particles are in the same field as liquid steel and liquid sodium. For particles (or droplets) in the same velocity field as the continuous liquid, the average velocity difference between the particles and liquid is zero by definition. Furthermore, the velocity of a small particle rapidly assumes the liquid velocity, even if the particle and liquid are put in different velocity fields, resulting in a negligible velocity difference. In the absence of a velocity difference, and disregarding natural convection, conduction is the only remaining heat

transfer mechanism. In fact, conduction alone will underpredict heat transfer rates since turbulence induces an apparent relative velocity between the fluid and the particles, which augments the conduction heat transfer.

Heat and mass transfer from a small particle in a turbulent fluid is discussed by Lee (the effect of freestream turbulence on heat transfer from large, fixed particles is discussed above).[23] The particle diameters considered are in the range 100 to 500 microns. Lee assumes that heat transfer can be calculated using one of the steady-state forced convection heat transfer correlations, discussed above for a single sphere. The problem is: what is the equivalent convective velocity between the particle and the liquid? This requires a parameter to be chosen which characterizes the effect of turbulence in the liquid. The parameter recommended by Lee is the r.m.s. particle-fluid relative velocity. Lee notes that initial analyses underpredicted the measured heat transfer rates by as much as a factor of 2.5 because an incorrect slip velocity was estimated. Lee claims that a more accurate prediction of slip velocity results in better agreement with heat transfer from particles in stirred tanks.

Unfortunately the correct calculation of the r.m.s. fluid-particle relative velocity according to Lee, requires the solution of the unsteady equation of motion of the particle, which requires the Lagrangian energy spectrum of the fluid flow. This approach is not feasible in SIMMER-III. The easiest option for SIMMER-III is probably to use the r.m.s. velocity which is calculated by the IFA model. This is based on bubble buoyancy and shear stress at the wall (the contributions of other discontinuous components seem to be ignored). A further sophistication might be to use the r.m.s. velocity only if the turbulent eddies produced are similar in size to the particles and droplets from which heat transfer is being calculated. The velocity in the above correlations would then be the sum of the differential velocity (if there is one) and the r.m.s. velocity of the continuous fluid.

An alternative approach to including the effect of turbulence is used by the AFDM code.[24] In this approach a turbulent conductivity is calculated, and added to the molecular thermal conductivity. The turbulent conductivity is calculated using the Reynolds analogy, which connects the heat transfer exchange coefficient to the momentum exchange coefficient, and Prandtl's mixing length hypothesis. In fact, as is argued above, the heat transfer from spheres is not related to drag, because the resistance to flow is largely pressure drag rather than skin friction, which would seem to invalidate use of the Reynolds analogy. This method would therefore seem to be dubious.

B.10. Heat Transfer from Rigid Spheres in Other Codes

Heat transfer correlations used in other multi-component, multi-phase codes are listed in Table B-2. Most codes use one of the formulae compiled in Table B-1, particularly a correlation which is most appropriate to the code's main area of application. Note that although the heat transfer correlations are based on the formulae listed in Table B-2, they may be also modified to take account of other factors (e.g. in the CATHARE code[25] the Nusselt number is multiplied by a function to take account of mass transfer; in the IVA3 code[26] a time constant correction factor is applied).

It is not known in most cases which reference temperatures are used to evaluate the physical properties, but it would seem that the difference in physical properties between the interface and bulk fluid temperature is not corrected for. The influence of turbulence seems to be considered only in AFDM. A distinguishing

characteristic of SIMMER-III is that it must model heat transfer in low Prandtl number fluids such as liquid metals, which most of the above codes do not.

B.11. Recommendations for SIMMER-III

Heat transfer from particles and droplets to a continuous fluid are based on correlations derived for heat transfer from single rigid spheres. Although the most accurate correlation is given by Eq. (B-12), this expression is rather unwieldy if it is also desired that the code user has the flexibility to define his own expression. It is therefore recommended that the Nusselt number be calculated using an expression of the form:

$$\mathrm{Nu} = a + b\mathrm{Re}^{c}Pr^{d}\left(1 + e\mathrm{Re}^{f}\right), \tag{B-17}$$

where the constants a to f are user-input parameters for each fluid. Equation (B-17) can reproduce the full dependence of Nu on Re; the dependence on Pr is more restrictive, but since the value of Pr for a particular fluid is usually known to within an order of magnitude this is not so crucial. The recommended values of the parameters are obtained by reference to Eq. (B-12):

$$\mathrm{Nu} = 2 + 0.510\mathrm{Re}^{1/2}\mathrm{Pr}^{0.4}\left(1 + 0.015\mathrm{Re}^{1/3}\right) \text{ for water } (\mathrm{Pr} \cong 5), \tag{B-18a}$$

$$\mathrm{Nu} = 2 + 0.542\mathrm{Re}^{1/2}\mathrm{Pr}^{0.45}\left(1 + 0.012\mathrm{Re}^{1/3}\right) \text{ for gas, fuel } (\mathrm{Pr} \cong 0.7), \tag{B-18b}$$

$$\mathrm{Nu} = 2 + 0.646\mathrm{Re}^{1/2}\mathrm{Pr}^{0.5}\left(1 + 0.008\mathrm{Re}^{1/3}\right) \text{ for steel } (\mathrm{Pr} \cong 0.07), \text{ and} \tag{B-18c}$$

$$\mathrm{Nu} = 2 + 0.68\mathrm{Re}^{1/2}\mathrm{Pr}^{0.5} \text{ for sodium } (\mathrm{Pr} \cong 0.007). \tag{B-18d}$$

The above expressions are evaluated at the fluid bulk temperature because in SIMMER-III it is too inconvenient to evaluate interface temperatures simultaneously with Nusselt numbers.

It is not currently recommended to modify the heat transfer correlations explicitly for turbulence in the flow field, though this might be a future development. Currently the velocity used in the correlations is the average slip velocity, although in future it might be more accurate to sum the average slip velocity and the r.m.s. velocity:

$$V = \Delta\hat{V} + V_{rms}\,. \tag{B-19}$$

Also it is not currently recommended to modify the heat transfer correlations for multi-particle effects, although this would be required if SIMMER-III is to be applied to debris beds, for example.

References for Appendix B

1) Clift, R. et al., Bubbles, Drops, and Particles, Academic Press, 1978, 380p.

2) Hayward, G.L., Pei, D.C.T., Local heat transfer from a single sphere to a turbulent air stream, Int. J. Heat Mass Transfer, Vol. 21, No. 1, 1978, pp. 35–41.

3) Whitaker, S., Forced convection heat transfer correlations for flow in pipes, past flat plates, single cylinders, single spheres, and for flow in packed beds and tube bundles, AIChE J., Vol. 18, No. 2, 1972, pp. 361–371.

4) Churchill, S.W., A comprehensive correlating equation for laminar, assisting, forced and free convection, AIChE J., Vol. 23, No. 1, 1977, pp. 10–16.

5) Holman, J.P., Heat Transfer, McGraw-Hill, 1989, 752p.

6) Dwyer, O.E., Chapter 2 of "Sodium-NaK engineering handbook Vol II", edited by Foust, O.J., Gordon and Breach, 1976.

7) Hsu, C.-J., Heat transfer to liquid metals flowing past spheres and elliptical-rod bundles, Int. J. Heat Mass Transfer, Vol. 8, No. 2, 1965, pp. 303–315.

8) Vliet, G.C., Leppert, G., Forced Convection Heat Transfer From an Isothermal Sphere to Water, ASME J. Heat Transfer, Vol. 83, No. 2, 1961, pp. 163–170.

9) Torii, K., Yoshida, M., "Free stream turbulence effects on heat and mass transfer from spheres" of "Structure of turbulence in heat and mass transfer", p. 245, Hemisphere, 1982.

10) Achenbach, E., Heat transfer from spheres up to Re 6 x 10 to the 6th power, Proceedings of the 6th Int. Heat Transfer Conf., Washington, D.C., 1978, Vol. 5, pp. 341–346.

11) McAdams, W.H., Heat Transmission, McGraw-Hill, 1954.

12) Lee, K., Ryley, D.J., The Evaporation of Water Droplets in Superheated Steam, ASME J. Heat Transfer, Vol. 90, No. 4, 1968, pp. 445–451.

13) Ranz, W.E., Marshall, W.R., Evaporation from Drops Part I, Chem. Eng. Prog., Vol. 48, No. 3, 1952, pp. 141–146.

14) Ranz, W.E., Marshall, W.R., Evaporation from Drops Part II, Chem. Eng. Prog., Vol. 48, No. 3, 1952, pp. 173–180.

15) Brown, W.S., Pitts, C.C. et al., Forced Convection Heat Transfer From a Uniformly Heated Sphere, ASME J. Heat Mass Transfer, Vol. 84, No. 2, 1962, pp. 133–140.

16) Witte, L.C., An Experimental Study of Forced-Convection Heat Transfer From a Sphere to Liquid Sodium, ASME J. Heat Transfer, Vol. 90, No. 1, 1968, pp. 9–12.

17) Churchill S.W., Bernstein, M., A Correlating Equation for Forced Convection From Gases and Liquids to a Circular Cylinder in Crossflow, ASME J. Heat Transfer, Vol. 99, No. 2, 1977, pp. 300–306.

18) Ishiguro, R., et al., Heat transfer around a circular cylinder in liquid sodium crossflow, Int. Chem. Eng., Vol. 16, No. 2, 1976, p. 249–253.

19) Reed, C.B., Chapter 8 of "Handbook of single-phase convective heat transfer", edited by Kakic et al, John Wiley and Sons, 1987.

20) Aminzadeh, K., Taha, T.R. Al et al., Mass transport around two spheres at low Reynolds numbers, Int. J. Heat Mass Transfer, Vol. 17, No. 12, 1974, pp. 1425–1436.

21) Wang, B., Liu, T., Research on hydrodynamics and heat transfer for fluid flow around heating spheres in tandem, Int. J. Heat Mass Transfer, Vol. 35, No. 2, 1992, pp. 307–317.

22) Pei, D.C.T., Hayward, G., Local heat transfer rates from two adjacent spheres in turbulent axisymmetric flow, Proceedings of the 7th Int. Heat Transfer Conf., Munich, 1982, Vol. 3, pp. 201–206.

23) Lee, L.W., "Multi-phase flow and heat transfer III", Part B, Veziroglu and Bergles (editors), p. 605, Elsevier Science, 1984.

24) Berthier, J. et al., AFDM: An Advanced Fluid Dynamics Model, Volume III: AFDM Heat-Transfer and Momentum-Exchange Coefficients, LA-11692-MS, Vol. III, Los Alamos National Laboratory, 1990.

25) Bestion, D., The physical closure laws in the CATHARE code, Nucl. Eng. Des., Vol. 124, No. 3, 1990, pp. 229–245.

26) Kolev, N.I., IVA3 Code Manual Part 2, KfK 4949, 1991.

27) Frossling, N., Uber die Verdunstung fallender Tropfen, Beitr. Geophys. Gerlands, Vol. 52, 1938, pp. 170–216.

28) Garner, F.H., Suckling, R.D., Mass transfer from a soluble solid sphere, AIChE J., Vol. 4, No. 1, 1958, pp. 114–124.

29) Kramers, H., Heat transfer from spheres to flowing media, Physica, Vol. 12, Nos. 2–3, 1946, pp. 61–80.

30) Steinberger, R.L., Treybal, R.E., Mass transfer from a solid soluble sphere to a flowing liquid stream, AIChE J., Vol. 6, No. 2, 1960, pp. 227–232.

31) Davis, F.J. et al., IFCI 6.0 user's manual, NUREG/CR-6211, 1994.

32) Theofanous, T.G. et al., Steam Explosions, NUREG/CR-5960, 1994.

33) Birgersson, G. et al., SAS4A Manual, ANL/RAS 83-38, 1983.

34) Nigmatulin, R.I., Basics of the mechanics of the heterogeneous fluids, Nauka, 1978.

Nomenclature for Appendix B

c_p	Specific heat capacity of external fluid	
D	Diameter of a sphere	
h	Heat transfer coefficient (HTC)	$h = \frac{k}{D}\mathrm{Nu}$
k	Thermal conductivity of the external fluid	
Nu	Nusselt number:	
	Nu_0 is the Nusselt number for stagnant flow conditions	
	Nu_{nt} is a Nusselt number evaluated for no freestream turbulence	
	Nu_c is a Nusselt number evaluated at the critical transition.	
Pe	Peclet number	$\mathrm{Pe} = \mathrm{RePr} = \frac{\rho c_p V D}{k}$
Pr	Prandtl number	$\mathrm{Pr} = \frac{\mu c_p}{k}$
Re	Reynolds number	$\mathrm{Re} = \frac{\rho V D}{\mu}$
Tu	Turbulence intensity	$\mathrm{Tu} = \frac{V_{rms}}{V}$
V	Velocity of sphere relative to the external freestream velocity	
V_{rms}	Root mean square velocity of the fluid	

Greek symbols

μ	Viscosity of external fluid
ρ	Density of external fluid

Subscripts

c	Evaluated at the critical transition
local	A local heat or mass transfer variabl
nt	Zero (no) freestream turbulence conditions
rms	Root mean square velocity
w	Wall (interface) properties

Table B-1 Correlations for single rigid spheres (1/2).

References	Equation	Restrictions
[Theory]		
	$\mathrm{Nu} = 2$	$\mathrm{Re} = 0$ - steady-state conduction
Clift (1978)[1)]	$\mathrm{Nu} = 1 + (1 + \mathrm{Pe})^{1/3}$	$\mathrm{Re} \leq 0$ - creeping flow
Clift (1978) [1)]	$\mathrm{Nu} = 1 + (1 + \mathrm{Pe})^{1/3}\mathrm{Re}^{0.08}$	$1 \leq \mathrm{Re} \leq 400$ and $0.25 \leq \mathrm{Pr} \leq 100$
	$\mathrm{Nu} \propto \mathrm{Re}^{0.5}$ (laminar boundary layer)	$\mathrm{Re} > 400$ - high subcritical Re
	$\mathrm{Nu} \propto \mathrm{Re}^{0.8}$ (turbulent boundary layer)	
Hsu (1965) [7)]	$\mathrm{Nu} = 1.13\mathrm{Pe}^{1/2}$	$\mathrm{Re} < 200{,}000$ - high subcritical liuqid metals
[Empirical (both heat and mass transfer)]		
Achenbach (1978) [10)]	$\mathrm{Nu} = 2 + (0.25Re + 0.0003Re^{1.6})^{1/2}$	$100 < \mathrm{Re} < 3 \times 10^5$; air($\mathrm{Pr} = 0.71$)
Clift (1978)[1)]	$\mathrm{Nu} = 1 + 0.752\mathrm{Re}^{0.139}(1 + \mathrm{Pe})^{1/3}$	$100 < \mathrm{Re} < 2000$ and $\mathrm{Pr} \geq 0.7$
	$\mathrm{Nu} = 1 + (0.44\mathrm{Re}^{1/2} + 0.034\mathrm{Re}^{0.71})\mathrm{Pr}^{1/3}(1 + 1/\mathrm{Pe})^{1/3}$	$2000 < \mathrm{Re} \leq 1 \times 10^5$ and $\mathrm{Pr} \geq 0.7$
Frossling (1938) [27)]	$\mathrm{Nu} = 2 + 0.552\mathrm{Re}^{1/2}\mathrm{Pr}^{1/3}$	$2 < \mathrm{Re} \leq 1000$ and $\mathrm{Pr} \approx 1$
Garner (1958) [28)]	$\mathrm{Nu} = 2 + 0.95\mathrm{Re}^{1/2}\mathrm{Pr}^{1/3}$	$60 < \mathrm{Re} < 600$ and $\mathrm{Pr} > 1$
Kramers (1946) [29)]	$\mathrm{Nu} = (0.97 + 0.68\mathrm{Re}^{1/2})\mathrm{Pr}^{0.3}$	$1 < \mathrm{Re} < 2000$; water and oil
	$\mathrm{Nu} = 2 + 1.3\,\mathrm{Pr}^{0.15} + 0.66\mathrm{Re}^{1/2}\mathrm{Pr}^{0.31}$	$0.4 < \mathrm{Re} < 10^5$ and $0.7 < \mathrm{Pr} < 400$
Lee & Ryley (1968) [12)]	$\mathrm{Nu} = 2 + 0.74\mathrm{Pe}^{1/2}$	water droplets in steam

Table B-1 Correlations for single rigid spheres (2/2).

References	Equation	Restrictions
McAdams (1954) [11]	$\mathrm{Nu} = 2 + 0.3\mathrm{Pe}^{0.6}$	$17 < \mathrm{Re} < 70{,}000$; flowing gas
Ranz (1952) [13]	$\mathrm{Nu} = 2 + 0.6\mathrm{Re}^{1/2}\mathrm{Pr}^{1/3}$	$1 < \mathrm{Re} < 70{,}000$ and $\mathrm{Pr} \approx 1$
Steinberger (1960) [30]	$\mathrm{Nu} = 2 + 0.347\mathrm{Re}^{0.62}\mathrm{Pr}^{0.31}$	$\mathrm{Re} < 10^4$ and $0.7 < \mathrm{Pr} < 380$
Torii (1982) [9]	$\mathrm{Nu} = 2 + 0.285\mathrm{Re}^{0.59}\mathrm{Pr}^{0.4}$	$16{,}000 < \mathrm{Re} < 1.4 \times 10^5$ and $0.7 < \mathrm{Pr} < 2.6$
Vliet (1961) [8]	$\mathrm{Nu} = (1.2 + 0.53\mathrm{Re}^{0.54})\mathrm{Pr}^{0.3}\left(\frac{\mu}{\mu_w}\right)^{0.25}$	$16{,}000 < \mathrm{Re} < 1.4 \times 10^5$ and $0.7 < \mathrm{Pr} < 2.6$
Whitaker (1972) [3]	$\mathrm{Nu} = 2 + (0.4\mathrm{Re}^{1/2} + 0.06\mathrm{Re}^{2/3})\mathrm{Pr}^{0.4}\left(\frac{\mu}{\mu_w}\right)^{1/4}$	$3.5 < \mathrm{Re} < 80{,}000$ and $0.7 < \mathrm{Pr} < 380$
Witte (1968) [16]	$\mathrm{Nu} = 2 + 0.386\mathrm{Pe}^{1/2}$	$35{,}000 < \mathrm{Re} < 153{,}000$ and sodium ($\mathrm{Pr} \cong 0.005$)

Table B-2 Correlations for particles used in various codes.

Code	Equation	Note	Origin (see Table B-1)
AFDM[24]	$\mathrm{Nu} = 2 + 0.55\,\mathrm{Re}^{1/2}\,\mathrm{Pr}^{1/3}$ for Pr > 1		Frossling (1938)
	$\mathrm{Nu} = 2 + 0.95\,\mathrm{Re}^{1/2}\,\mathrm{Pr}^{1/3}$ for Pr > 1	Particles and non-circulating droplets to liquids, vapor	Garner (1958)
CATHARE[25]	$\mathrm{Nu} = 2 + 0.386\mathrm{Pe}^{1/2}$	Water droplets to superheated vapor	Frossling (1938)
IFCI 6.0[31]	$\mathrm{Nu} = 2 + 0.74\mathrm{Re}^{1/2}$	Droplets to vapor	Lee & Ryley (1968)
	$\mathrm{Nu} = 2 + 0.6\,\mathrm{Re}^{1/2}\,\mathrm{Pr}^{1/3}$	Vapor film to bulk coolant in the film boiling model	Ranz (1952)
IVA3[26]	$\mathrm{Nu} = 2 + 0.6\,\mathrm{Re}^{1/2}\,\mathrm{Pr}^{1/3}$	Droplets to vapor	Ranz (1952)
	$\mathrm{Nu} = 2 + \frac{0.65\mathrm{Pe}^{1.7}}{(1 + \mathrm{Pe}^{1.3})}$	Solid particles and bubbles to liquid	Nigmatulin (1978)[34]
	$\mathrm{Nu} = 2 + \frac{0.33\mathrm{Pe}^{0.84}}{(1 + 0.33\mathrm{Pe}^{0.51})}$	Solid particles to gas	Nigmatulin (1978)[34]
PM-ALPHA[32]	$\mathrm{Nu} = 2 + 0.6\,\mathrm{Re}^{1/2}\,\mathrm{Pr}^{1/3}$	Liquid droplets to gas and gas bubbles to liquid	Ranz (1952)
SAS4A (PLUTO2)[33]	$\mathrm{Nu} = 2 + 0.54\mathrm{Re}^{1/2}$	Fuel particles to vapor; assumes vapor Pr ~ 1	Ranz/Frossling

Appendix C: Forced Convection Heat Transfer from Fluid Particles

C.1. Introduction

This Appendix discusses the approach used to evaluate forced convection heat transfer between a fluid particle and an external fluid (liquid or gas). The internal and external heat transfers in rigid particles are described in Appendices A and B, and this Appendix concentrates on the modifications which should be made to the rigid heat transfer correlations to take account of the peculiar characteristics of fluid particles. The equivalence of heat and mass transfer is assumed, since most data is available for mass transfer, so the Nusselt number is freely interchanged with the Sherwood number. The review relies heavily on Clift et al.[1] and Sideman[2), 3)], but also on theoretical and experimental investigations of condensation of vapor on droplets.

Fluid particles, which may be droplets or bubbles, differ from rigid spheres in three respects:

- The differential velocity between the external fluid and the particle promotes internal circulation which enhances both internal and external heat transfer. Internal circulation also modifies the flow behavior around the particle.
- The fluid particle can deform.
- The fluid particle can oscillate, which both enhances the area available for heat transfer and promotes mixing and thus heat transfer inside the droplet.

The degree to which fluid particles differ from rigid particles is determined by the flow conditions (i.e. Reynolds number and particle size) and by physical properties of the two fluids. In particular the ratio of the fluids' viscosities strongly influences the extent to which internal circulation can occur. The viscosity ratio is defined as:

$$\kappa = \frac{\mu_{dp}}{\mu_{cp}}, \tag{C-1}$$

where $\kappa = 0$ corresponds to a highly circulating fluid particle, whilst $\kappa = \infty$ corresponds to a rigid particle. In general gas and vapor bubbles in a continuous liquid are liable to circulate freely, whilst liquid droplets in gas are less likely to circulate for the same particle size and external flow velocity. Liquid steel droplets in a molten fuel pool are also susceptible to circulation caused by the flow of molten fuel.

The other parameter which strongly influences the behavior of fluid particles is the system purity. The presence of surface-active contaminants has a major influence on particle internal circulation and oscillatory behavior. Unfortunately, the extent of contamination is almost always not known for problems to which SIMMER-III is applied, and even if it is there is no suitable way to use the information quantitatively. The effect of contamination must therefore be parameterized, and possible values of the parameters are obtained from simulant experiments. Realistically, since very small quantities of contaminants can eliminate internal circulation, the most valuable experimental data for the purpose of SIMMER-III applications is from contaminated systems.

In order to evaluate the heat transfer behavior of fluid particles, it is necessary to be aware of the conditions in which fluid particles are likely to circulate, deform and oscillate. This Appendix is therefore organized as follows. The conditions in which fluid particles deform and break-up are briefly summarized at first, since this gives an indication of the range of application of formulae derived for fluid spheres. Criteria for the onset of fluid particle oscillation and internal circulation are then proposed. Then internal heat transfer formulae for circulating and oscillating fluid particles are reviewed, followed by external heat transfer correlations. Finally, formulae are recommended for SIMMER-III.

C.2. Behavior of Fluid Particles

(1) Deformation and break-up of fluid particles

The simplest fluid particles to treat theoretically are spherical particles. However, since fluid particles are more likely to deform and break up with increasing Reynolds and Eotvos numbers, it is useful to be aware of the range over which fluid particles can exist and can legitimately be treated as spherical.

A shape regime for bubbles and drops in unhindered gravitational motion through liquids is discussed in Ref. 1). Using the Morton numbers and Eotvos numbers for a 1 mm bubble in some relevant liquids, bubbles can be regarded are spherical at very low Re (Re < 2) and for Eo < 0.3. The latter requirement is satisfied for bubbles of diameter 1 mm or less in relevant liquids. Larger bubbles are likely to assume an ellipsoid shape, with the extent of deformation sensitive to system contamination. The shape regime map is consistent with data for air bubbles rising in water.[1)] At the transition between spherical and ellipsoidal the Eotvos number is ~ 0.15 - 0.4, corresponding to a bubble diameter 1 - 2 mm, whilst the Reynolds number is ~ 200 - 500.

At high velocity differentials the fluid particle breaks up, and this limits the extent of deformation. Particle break-up is a time-dependent process, but it can nevertheless provide some rough limits on particle size. Even for stagnant media the maximum stable diameter for systems with $\kappa > 0.5$ (i.e. liquid drops in gases and fuel droplets in a steel pool) is said to be an Eotvos number of Eo = 16.[1)] This rules out the spherical cap shape regime for these systems. A Weber number break-up criterion is used in SIMMER-III. The Weber number, We, is defined as:

$$\mathrm{We} = \frac{\rho D V^2}{\sigma}. \tag{C-2}$$

Break-up is assumed to accelerate at a critical Weber number, We_c, which is currently set to $\mathrm{We}_c = 12$. Equation (C-2) can be rearranged in the form a critical Reynolds number for break-up:

$$\mathrm{Re}_c = \left(\frac{\mathrm{We}_c{}^2 \mathrm{Eo}}{\mathrm{M}}\right)^{1/4}. \tag{C-3}$$

It seems that fluid particles can survive at relatively high Re, up to Re ~ 10,000, in liquid sodium and liquid steel. However, in liquid fuel and in water the upper limit to Re is about 1000 - 3000. Thus external heat transfer correlations are required for a much more restrictive range of Re than for solid particles. Fluid particles can very reasonably be treated as spherical up to Eo ~ 0.3, and ellipsoidal for most of the remaining flow conditions of interest.

(2) Effect of deformation

Deformation on does not seem to influence heat transfer greatly.[1)] For example the experimental data from ellipsoidal drops which is discussed below, for both internal and external heat transfer, seems to be explicable using formulae derived for fluid spheres. Furthermore, the theoretical solution for heat transfer due to potential flow around highly deformed oblate spheroids does not differ greatly from heat transfer for an equivalent sphere.

It therefore seems reasonable to base heat transfer correlations on spheres since approximately spherical fluid particles exist over a wide range of conditions, and deformation does not greatly influence heat transfer. Internal circulation or oscillation of fluid particles has a more important effect on heat transfer.

(3) Onset and effect of oscillations

Ellipsoidal particles in pure systems start oscillating when Re exceeds a value of order 1000; in contaminated systems oscillations can apparently occur when Re > 200,[1),4)] although the amplitude of the oscillations is sensitive to the degree of contamination. For air bubbles rising in pure water oscillations apparently occur for Re ~ 450. Oscillations may also be induced in droplets produced in experiments by ejection from a needle or nozzle i.e. by the droplet formation process (e.g. see Refs. 5), 6)).

The effect of oscillations are to decrease the internal thermal resistance of the fluid particle, but the external resistance need not be affected if Re is sufficiently high. A thorough treatment of heat transfer from oscillating fluid particles requires the amplitude and frequency of oscillation.

(4) Onset and effect of internal circulation

In principle a fluid particle should exhibit internal circulation for any velocity difference between the particle and the continuous fluid. In practice internal circulation is usually absent from small bubbles and droplets, almost certainly due to the presence of surface-active contaminants at the interface of the two fluids.[1)] On the other hand, bubbles and droplets become deformed and start to oscillate with increasing size, and this promotes internal circulation even in contaminated systems. The most studied gas bubbles/liquid system is air bubbles in water. From the difference in terminal velocity of air bubbles between pure and contaminated water, internal circulation appears to have a measurable effect on bubble drag for Re ~ 40 and greater. Thus, internal circulation in a pure system occurs for Re = 40 or lower. It is suggested that even for contaminated systems internal circulation can be induced for Re ~ 50.

A theoretical treatment of heat transfer to moving circulating drops with Re = 100 is described in Ref. 7). The authors used their treatment to interpret experiments involving droplets with Re ~ 225.

(5) Proposal for simple treatment of heat transfer for fluid spheres

Internal and external heat transfer are treated independently, to be consistent with the heat transfer modeling philosophy in SIMMER-III. Nusselt numbers are based on quasi-steady state analytical solutions and empirical correlations, where available. The influence of particle deformation will be neglected. However Nusselt numbers are modified where required to take account of (a) internal circulation, and (b) oscillations. The criteria for the onset of internal circulation and oscillatory behavior are Reynolds numbers Re_{ic} and Re_{os},

respectively. These criteria will vary according to system purity, and perhaps according to personal judgement. Therefore three regimes are modeled:

- ***Rigid particle,*** $0 \leq \mathrm{Re} \leq \mathrm{Re}_{ic}$. No internal circulation; no oscillatory behavior. Internal and external Nusselt numbers calculated as for a rigid particle. A suggested value of Re_{ic} is $\mathrm{Re}_{ic} = 50$, though it seems legitimate for Re_{ic} to be any value between 10 and 200.
- ***Circulating particle***, $\mathrm{Re}_{ic} \leq \mathrm{Re} \leq \mathrm{Re}_{os}$. Internal circulation occurs, but the particle is not oscillating. Both internal and external Nusselt numbers are affected. A suggested value of Re_{os} is $\mathrm{Re}_{os} = 300$, although it seems legitimate for Re_{os} to have any value between 200 and 1000.
- ***Oscillating particle***, $\mathrm{Re}_{os} \leq \mathrm{Re}$. Internal circulation not only occurs, the particle is also oscillating. The internal Nusselt number is strongly affected because mixing reduces the thermal resistance.

In the literature describing direct contact heat transfer to droplets (e.g. Refs. 2), 8)), heat transfer in the droplet is often described in terms of three models: (a) droplet with maximum internal resistance/rigid drop, (b) internal resistance with partial mixing/drop with internal circulation, and (c) no internal resistance/completely mixed drop. It is assumed that these three models correspond to the three regimes described above.

C.3. Formulae for Internal Heat Transfer

Heat transfer in a rigid particle is described in Appendix A, so the following review concentrates on corrections required for circulating and oscillating fluid particles. The external resistance is ignored when formulating the internal Nusselt number (i.e. it is treated as negligible) and the external fluid is assumed to have constant temperature. A time-independent Nusselt number is required for SIMMER-III.

The formulae which are recommended in the literature are generally a function of a particle Peclet number Pe_{dp}^{*}: for low values of Pe_{dp}^{*} heat transfer in the particle is well-approximated by the rigid particle Nusselt number, whereas for high values of Pe_{dp}^{*} the effect of internal circulation and oscillation can be significant. Pe_{dp}^{*} is defined by:

$$\mathrm{Pe}_{dp}^{*} = \frac{\mathrm{Pe}_{dp}}{(1+\kappa)} \ , \text{ where } \mathrm{Pe}_{dp} = \frac{VD}{\alpha_{dp}} = \mathrm{RePr}_{cp}\frac{\alpha_{cp}}{\alpha_{dp}} = \mathrm{RePr}_{dp}\frac{v_{cp}}{v_{dp}}. \tag{C-4}$$

The equations in the literature for the fractional approach to thermal equilibrium, $F(t)$, are listed in Table C-1, including the rigid particle described in Appendix A.

(1) Rigid particle

Although heat transfer in a rigid particle ($\mathrm{Pe}_{dp}^{*} = 0$) is described in Appendix A, it is useful to reproduce here the transient conduction solution for a sphere at initially uniform temperature. The fractional approach to thermal equilibrium and the instantaneous Nusselt number are:

$$F(t) = 1 - \frac{6}{\pi^2}\sum_{n=1}^{\infty}\frac{1}{n^2}\exp\left(\frac{-n^2 t}{\tau}\right) \text{, and}$$

$$\mathrm{Nu}(t) = \frac{2\pi^2}{3}\sum_{n=1}^{\infty}\exp\left(\frac{-n^2 t}{\tau}\right)\Big/\sum_{n=1}^{\infty}\frac{1}{n^2}\exp\left(\frac{-n^2 t}{\tau}\right). \quad \text{(C-5)}$$

The expressions are clearly time-dependent, but SIMMER-III is constrained to use a time-independent Nusselt number to approximate heat transfer.

(2) Circulating particle

The Kronig-Brink analytical solution describes the transient heat transfer behavior of a freely circulating fluid particle at low Reynolds numbers.[1),2)] The solution is strictly applicable for fluid spheres in the creeping flow regime, i.e. $\mathrm{Re} \to 0$. However experimental data for fluid particles in the ellipsoidal regime indicates that the solution is applicable even up to Re = 3000.[1)] The main reason for discrepancies between the Kronig-Brink solution and experimental data is believed be the presence of surface-active agents in impure systems and oscillatory behavior at high Re.

For a freely circulating sphere with $\mathrm{Pe}_{dp}^{*} \to \infty$, heat transfer in the particle is partly transferred to the surface by internal circulation, although heat transfer across closed streamlines must occur by conduction. If the temperature contours are assumed to coincide with Hadamard-Rybczynski streamlines, transient heat transfer is described by the Kronig-Brink solution:[9)]

$$F(t) = 1 - \frac{3}{8}\sum_{n=1}^{\infty} A_n^2 \exp\left(\frac{-16\lambda_n t}{\pi^2 \tau}\right), \text{ and}$$

$$\mathrm{Nu}(t) = \frac{32}{3}\sum_{n=1}^{\infty} A_n^2 \lambda_n^2 \exp\left(\frac{-16\lambda_n t}{\pi^2 \tau}\right)\Big/\sum_{n=1}^{\infty} A_n^2 \exp\left(\frac{-16\lambda_n t}{\pi^2 \tau}\right), \quad \text{(C-6)}$$

where the constants A_n and λ_n are Kronig-Brink coefficients. The Kronig-Brink solution (Eq. (C-6)) is in fact well-approximated by the transient conduction solution (Eq. (C-5)) if the thermal diffusivity of the particle is multiplied by a factor 2.5. Furthermore, the asymptotic value of Nu in the Kronig-Brink solution is 17.66, which is a factor of 2.68 times the transient conduction asymptote. Thus internal circulation can enhance the rigid sphere Nusselt number by between a factor of 2 to 3. This is because the assumed circulation pattern in the droplet reduces the effective drop diameter by about half.

The Kronig-Brink solution predicts transient Nusselt numbers, which is awkward from the point of view of heat transfer modeling in SIMMER-III. The simplest way to modify the internal Nusselt number for a circulating particle is by:

$$\mathrm{Nu}_{ic} = \mathrm{Nu}_{rg} f\,, \quad \text{(C-7)}$$

where Nu_{rg} is the rigid particle Nusselt number, and *f* is a function to be determined, but varies from 1 to 2.68 with Pe_{dp}^{*}.

The transition from a rigid sphere to a freely circulating particle occurs around Pe_{dp}^{*} ~ 50 to 200. If the variation of the asymptotic value of *Nu* is used to obtain *f*, then the following correlation reproduces Nusselt number from the Kronig-Brink solution:

$$f = 1 + 0.842\left\{1 + \tanh\left[1.025 \ln\left(\frac{\mathrm{Pe}_{dp}^{*}}{60.9}\right)\right]\right\}, \tag{C-8}$$

where the value of Nu_{rg} should be taken as 6.58. However, Eq. (C-8) does not reproduce the variation in the fractional approach to equilibrium well. This is partly because the instantaneous Nu conforms to the rigid sphere Nu at short times before deviating toward the asymptotic value, and also because the average Nusselt number is a more useful quantity to estimate the time to equilibrium. (In fact the latter consideration implies that a value of 10 should be used in SIMMER-III for Nu_{rg} instead of 6.58 - see Appendix A.)

The SIMMER-III formulation, using a time-independent *Nu*, gives the following equation for the fractional approach to equilibrium:

$$F(t) = 1 - \exp\left(\frac{-3f\mathrm{Nu}_{rg}t}{2\pi^2\tau}\right). \tag{C-9}$$

This equation cannot be equated to Eq. (C-5), so the value of $\mathrm{Nu}_{rg} = 10$ was chosen to best estimate the timescale in which the particle achieves thermal equilibrium. The above formulation was quantified to examine how it fit the Kronig-Brink solution. The result was not satisfactory. However a correlation which is a simple variation of Eq. (C-8) produces better fitting:

$$f = 1 + 0.842\left\{1 + \tanh\left[1.025 \ln\left(\frac{\mathrm{Pe}_{dp}^{*}}{200}\right)\right]\right\}. \tag{C-10}$$

It is clear that the SIMMER-III formulation is a poor approximation to both the transient conduction and Kronig-Brink solutions because we are constrained to use a time-independent Nu. However, the timescale for the particle to achieve thermal equilibrium with the surrounding fluid is correct if we choose $\mathrm{Nu}_{rg} = 10$ and use Eq. (C-10) as the correlation for *f*. The error if no correction for internal circulation is made is that the timescale to equilibrium is overestimated by a factor of 2 to 3.

(3) Oscillating particle

Oscillations are assumed to be sufficiently violent to mix the contents of a fluid particle efficiently, which promotes a constant average internal thermal resistance. This process implies that the assumption of a constant internal Nusselt number is more valid and that the internal Nusselt number should be higher than that obtained from the Kronig-Brink solution. Experimental data seems to support this inference. The internal resistance for gas bubbles in liquids might also be expected to be more affected by oscillations than internal circulation.

The Handlos and Baron model[2] assumes that transfer within an oscillating droplet is entirely by turbulent motion (i.e. Re ~ 1000). Although heat transfer is expressed as a series solution, at long times only the first term is required and the internal Nu is given by:

$$\mathrm{Nu}_{os} = 0.00375\mathrm{Pe}_{dp}^{*}\,. \tag{C-11}$$

Apparently Handlos and Baron obtained experimental data in agreement with their prediction, but the model assumptions are criticized in Ref. 1).

It is convenient to treat the effect of oscillations on internal heat transfer as a multiplication factor which enhances the rigid sphere Nusselt number:

$$\mathrm{Nu}_{os} = \mathrm{Nu}_{rg} g \,, \tag{C-12}$$

where g is likely to be a function of Pe^*_{dp}. (This formulation is the same as used in Ref. 2).) In this format Eq. (C-11) can be rewritten as:

$$g = 1 + \frac{\mathrm{Pe}^*_{dp}}{2670}. \tag{C-13}$$

Celata et al.[6] have reviewed experiments and models concerned with the condensation of steam on water droplets, with emphasis on the Reynolds number range 150 to 2000. This corresponds mainly to the regime in which oscillating droplets are expected. They conclude that the only way to define the turbulent contribution inside an oscillating droplet is by an empirical factor. They recommended multiplying the particle diffusivity in the transient conduction equation (Eq. (C-5)) by a factor *C*:

$$C = 0.153\left(\mathrm{Pe}^*_{dp}\right)^{0.454}. \tag{C-14}$$

Note that Celata's procedure implies a transient Nusselt number, which is contrary to the idea that internal mixing caused by oscillations can be represented by a constant internal Nusselt number. Nevertheless, the reasoning behind Eq. (C-14) suggests that *C* can be replaced by *g*.

Equations (C-13) and (C-14) imply that oscillations have an important influence on internal Nusselt number for liquid droplets in gas at high Re. For $\mathrm{Pe}^*_{dp} \sim 10{,}000$, Eq. (C-13) implies an increase over the rigid particle Nusselt number of only 5, whereas Eq. (C-14) implies a factor of 10. On the other hand it is claimed in Ref. 3) that g should vary from 2.5 up to 70 for moderate and high Re. Hijikata et al.[5] have also estimated the internal Nusselt numbers for droplets of ethanol and R113 falling at their terminal velocity (Pe ~ 2000), and concluded that the rigid particle internal Nusselt numbers should be multiplied by up to a factor of 10. Equations (C-13) and (C-14) imply that oscillations have little effect on gas bubbles in liquids, whereas oscillations would be expected to reduce the internal heat transfer resistance in bubbles significantly. The equations are probably applicable to liquid droplets only.

In summary, it seems clear that heat transfer in oscillating droplets is enhanced significantly above the rigid drop values, but there does not seem to be a consistent, agreed treatment of oscillating droplets. Equation (C-14) appears to be the most reliable correlation, though the simplest way of treating the effect of oscillations is by assigning a constant value to g.

C.4. Formulae for External Heat Transfer

Heat transfer from a rigid particle is obtained using empirical correlations which are described in Appendix B. The review below concentrates on corrections for circulating and oscillating fluid particles. As for a rigid particle, the internal resistance is ignored and the particle is assumed to have constant temperature. A Nusselt number which is a function of instantaneous flow conditions is required for SIMMER-III.

(1) Rigid particles

Although Nusselt number correlations are discussed in more detail in Appendix B, it is useful to reproduce a correlation against which corrections for fluid particles may be compared. For fluids with Pr > 0.7 and Re < 2000, the following simple formula is applicable:

$$\mathrm{Nu} = 0.55\mathrm{Re}^{1/2}\mathrm{Pr}^{0/4} . \quad \text{(C-15)}$$

(2) Circulating particles

Numerical solutions are available for heat transfer from fluid spheres in creeping flow,[1)] but these are not very useful because they are only applicable to fluids with relatively high Prandtl numbers. No analytical solution seems to exist for heat transfer from fluid particles for Re > 1. For fluid spheres, an asymptotic theoretical solution for $\mathrm{Re} \to \infty$ can be derived using an assumption of a thin concentration boundary layer and potential flow surface velocity:

$$\mathrm{Nu} = \frac{2}{\sqrt{\pi}}\mathrm{Pe}^{1/2} = 1.13\mathrm{Pe}^{1/2} . \quad \text{(C-16)}$$

Equation (C-16) describes the Nusselt number in the case of $\kappa = 0$ (and no surface contamination). At intermediate *Re*, Eq. (C-16) is 2 to 3 times higher than the correlations for rigid spheres. A formula which takes account of the viscosity ratio, and so can be applied to both bubbles and droplets, was obtained by approximating to boundary layer calculations:

$$\mathrm{Nu} = \frac{2}{\sqrt{\pi}}\left[1 - \frac{(2.89 + 2.15\kappa^{0.64})}{\mathrm{Re}^{1/2}}\right]^{1/2} \mathrm{Pe}^{1/2} . \quad \text{(C-17)}$$

Equation (C-17) is valid for $\kappa < 2$ and $\mathrm{Re} > 70$ (and neglects the influence of surface-active agents). For $\kappa \geq 2$ and low Re the Nusselt number correlations for a rigid particle should be used (and in any case Eq. (C-17) should not be used to predict values of Nu lower than the rigid particle values). A more complex formula which covers the range $\mathrm{Re} < 70$ is also quoted by Clift et al.[1)] Equation (C-17) may well be applicable to liquid metals, since heat transfer correlations from rigid spheres to liquid metals is based on potential flow theory, but experimental data is unsurprisingly absent. Experimental justification for Eq. (C-17) was attempted.

Equation (C-17) seems to be the best compromise between range of applicability and simplicity. In fact, heat transfer from all liquid droplets in gases, and liquid fuel droplets in liquid steel, can be treated adequately using the rigid particle Nusselt number correlations. For bubbles in liquids, and liquid steel droplets in liquid fuel, the increased external heat transfer should be treated according to Eq. (C-17). For bubbles at moderate and high values of Re, Nu should approach the value predicted by potential flow, as is the case for bubbles in water.

(3) Oscillating fluid particles

For liquid drops in gases oscillations seem to have virtually no effect on heat transfer, although for drops and bubbles in liquids the influence can be significant.[1)] Unfortunately theoretical formulae require a

knowledge of the amplitude and frequency of the oscillations, so it does not seem feasible to explicitly treat heat transfer from oscillating fluid particles in SIMMER-III.

C.5. Treatment of Fluid Particles by Other Computer Codes

AFDM explicitly takes account of internal circulation in fluid particles. The internal Nusselt number is modified according to the expression derived by Handlos and Baron for oscillating particles (Eq. (C-11)), although it seems to have been applied even to Reynolds numbers as low as 50. The external Nusselt number is the one attributed to Griffith in Table C-2, which is similar to Eq. (C-17).

C.6. Recommendations for SIMMER-III

Reynolds number criteria for the onset of internal circulation and oscillation, Re_{ic} and Re_{os}, respectively should be user-input data items. For maximum flexibility they would be specified for each potential fluid/fluid combination, but this is too complex. It is reasonable to apply the same value of Re_{ic} and Re_{os}, say 50 and 300, respectively, to all fluid combinations.

For internal heat transfer, the internal Nusselt numbers of liquid droplets should be enhanced to take account of internal circulation, i.e. for $\mathrm{Re} > \mathrm{Re}_{ic}$. There is no practical advantage of enhancing the Nusselt numbers of bubbles. The enhancement should be done using Eq. (C-7), where *f* is defined by:

$$f = 1 + a\left\{1 + \tanh\left[b \ln\left(\frac{\mathrm{Pe}^{*}_{dp}}{c}\right)\right]\right\}, \tag{C-18}$$

where *a, b* and *c* are user-input constants. The recommended values of the constants are the same as in Eq. (C-10). When oscillations occur, i.e. for $\mathrm{Re} > \mathrm{Re}_{os}$, then a Nusselt number according to Eq. (C-12) should be calculated for both droplets and bubbles, where g is a user-input data item. There currently seems no justification for defining a function for g; a default value of g = 2.7 would correspond to the maximum effect of internal circulation. The maximum value from *f* or g should be used to calculate the Nusselt number in the oscillating particle regime.

For external heat transfer, the external Nusselt number should be enhanced to take account of internal circulation only for bubbles in liquids and liquid-liquid systems. Heat transfer from liquid droplets in gas can be treated satisfactorily using rigid particle correlations. The Nusselt number for internal circulation, i.e. for $\mathrm{Re} > \mathrm{Re}_{ic}$, is defined by:

$$\mathrm{Nu} = 2 + a\left[1 - \frac{(b + c\kappa^{d})}{\mathrm{Re}^{1/2}}\right]^{e} \mathrm{Pe}^{f}, \tag{C-19}$$

where *a*, *b*, *c*, *d*, *e* and *f* are input-data constants, and the constant "2" accounts for the minimum heat transfer to a stagnant fluid. Recommended values for the constants are shown in Eq. (C-17). The maximum value of Nu given by either Eq. (C-19) or the rigid particle correlation should be used as the final value of Nu. There currently seems no justification for modifying the external Nusselt number to take account of oscillations.

References for Appendix C

1) Clift, R. et al., Bubbles, Drops, and Particles, Academic Press, 1978, 380p.

2) Sideman, S., Shabtai, H., Direct contact heat transfer between a single drop and an immiscible liquid medium, Can. J. Chem. Eng., Vol. 42, No. 3, 1964, pp. 107–116.

3) Sideman, S., Direct contact heat transfer between immiscible liquids, Advances in Chemical Engineering, Vol. 6, 1966, pp. 207–286.

4) Celata, G.P., Direct contact condensation of steam on subcooled water, Energia Nucleare, Vol. 7, No. 2, 1990, pp. 17–42.

5) Hijikata, K., Mori, Y. et al., Direct contact condensation of vapor to falling cooled droplets, Int. J. Heat Mass Transfer, Vol. 27, No. 9, 1984, pp. 1631–1640.

6) Celata, G.P., Cumo, M. et al., Direct contact condensation of steam on droplets, Int. J. Multiphase Flow, Vol. 17, No. 2, 1991, pp. 191–211.

7) Huang, L.J., Ayyaswamy, P.S., Heat and mass transfer associated with a spray drop experiencing condensation, Int. J. Heat Mass Transfer, Vol. 30, No. 5, 1987, pp. 881–891.

8) Kulic, E., Rhodes, E., Direct contact condensation from air-stream mixtures on a single droplet, Can. J. Chem. Eng., Vol. 55, No. 2, 1977, pp. 131–137.

9) Kronig, R., Brink, J.C., On the theory of extraction from falling droplets, Appl. Sci. Res., Section A, Vol. 2, 1950, pp. 142–154.

10) Calderbank, P.H., Korchinski, I.J.O., Circulation in liquid drops: (A heat-transfer study), Chem. Eng. Sci., Vol. 6, No. 2, 1956, pp. 65–78.

11) Iguchi, M. et al., Bubble characteristics and heat transfer between bubble and liquid during cold gas injection, Proc. Int. Conf. Multiphase flows ’91-TSUKUBA, Vol. 2, 1991, pp. 387–390.

Nomenclature for Appendix C

A	Constant in Kronig-Brink solution (Eq. (C-5))	
D	Diameter of a sphere	
Eo	Eotvos number	
h	Heat transfer coefficient (HTC)	$h = \frac{k}{D}\mathrm{Nu}$
f	Factor to account for internal circulation (see Eq. (C-7))	
F	Fractional approach to equilibrium	
g	Factor to account for oscillations (see Eq. (C-12))	
M	Morton number	
Nu	Nusselt number (used to denote both internal and external *Nu*)	
	Nu_{rg} is a rigid particle Nusselt number	
	Nu_{ic} is a Nusselt number for internal circulation regime	
	Nu_{os} is a Nusselt number for oscillating regime	
Pe	Peclet number	$\mathrm{Pe} = \mathrm{RePr} = \frac{\rho c_p V D}{k}$
Pe_{dp}	Peclet number of the particle	$\mathrm{Pe}_{dp} = \frac{VD}{\alpha_{dp}}$
Pe^*_{dp}	See Eq. (C-4)	
Pr	Prandtl number	$\mathrm{Pr} = \frac{\mu c_p}{k}$
R	Radius of particle	
Re	Reynolds number (based on CP fluid properties)	$\mathrm{Re} = \frac{\rho V D}{\mu}$
V	Velocity of sphere relative to the external freestream velocity	
We	Weber number	

Greek symbols

α	Thermal diffusivity	
λ	Eigenvalue in Kronig-Brink solution (Eq. (C-5))	
τ	Thermal time constant of the particle	
κ	Viscosity ratio	$\kappa = \frac{\mu_{dp}}{\mu_{cp}}$
μ	Viscosity of external fluid	
ν	Kinematic viscosity	
ρ	Density of external fluid	

σ	Surface tension

Subscripts

c	Critical (Weber number)
cp	Continuous phase (external fluid)
dp	Dispersed phase (particle)
ic	Internal circulation
os	Oscillating particle
rg	Rigid particle

Table C-1 Internal heat transfer for fluid spheres.

Name	Equation for *F* (fractional approach to thermal equilibrium)	Restrictions
[Rigid]		
Conduction	$1-\frac{6}{\pi^2}\sum_{n=1}^{\infty}\frac{1}{n^2}\exp\left(\frac{-n^2t}{\tau}\right)$	Negligible external resistance
SIMMER-III	$1-\exp\left(\frac{-3\mathrm{Nu}t}{2\pi^2\tau}\right)$	$\mathrm{Nu}_{rig}=10$ is recommended
[Circulating]		
Kronig-Brink	$1-\frac{3}{8}\sum_{n=1}^{\infty}A_n^2\exp\left(\frac{-16\lambda_n t}{\pi^2\tau}\right)$	$\frac{\mathrm{Pe}_{dp}}{(1+\kappa)}\to\infty,\mathrm{Re}\to 0$
Calderbank[10]	$\left[1-\exp\left(\frac{-2.25t}{\tau}\right)\right]^{1/2}$	Empirical; $10<\mathrm{Re}\leq 200$ and $6\leq\mathrm{Pr}$
[Oscillating and circulating]		
Sideman	$1-\frac{6}{\pi^2}\sum_{n=1}^{\infty}\frac{1}{n^2}\exp\left(\frac{-Yn^2t}{\tau}\right)$	Empirical; *Y* is a parameter
Handlos	$1-\exp\left(\frac{-0.00562\mathrm{Pe}_{dp}t}{\pi^2(1+\kappa)\tau}\right)$	$\mathrm{Re}=1000$
Iguchi[11]	$1-\exp\left[\frac{-3.3t}{2\pi^2\tau}\left(\frac{\mathrm{Pe}_{cp}}{1+\kappa}\right)^{0.7}\right]$	$50<\frac{\mathrm{Pe}_{cp}}{(1+\kappa)}<800$

Table C-2 External heat transfer formulae for fluid spheres.

Name	Equation for Nu	Restrictions
Potential flow	$\mathrm{Nu} = \frac{2}{\sqrt{\pi}}\mathrm{Pe}^{1/2} = 1.13\mathrm{Pe}^{1/2}$	$\mathrm{Re} \to \infty$
Boundary layer	$u = \frac{2}{\sqrt{\pi}}\left[1 - \frac{2.89}{\mathrm{Re}^{1/2}}\right]^{1/2}\mathrm{Pe}^{1/2}$	$\mathrm{Re} > 70,\ \kappa < 2$
Clift (1)	$\mathrm{Nu} = \frac{2}{\sqrt{\pi}}\left[1 - \frac{(2.89 + 2.15\kappa^{0.64})}{\mathrm{Re}^{1/2}}\right]^{1/2}\mathrm{Pe}^{1/2}$	$\mathrm{Re} > 70,\ \kappa < 2$
Clift (2)	$\mathrm{Nu} = \frac{2}{\sqrt{\pi}}\left[1 - \frac{\left(\frac{2+3\kappa}{3(1+\kappa)}\right)}{\left\{1 + \left[\frac{(2+3\kappa)Re^{1/2}}{(1+\kappa)(8.67+6.45\kappa^{0.64}}\right]^{(4/3+3\kappa)}\right\}^{\frac{1}{(4/3+3\kappa)}}}\right]^{1/2}\mathrm{Pe}^{1/2}$	$\kappa < 2$
Elzinger	$\mathrm{Nu} = \sqrt{\frac{12}{\pi}}\mathrm{Pe}^{1/2} = 1.95\mathrm{Pe}^{1/2}$	Maximum possible Nu
Griffith	$\mathrm{Nu} = \frac{2}{\sqrt{\pi}}\left[1 - \frac{1.43}{\mathrm{Re}^{1/2}}\right]^{1/2}\mathrm{Pe}^{1/2}$	$\mathrm{Pe} >> 1,\ \kappa < 2,\ \mathrm{Re} < 1000$

NB: Add a constant factor 2 to the above correlations to correct for the minimum Nu for a sphere in a stagnant fluid.

Appendix D: External Heat Transfer from Spheres by Natural Convection

D.1. Introduction

This appendix summarizes the approach used to evaluate natural convection heat transfer between particles and a fluid (liquid or gas) in SIMMER-III. A fluid-side (external) Nusselt number is required in order to calculate heat transfer from particles and non-circulating droplets to continuous vapor or liquid when flow velocities are low. Since SIMMER-III is applied to various LMFR accident situations and experiments which involve stationary particles, a selection of heat transfer correlations is collated so that the code user can choose a correlation most appropriate to the conditions being modeled. The particles can be solid particles, liquid droplets or bubbles. Although particles, fluid particles in particular, do in reality assume shapes other than spheres, they are treated as spheres in SIMMER-III.

Natural convection is driven by a density difference between fluid at the surface of the sphere and the bulk external fluid. The buoyancy force can in nature originate by a temperature difference which induces thermal expansion, or by an accumulation or depletion of material at the surface arising from mass transfer. In SIMMER-III the concentrations of materials are currently not calculated at the interfaces, so the only mechanism modeled is thermal expansion-driven natural convection.

This appendix is subdivided as follows. The Grashof number and Rayleigh number ranges of application of SIMMER-III are first identified, and suitable correlations derived for rigid spheres are identified. Means of combining natural and forced convection are then briefly reviewed, as is the need to adapt the rigid particle correlations for fluid spheres. A non-iterative method for calculating natural convection Nusselt numbers in SIMMER-III is proposed, and the use of natural convection heat transfer in some other codes is briefly reviewed. Finally, formulae to calculate natural convection HTCs in SIMMER-III are recommended.

D.2. SIMMER-III Range of Application

In identifying suitable correlations for SIMMER-III there are two factors which must be taken into account. The first is that the correlation must be valid over the wide range of fluid Prandtl number to which the code will be applied: from a Prandtl number of about 7 (for water) to 0.005 (liquid sodium).

The second factor is the range of Grashof and Rayleigh numbers which the code will be used for, since at moderate values of Gr and Ra the boundary layer is laminar whereas at very high Ra the formation of a turbulent boundary layer must be treated. The Grashof number is:

$$\mathrm{Gr} = \frac{g\beta\Delta T_{ib} D^3}{\nu^2} = \mathrm{Gr}^* \Delta T_{ib} D^3 \,, \tag{D-1}$$

where Gr^* is a quantity which is a function only of physical properties, and which can be interpreted as the Grashof number for a temperature difference of 1000 K for a 10-cm diameter sphere. The Rayleigh number is:

$$\mathrm{Ra} = \mathrm{Gr}\,\mathrm{Pr} = \frac{g c_p \rho \beta \Delta T_{ib} D^3}{k\upsilon} = \mathrm{Ra}^* \Delta T_{ib} D^3 \,, \tag{D-2}$$

where Ra^* can similarly be interpreted as the Rayleigh number for a temperature difference of 1000 K for a 10-cm diameter sphere. Note that to evaluate Gr and Ra it is necessary to obtain the thermal expansion coefficient β. This can be obtained for liquids from the SIMMER-III EOS functions, and for an ideal gas it can be calculated from $\beta = \gamma_T$.[1] For practical purposes they have maximum values of $\mathrm{Gr}^* \sim 10^{11}$ and $\mathrm{Ra}^* \sim 10^{11}$, respectively, for all the materials with which we are concerned ($\mathrm{Ra}^* \sim 10^{10}$ for all materials except water). For the available experimental data the transition from the laminar to the turbulent regime is not achieved with spheres even up to $\mathrm{Ra}^* = 10^{10}$.[2]

Since the temperature difference in most SIMMER-III applications is less than 1000 K, and the particles much less than 10 cm, the quantities Gr^* and Ra^* can be regarded as maximum values of the Grashof and Rayleigh numbers, respectively. Thus for the purpose of SIMMER-III applications it is only necessary to consider heat transfer correlations for the laminar regime.

D.3. Theoretical Treatments for a Rigid Sphere

For a heated solid sphere the external flow is directed toward the surface over the bottom hemisphere and away from the surface over the top hemisphere. Over the lower hemisphere the buoyancy force is directed towards the surface and a laminar boundary layer forms. Over the upper hemisphere the buoyancy force is directed away from the surface and the flow is less stable. An axisymmetric plume forms at the top of the sphere which becomes turbulent at some distance from the sphere. As the Grashof number increases the position of the plume instability approaches the sphere until the flow over the rear hemisphere is disturbed at a sufficiently high Gr ("turbulent flow").[2]

The minimum Nusselt number is given by the steady-state conduction solution for a sphere surrounded by an infinite stagnant fluid:

$$\mathrm{Nu} = 2 \,. \tag{D-3}$$

There is no analytical solution for the limit $\mathrm{Gr} \to 0$ and so empirical correlations are required for this flow regime. However, for larger Gr the boundary layer approximations become appropriate, and an analytical solution is possible for the limit $\mathrm{Pr} \to \infty$:[2]

$$\mathrm{Nu} = 0.589 \mathrm{Ra}^{1/4} \,. \tag{D-4}$$

Equation (D-4) is said to represent the data well for high Pr and $\mathrm{Ra} > 10^5$. However, at high Ra the heat transfer at the top of the sphere is higher than predicted due to the instability of the flow. In the turbulent range the heat transfer relationship is expected to be $\mathrm{Nu} \propto \mathrm{Ra}^{1/3}$. However, the available experimental data for particles of various shapes conforms to the law $\mathrm{Nu} \propto \mathrm{Ra}^{1/4}$ even up to $\mathrm{Ra} = 10^{10}$.

Boundary layer theory can be used to make predictions about the Prandtl number dependence of Nusselt number. The Nusselt number is inversely proportional to the boundary layer thickness, and for a vertical plate is given by:[1]

$$\mathrm{Nu}_x \propto \frac{\mathrm{Gr}_x^{1/4}\mathrm{Pr}^{1/4}}{(1+0.952/\mathrm{Pr})^{1/4}}. \quad \text{(D-5)}$$

Although the analysis for a sphere yields different values for the constants, the Nusselt number for a sphere should also have the form $\mathrm{Nu} \propto \mathrm{Gr}^{1/4}\mathrm{Pr}^{1/4}$ for fluids with Pr >> 1, and $\mathrm{Nu} \propto \mathrm{Gr}^{1/4}\mathrm{Pr}^{1/2}$ for Pr << 1. A function describing the Pr-dependence of *Nu* for spheres has been deduced from boundary layer analysis by Churchill, [3] and Nu is described below.

D.4. Heat Transfer Correlations for Rigid Spheres

Although boundary layer solutions give theoretical solutions in the range $\mathrm{Ra} > 10^5$, it is necessary to use experimental data both to validate the correlations and to fill in the gaps (particularly for $\mathrm{Ra} < 10^4$ and at low Pr)

A number of theoretical and empirical heat transfer correlations are listed in Table D-1 (largely obtained from Ref. 4). The empirical correlations have been fitted to both heat and mass transfer data involving liquids as well as gases. Although some of the correlations are valid over a limited range of Rayleigh number, they collectively extend over the whole laminar flow range. Virtually all of the correlations are restricted to fluids with Prandtl number of order unity and higher. The Reynolds and Prandtl numbers in most of the correlations should be calculated using film or wall temperatures.

Virtually all of the correlations listed in Table D-1 have the form $\mathrm{Nu} \propto \mathrm{Gr}^{1/4}\mathrm{Pr}^{1/4}$. The main difference is in the constant of proportionality. The correlations of Clift et al.[2] and Churchill[3] are the only expressions to explicitly take account of the Pr-dependence of Nu, and to some extent they explain the discrepancy between the constants. For example, the correlation by Churchill reduces to the following equations for different values of Pr:

$$\mathrm{Nu} = 0.589\mathrm{Ra}^{1/4}, \quad \text{(D-6a)}$$

$$\mathrm{Nu} = 2 + 0.659\mathrm{Ra}^{1/4} \ \text{ as } \ \mathrm{Pr} \to \infty, \quad \text{(D-6b)}$$

$$\mathrm{Nu} = 2 + 0.605\mathrm{Ra}^{1/4} \ \text{ for } \ \mathrm{Pr} = 7 \ \text{(water)}, \quad \text{(D-6c)}$$

$$\mathrm{Nu} = 2 + 0.510\mathrm{Ra}^{1/4} \ \text{for } \ \mathrm{Pr} = 0.7 \ \text{(air)}, \text{and} \quad \text{(D-6d)}$$

$$\mathrm{Nu} = 2 + 0.805\mathrm{Ra}^{1/4}\mathrm{Pr}^{1/4} \ \text{ as } \ \mathrm{Pr} \to 0. \quad \text{(D-6e)}$$

Note that Eq. (D-6) predicts the correct form of the Prandtl number dependence for liquid metals.

The differences between the Nusselt numbers predicted by the correlations in Table D-1 can be deduced from the constants of proportionality "a" in the expression $\mathrm{Nu} = 2 + a\mathrm{Ra}^{1/4}$, except for the more complicated expressions of Churchill and Clift. Since the constants vary by over 20% for fluids with Pr between 0.7 and 10, it is desirable to use a formula which fully takes into account the fluid Prandtl number. This is particularly desirable for SIMMER-III since the code's application area includes heat transfer to liquid metals.

The correlations of Clift et al and Churchill differ in two respects. At high Ra, Churchill's expression is some 12% higher than Clift's, and Clift's expression tends to the boundary layer solution for $\mathrm{Pr} \to \infty$, whereas Churchill's expression is about 12% too high. Furthermore, at low values of Ra, Clift's expression is some 12 to 20% below that of Churchill. Clift's expression is in agreement with experimental data. However, Churchill's expression is easier to use. Thus a convenient correlation for natural convection heat transfer on rigid spheres is obtained by adjusting Churchill's expression to agree with Clift's expression at high Ra:

$$\mathrm{Nu} = 2 + \frac{0.589\mathrm{Ra}^{1/4}}{[1 + (0.45/\mathrm{Pr})^{9/16}]^{4/9}}. \tag{D-7}$$

Equation (D-7) agrees with the boundary layer solution for $\mathrm{Pr} \to \infty$, and with the expression of Clift at moderate and high Ra. Equation (D-7) differs from Clift's expression by at most 13% at very low Ra (Ra ~ 1), which is acceptable. Equation (D-7) gives the predicted Prandtl number dependence for liquid metals.

Note that the correlations shown in Table D-1 have been obtained for both heating the external fluid and melting from a cold sphere. It therefore seems reasonable for Eq. (D-7) to apply whether the external fluid is heated or cooled, and for evaporation and condensation where the mass transfer rates are low.

D.5. Combination of Natural and Forced Convection

Natural convection heat transfer dominates in stagnant flow conditions and at low Reynolds number, whereas forced convection dominates at high Reynolds number. The regime in which neither heat transfer mechanism is dominant is the mixed flow regime. It is necessary to propose a criterion for which forced convection becomes more important than natural convection, and how heat transfer should be treated in the mixed flow regime.

From the Boussinesq approximation applied to the Navier-Stokes equation, the relative effect of natural convection to forced convection is the quantity:

$$\eta_1 = \frac{\mathrm{Gr}}{\mathrm{Re}^2}. \tag{D-8}$$

Experimental data for heat transfer in combined convection to spheres suggests that natural convection dominates for $\eta_1 \geq 10$, whereas forced convection dominates for $\eta_1 \leq 0.1$.[2)] Mixed convection occurs in the range $0.1 < \eta_1 < 10$.

A second method of estimating the relative effects of natural and forced convection is to calculate the ratio of the respective Nusselt numbers. The natural convection Nusselt number, Nu_{nc}, is given by Eq. (D-7). If wake heat transfer is ignored a suitable forced convection Nusselt number is obtained from Appendix B.

$$\mathrm{Nu}_{nc} = 2 + \frac{0.593\mathrm{Re}^{1/2}\mathrm{Pr}^{1/3}}{[1 + (0.4/\mathrm{Pr})^{2/3}]^{1/4}}. \tag{D-9}$$

Thus by ignoring the conduction term in Eqs. (D-7) and (D-9) the relative effects of natural and forced convection are:

$$\eta_2 = \frac{\mathrm{Nu}_{nc}}{\mathrm{Nu}_{fc}} = \left(\frac{\mathrm{Gr}}{\mathrm{Re}^2}\right)^{\frac{1}{4}} g(\mathrm{Pr}) \text{ , where } g(\mathrm{Pr}) = \frac{\left[1 + (0.4/\mathrm{Pr})^{2/3}\right]^{1/4}}{\left[1 + (0.45/\mathrm{Pr})^{9/16}\right]^{4/9}\mathrm{Pr}^{1/12}}. \quad \text{(D-10)}$$

The transition between natural convection and forced convection predicted by comparison of the respective Nusselt numbers also occurs at $\eta_2 \sim 1$. Therefore, a criterion based on Nusselt number is consistent with the Navier-Stokes formulation.

The combination of the forced and natural convection Nusselt numbers in the mixed convection regime depends on whether the free stream velocity acts in the same direction as the buoyancy force ("aiding" or "assisted" flow), or opposes the buoyancy force ("opposing" flow), or else is perpendicular to the gravity vector ("crossflow"). Aiding flow and crossflow tends to enhance heat transfer whilst opposing flow reduces heat transfer. However, it seems that at high *Re* and *Ra* heat transfer in opposing flow is also enhanced by a complex turbulent flow over the rear of the particle.[2)]

Some quantification of how Nu_{nc} and Nu_{fc} might be combined in mixed flow is proposed by Yuge[5)] and Churchill.[3)] Yuge proposes a rather complex method and notes that although crossflow and aiding flow may be treated in the same way, opposing flow requires a different method. If simply the maximum of either Nu_{nc} or $\mathrm{Nu}_{fc}$is chosen, the maximum error in Nu is ~ 25% for crossflow and aiding flow. In opposing flow the error depends on the value of Re. Churchill correlated the combination of natural and forced convection for several bodies (mainly plates) in assisted flow by:

$$\mathrm{Nu}^n = \mathrm{Nu}_{nc}^n + \mathrm{Nu}_{fc}^n \text{ ,} \quad \text{(D-11)}$$

where $n = 3$ was found to be the best value of n. Therefore, if simply the maximum of eitherNu_{nc} or Nu_{fc} is chosen, the total Nusselt number Nu is underestimated by at most 21%.

It is not worthwhile to attempt to evaluate whether a particle is in assisted flow, crossflow or opposing flow in SIMMER-III, and then perform a complex combination of forced convection and natural convection Nusselt numbers. It seems adequate, to within an error of ~25%, to simply select the maximum of the two values Nu_{nc} and Nu_{fc}.

D.6. Fluid Spheres

Forced convection heat transfer correlations need to take account of internal circulation and oscillations of fluid particles. In particular, internal circulation was found to enhance the external heat transfer by between a factor of 2 to 3 for freely circulating fluid particles by thinning the external boundary layer. The question arises whether there are conditions in which natural convection heat transfer is also enhanced for fluid particles.

In Appendix C, it is noted that internal circulation does not occur for a high viscosity ratio between the fluid particle and the external fluid. Thus, internal circulation needs to be considered mainly for bubbles in liquids and liquid steel in liquid fuel. In the former case a velocity difference between the bubble and the liquid usually makes forced convection the dominant heat transfer mechanism, whereas in the latter case steel

vaporization and boiling is more of a concern. Thus it seems reasonable to treat fluid particles as rigid spheres when calculating natural convection heat transfer coefficients.

In the case of film boiling a particle is surrounded by a vapor film blanket, and heat transfer from the vapor-liquid interface to the bulk liquid often occurs by natural convection. In this case perhaps a non-zero vapor velocity in the film can reduce the thickness of the external boundary layer, and thus enhance heat transfer. In forced convection conditions the presence of surface-active contaminants was judged to inhibit internal circulation until a critical Reynolds number Re_c is achieved. The criteria for mixed flow conditions described above suggest a critical Grashof number for circulation analogous to the critical Reynolds number:

$$\frac{\mathrm{Gr}_c}{\mathrm{Re}_c^2} \sim 1 \,, \tag{D-12}$$

which implies a critical Grashof number of $\mathrm{Gr}_c \sim 3000$. This value is 00easily achieved for liquids. For film boiling it seems plausible that the natural convection heat transfer coefficient is enhanced, but there seems to be no clear experimental evidence and no theoretical treatments.

D.7. Combined Internal and External Heat Transfer in SIMMER-III

To calculate the natural convection Nusselt number it is necessary to know the particle surface temperature. Unfortunately this presents a problem in SIMMER-III because the surface temperature is in itself a function of the natural convection Nusselt number. Either an iterative method is necessary, or else an approximate method needs to be formulated, to estimate the surface temperature. This subsection shows how an approximate, non-iterative, method can be used to estimate the surface temperature with good accuracy.

The particle (dispersed phase) is treated as rigid, in which case the Nusselt number is a constant Nu_{dp} (see Appendix B). The heat transfer in the external fluid is subdivided into a steady-state conduction term Nu_{cd} and a natural convection heat transfer term Nu_{nc} which is a function of Grashof number and Prandtl number:

$$\mathrm{Nu}_{dp} = \text{constant, and} \tag{D-13a}$$

$$\mathrm{Nu}_{cp} = \mathrm{Nu}_{cd} + \mathrm{Nu}_{nc} \quad \text{where } \mathrm{Nu}_{cd} = \text{constant, and } \mathrm{Nu}_{nc} = a(GrPr^b)^c \,. \tag{D-13b}$$

Values for *a*, *b* and *c* are recommended at the end of Appendix D. The Grashof number in Eq. (D-13b) is a function of the interface temperature T_I:

$$Gr = \frac{g\beta(T_{cp})D^3}{\nu(T_{cp})^2}\left|T_I - T_{cp}\right| = Gr_m\left(\frac{T_I - T_{cp}}{T_{dp} - T_{cp}}\right), \tag{D-14}$$

where T_{cp} is the bulk temperature of the external fluid and T_I is between the particle and external fluid temperatures T_{dp} and T_{cp}. (In addition T_I is not allowed to exceed the continuous phase liquid saturation temperature, or fall beneath the melting point, at interfaces where non-equilibrium phase changes are allowed.) Gr_m is the Grashof number if the particle temperature is used as the surface temperature (i.e. the maximum Grashof number).

If there is no phase change (which is the general case) the interface temperature is obtained by equating heat fluxes in the particle and bulk fluid:

$$T_I = \frac{h_{dp}T_{dp} + h_{cp}(T_{cp})T_{cp}}{h_{dp} + h_{cp}(T_{cp})} = \frac{k_{dp}\mathrm{Nu}_{dp}T_{dp} + k_{cp}\mathrm{Nu}_{cp}T_{cp}}{k_{dp}\mathrm{Nu}_{dp} + k_{cp}\mathrm{Nu}_{cp}}. \tag{D-15}$$

Equation (D-15) can be rewritten in terms of fractional interface temperature:

$$\tau = \frac{T_I - T_{cp}}{T_{dp} - T_{cp}} = \frac{1}{1 + \frac{k_{cp}\mathrm{Nu}_{cp}}{k_{dp}\mathrm{Nu}_{dp}}} = \frac{1}{1 + \frac{k_{cp}\mathrm{Nu}_{cp}}{k_{dp}\mathrm{Nu}_{dp}} + \frac{k_{cp}a(\mathrm{Gr}_m\mathrm{Pr}^b)^c}{k_{dp}\mathrm{Nu}_{dp}}\tau^c}. \tag{D-16}$$

Equation (D-16) can be expressed even more succinctly:

$$\tau = \frac{1}{1 + A + B\tau^c}, \tag{D-17}$$

where A and B are constants which are easily identified from Eq. (D-16), and the constant c has a value $c \sim 0.25$. Equation (D-17) should be solved by iteration to find τ, but good estimate of τ can be obtained by considering the solutions of Eq. (D-17) as $B \to 0$ and $B \to \infty$:

$$\tau = \frac{1}{1 + A + B\tau^{1/(1+c)}}. \tag{D-18}$$

The natural convection Nusselt numbers calculated by iteration (Eq. (D-17)) and by approximation (Eq. (D-18)) are compared. The error in the approximation is negligible in all cases, and is in any case much less than the error in assuming constant material properties. Thus Eq. (D-18) is adequate for estimating the interface temperature, and hence for calculating the natural convection Nusselt number.

D.8. Secondary Effects

There are several secondary effects, some of which are discussed in Appendix B.

One important effect is the variation of physical properties between the particle surface and the bulk fluid. The Reynolds and Prandtl numbers in most of the correlations discussed above should be calculated using film or wall temperatures. However in SIMMER-III it is too costly to evaluate properties at the wall temperatures, and so bulk temperatures only are used to evaluate the correlations. Since Gr and Ra may vary by several orders of magnitude, this assumption can result in quite large errors in the calculated Nusselt number (~ factor of 2) in extreme conditions for some materials.

SIMMER-III is typically applied to transient conditions, whereas natural convection takes some time to become established. This time period is ignored. Furthermore it is assumed that natural convection around a particle takes place within a SIMMER-III mesh-cell, and no allowance is made for the presence of other particles.

D.9. Heat Transfer from Rigid Spheres in Other Codes

Heat transfer correlations used in codes which perform some similar functions as SIMMER-III are listed in Table D-1. The correlations used by the codes are based on one or more of the many empirical formulae also listed in Table D-1. In most cases a natural convection heat transfer coefficient is calculated only for use in a film boiling model, though in the CATHARE code[6] it is also used to calculate a minimum heat transfer from water droplets.

A distinguishing characteristic of SIMMER-III is that it models heat transfer in low Prandtl number fluids such as liquid metals, which most codes do not. No code seems to explicitly model enhanced natural convection heat transfer coefficients due to a circulating fluid particle.

D.10. Recommendations for SIMMER-III

Heat transfer from particles and droplets to a continuous fluid are based on correlations derived for heat transfer from single rigid spheres. Although a sufficiently accurate correlation is given by Eq. (D-7), this expression is rather unwieldy. It is therefore recommended that the Nusselt number in SIMMER-III be calculated using a simplified expression of the form:

$$\mathrm{Nu} = 2 + a(\mathrm{GrPr}^{\mathrm{b}})^{1/4}\,, \tag{D-19}$$

where the constants a and b are Pr-dependent, and so need to be user-input parameters for each fluid. The constants can be calculated from Eq. (D-7) using the following method:

$$b(\mathrm{Pr}) = \frac{4\mathrm{Pr}}{(\mathrm{Nu}-2)}\frac{\partial \mathrm{Nu}}{\partial \mathrm{Pr}} = 1 + \frac{1}{[1+(\mathrm{Pr}/0.45)^{9/16}]}\,, \text{and} \tag{D-20a}$$

$$a(\mathrm{Pr}) = \frac{0.589}{\mathrm{Pr}^{(b-1)/4}[1+(\mathrm{Pr}/0.45)^{9/16}]^{4/9}}\,. \tag{D-20b}$$

The recommended heat transfer correlations for some relevant materials are:

$$\mathrm{Nu} = 2 + 0.5(\mathrm{GrPr}^{1.18})^{1/4} \text{ for water } (\mathrm{Pr} \cong 0.7)\,, \tag{D-21a}$$

$$\mathrm{Nu} = 2 + 0.474(\mathrm{GrPr}^{1.44})^{1/4} \text{ for gas, fuel } (\mathrm{Pr} \cong 0.7)\,, \tag{D-21b}$$

$$\mathrm{Nu} = 2 + 0.53(\mathrm{GrPr}^{1.74})^{1/4} \text{ for steel } (\mathrm{Pr} \cong 0.07)\,, \text{and} \tag{D-21c}$$

$$\mathrm{Nu} = 2 + 0.62(\mathrm{GrPr}^{1.91})^{1/4} \text{ for sodium } (\mathrm{Pr} \cong 0.007)\,. \tag{D-21d}$$

The thermal expansion coefficient β can be obtained for liquids from the SIMMER-III TPP functions, and for an ideal gas it can be calculated from $\beta = \gamma_T$. The surface temperature used to calculate the Grashof number where there is no phase change should be calculated according to Eq. (D-18), to avoid the need for iteration.

References for Appendix D

1) Holman, J.P., Heat Transfer, McGraw-Hill, 1989, 752p.

2) Clift, R. et al., Bubbles, Drops, and Particles, Academic Press, 1978, 380p.

3) Churchill, S.W., A comprehensive correlating equation for laminar, assisting, forced and free convection, AIChE J., Vol. 23, No. 1, 1977, pp. 10–16.

4) Amoto, W.S., Tien, C.L., Free convection heat transfer from isothermal spheres in water, Int. J. Heat Mass Transfer, Vol. 15, No. 2, 1972, pp. 327–339.

5) Yuge, T., Experiments on Heat Transfer From Spheres Including Combined Natural and Forced Convection, ASME J. Heat Transfer, Vol. 82, No. 3, 1960, pp. 214–220.

6) Bestion, D., The physical closure laws in the CATHARE code, Nucl. Eng. Des., Vol. 124, No. 3, 1990, pp. 229–245.

7) Acrivos, A., A theoretical analysis of laminar natural convection heat transfer to non-Newtonian fluids, AIChE J., Vol. 6, No. 4, 1960, pp. 584–590.

8) Merk, H.J., Prins, J.A., Thermal convection in laminary boundary layers, Appl. Sci. Res., Section A, Vol. 4, 1953–1954, pp. 11–24, pp. 195–206, pp. 207–222.

9) Boberg, J.E., Starrett, P.S., Determination of free convection heat transfer properties of fluids, Ind. Eng. Chem., Vol. 50, No. 5, 1958, pp. 807–810.

10) Garner, F.H., Keey, R.B., Mass-transfer from single solid spheres—I: Transfer at low Reynolds numbers, Chem. Eng. Sci., Vol. 9, Nos. 2–3, 1958, pp. 119–129.

11) Garner, F.H., Hoffman, J.M., Mass transfer from single solid spheres by free convection, AIChE J., Vol. 7, No. 1, 1961, pp. 148–152.

12) Jakob, M., Linke, W., Der Wärmeübergang von einer waagerechten Platte an siedendes Wasser, Forsch. Geb. Ing., Vol. 4, 1933, pp. 75–81.

13) Kyte, J.R. et al., Natural convection heat transfer at reduced pressure, Chem. Eng. Prog., Vol. 49, No. 12, 1953, pp. 653–662.

14) Ranz, W.E., Marshall, W.R., Evaporation from drops, Chem. Eng. Prog., Vol. 48, No. 3, 1952, pp. 141–146, pp. 173–180.

15) Schenkels, F., Schenk, J., Dissolution of solid spheres by isothermal free convection, Chem. Eng. Sci., Vol. 24, No. 3, 1969, pp. 585–593.

16) Schenk, J., Schenkels, F., Thermal free convection from an ice sphere in water, Appl. Sci. Res., Section A, Vol. 19, 1968, pp. 465–476.

17) Schulz, G., Natural convection mass-transfer measurements on spheres and horizontal cylinders by an electrochemical method, Int. J. Heat Mass Transfer, Vol. 6, No. 10, 1963, pp. 873–879.

18) J. Van der Burgh, Thermal convection at a melting benzene surface, Appl. Sci. Res., Section A, Vol. 9, 1960, pp. 293–296.

19) C. R. Vanier, Tien, Chi, Free convection melting of ice spheres, AIChE J., Vol. 16, No. 1, 1970, pp. 76–82.

20) Farahat, M., Eggen, D.T., Pool Boiling in Subcooled Sodium at Atmospheric Pressure, Nucl. Sci. Eng., Vol. 53, No. 2, 1974, pp. 240–254.

21) Berthier, J. et al., AFDM: An Advanced Fluid Dynamics Model, Volume III: AFDM Heat-Transfer and Momentum-Exchange Coefficients, LA-11692-MS, Vol. III, Los Alamos National Laboratory, 1990.

22) Davis, F.J. et al., IFCI 6.0 user's manual, NUREG/CR-6211, 1994.

23) Kolev, N.I., IVA3 Code Manual Part 2, KfK 4949, 1991.

24) Kolev, N.I., IVA4 computer code: the model for film boiling on a sphere in subcooled, saturated and superheated water, Proc. 2nd Int. Conf. Multiphase Flow ’95-KYOTO, 1995, P2-11.

Nomenclature for Appendix D

c_p	Specific heat capacity of external fluid	
D	Diameter of a sphere	
g	Gravitational acceleration	
Gr	Grashof number	$\mathrm{Gr} = \frac{g\beta\Delta T_{ib} D^3}{\nu^2} = \mathrm{Gr}^* \Delta T_{ib} D^3$
	Gr^* is Grashof number for unit temperature difference and unit diameter sphere	
h	Heat transfer coefficient (HTC)	$h = \frac{k}{D}\mathrm{Nu}$
k	Thermal conductivity of the external fluid	
Nu	Nusselt number:	
	Nu_{dp} is the Nusselt number for the particle	
	Nu_{cp} is a Nusselt number for the external fluid	
	Nu_{cd} is a conduction Nusselt number in the external fluid	
Pr	Prandtl number	$\mathrm{Pr} = \frac{\mu c_p}{k}$
Ra	Rayleigh number	$\mathrm{Ra} = \mathrm{Gr}\,\mathrm{Pr} = \frac{g c_p \rho \beta \Delta T_{ib} D^3}{k\nu}$
	Ra^* is Rayleigh number for unit temperature difference and unit diameter sphere	
Re	Reynolds number	$\mathrm{Re} = \frac{\rho V D}{\mu}$
T	Temperature:	
	ΔT_{ib} is temperature difference between particle surface and bulk external fluid	

Greek symbols

β	Thermal expansion coefficient	
μ	Dynamic viscosity of external fluid	
ρ	Density of external fluid	
ν	Kinematic viscosity of external fluid	
τ	Fractional interface temperature (see Eq. (D-16))	
η	Ratio of natural to forced convection	$\eta = \frac{\mathrm{Gr}}{\mathrm{Re}^2}$

Subscripts

cp	Continuous phase (external fluid)
dp	Dispersed phase (particle)

nc	Natural convection
fc	Forced convection
c	Denotes onset of internal circulation given by Re or Gr
I	Interface
x	Distance (along a plate)

Table D-1 Correlations for single rigid spheres (1/2).

References	Equation	Restrictions/origin
[Theory]		
	$\mathrm{Nu} = 2$	$\mathrm{Gr} = 0$ - steady-state conduction
Acrivos (1960) [7]	$\mathrm{Nu} = 0.589\mathrm{Ra}^{1/4}$	$\mathrm{Pr} \rightarrow \infty$
Merk (1954) [8]	$\mathrm{Nu} = 0.558\mathrm{Ra}^{1/4}$	$\mathrm{Pr} \rightarrow \infty$
[Empirical (both heat and mass transfer)]		
Amoto (1972) [4]	$\mathrm{Nu} = 2 + 0.50\mathrm{Ra}^{1/4}$	water; $3 \times 10^5 < \mathrm{Ra} < 8 \times 10^8$
Boberg (1958) [9]	$\mathrm{Nu} = 0.51\mathrm{Ra}^{1/4}$	Heat transfer
Churchill (1977) [3]	$\mathrm{Nu} = 2 + \frac{0.659\mathrm{Ra}^{1/4}}{[1 + (0.45/\mathrm{Pr})^{9/16}]^{4/9}}$	$\mathrm{Ra} < 10^9$
Clift (1978) [2]	$\mathrm{Nu} = 1.7 + 0.3\left\{1 + \frac{14.6\mathrm{Ra}}{[1 + (0.5/\mathrm{Pr})^{9/16}]^{16/9}}\right\}^{1/4}$	$1 < \mathrm{Ra} < 10^{10}$
Garner (1958) [10]	$\mathrm{Nu} = 23 + 0.585\mathrm{Ra}^{1/4}$	Mass transfer
Garner (1961) [11]	$\mathrm{Nu} = 5.4 + 0.44\mathrm{Ra}^{1/4}$	Mass transfer
Jakob (1933) [12]	$\mathrm{Nu} = 0.555\mathrm{Ra}^{1/4}$	Heat transfer for various body shapes
Kyte (1953) [13]	$\mathrm{Nu} = 2 + 0.399\mathrm{Ra}^{1/4}$	Heat transfer to air
Ranz (1952) [14]	$\mathrm{Nu} = 2 + 0.60\mathrm{Gr}^{1/4}\mathrm{Pr}^{1/3}$	Droplet evaporation, $\mathrm{Gr}^{1/4}\mathrm{Pr}^{1/3} < 200$
Schenkels (1969) [15]	$\mathrm{Nu} = 2 + 0.59\mathrm{Ra}^{1/4}$	Melting – organic shperes

Table D-1 Correlations for single rigid spheres (2/2).

References	Equation	Restrictions/origin
Schenk (1968) [16]	$\mathrm{Nu} = 2 + 0.56\mathrm{Ra}^{1/4}$	Melting – ice sheres
Schutz (1963) [17]	$\mathrm{Nu} = 2 + 0.59\mathrm{Ra}^{1/4}$	Mass transfer
Van der Burgh (1960) [18]	$\mathrm{Nu} = 0.525\mathrm{Ra}^{1/4}$	Melting - benzene
Vanier (1970) [19]	$\mathrm{Nu} = 2 + 0.52\mathrm{Ra}^{1/4}$	Melting – ice sheres
Yuge (1960) [5]	$\mathrm{Nu} = 2 + 0.43\mathrm{Ra}^{1/4}$	air; $1 < \mathrm{Ra} < 10^5$
[Computer codes and film boiling analysis]		
Farahat (1974) [20]	$\mathrm{Nu} = 0.75\mathrm{Ra}^{1/4}\mathrm{Pr}^{1/4}$	Liquid metal ($\mathrm{Pr} \ll 1$)
AFDM[21]	$\mathrm{Nu} = 0.586\mathrm{Ra}^{1/4}$ for $\mathrm{Pr} > 1/2$	In film boiling model
	$\mathrm{Nu} = 0.586\mathrm{Ra}^{1/4}\mathrm{Pr}^{1/4}$ for $\mathrm{Pr} < 7/15$	
CATHARE[6]	$\mathrm{Nu} = 0.401\mathrm{Ra}^{1/4}$	Water droplets to superheated vapor
	$\mathrm{Nu} = 0.12\mathrm{Ra}^{1/3}$	
IFCI 6.0[22]	$\mathrm{Nu} = 2 + 0.60\mathrm{Gr}^{1/4}\mathrm{Pr}^{1/3}$	In film boiling model
IVA3[23]	$\mathrm{Nu} = 0.9\mathrm{Ra}^{1/4}$	In film boiling model
IVA4[24]	$\mathrm{Nu} = 3.71 + 0.402\mathrm{Ra}^{1/4}$	In film boiling model

Appendix E: Heat Transfer to Structure

E.1. Introduction

This Appendix describes the heat transfer correlations used in SIMMER-III for heat transfer from liquid, solid particles and gas to structure. The structure modeled by SIMMER-III calculations could conceivably represent a pipe (e.g. a control rod guide-tube), a bundle of tubes (i.e. fuel pins in a subassembly) or the wall of a container (e.g. can-wall containing a boiling pool). Currently quasi-steady state correlations obtained for forced convection heat transfer in smooth pipes or tubes are used.

Heat transfer from a multi-component, multi-phase mixture to structure must be modeled for several topologies: the bubbly flow regime, the dispersed flow regime and annular flow. In each topology, HTCs are required for both continuous and discontinuous components to structure.

This Appendix is subdivided as follows. Heat transfer by conduction from a stationary or slow-moving multi-component mixture is first described. Then convection heat transfer from liquids or gas in turbulent tube flow is discussed, and correlations are proposed. A formula to calculate heat transfer from an annular liquid film on structure is then presented. The possibility of modeling natural convection in pools more explicitly and the role of discontinuous components in turbulent flow is also discussed briefly. Finally, recommendations are made for SIMMER-III modeling.

E.2. Conduction Heat Transfer

(1) Single-component fluid

Heat is transferred from a fluid in laminar flow to structure by conduction only. For single-component laminar flow in a tube the heat transfer coefficient depends on a constant value Nusselt number:

$$h = \frac{k\mathrm{Nu}_{la}}{D_h}, \tag{E-1}$$

where k is the thermal conductivity of the fluid. The theoretical value of Nu_{la} depends upon the assumed velocity distribution in the liquid and the temperature/heat flux boundary condition applied at the wall surface.[1)] For the usual parabolic velocity distribution Nu_{la} is 3.66 for a constant temperature wall and 4.36 for a constant flux boundary condition. For a constant velocity (plug flow) the respective values of Nu_{la} are 5.8 and 8.0. An empirical value of 3.66 for Nu_{la} is recommended by Holman.[2)] Many workers use a value 5.0 as a compromise where the boundary and flow conditions are not well defined.

For low fluid velocities, natural convection augments, and perhaps dominates, heat transfer to structure. However natural convection heat transfer to structure is currently not explicitly treated in SIMMER-III.

(2) Multi-component mixture

Consider a mixture of liquid and solid particles which is either moving slowly or has stopped moving next to a wall. Heat transfer from the mixture to the wall causes the liquid to cool down and freeze until most of the liquid has solidified, with the resultant frozen solid in good thermal contact with the wall. The solid acts as solder which fuses the mixture together and to the wall. In this situation, it is realistic to calculate heat

loss from the mixture as a whole rather than from the individual components which comprise the mixture. This is because it is difficult to think of an appropriate geometrical dimension to characterize heat transfer to the wall from the discontinuous components in the mixture, whereas the hydraulic diameter can be used for the mixture as a whole.

A single conduction HTC is required for the multi-component, multi-phase, bubbly flow mixture. The mixture HTC h_{mix} is calculated from a mixture thermal conductivity and a constant Nusselt number:

$$h_{mix} = \frac{k_{mix}}{D_h} \mathrm{Nu}_{mix} \,, \tag{E-2}$$

where Nu_{mix} is a constant value Nusselt number. The mixture thermal conductivity k_{mix} needs to be calculated from the thermal conductivities of the individual components of the mixture. The following formula is flexible:

$$k_{mix}^{y} = \left(\sum_{i=1}^{7} \alpha_i k_i^{y} + \alpha_{g,bub} k_g^{y} \right) \Big/ \alpha_{bub} \,, \tag{E-3}$$

where the exponent *y* is a variable, α_{bub} is the volume fraction of the bubbly region, α_i is the volume fraction of liquid energy component *i* in the bubbly region and $\alpha_{g,bub}$ is the volume fraction of the vapor mixture in the bubbly flow. Volume fractions in the bubbly region are used because the mixture HTC is applied only to components in bubbly flow.

The form of Eq. (E-3) ensures that the thermal conductivity of the mixture lies between the minimum and maximum individual thermal conductivities. Nevertheless, the exponent *y* in Eq. (E-3) is crucial for determining how the thermal conductivity of the mixture varies as a function of volume fraction of the components, for example:

$$y = 1 \quad \Rightarrow \quad k_{mix} = \sum_{i=1}^{n} \alpha_i k_i \quad \text{(thermal resistance in parallel)} \,, \tag{E-4a}$$

$$y = -1 \quad \Rightarrow \quad \frac{1}{k_{mix}} = \sum_{i=1}^{n} \frac{\alpha_i}{k_i} \quad \text{(thermal resistance in series)} \,, \tag{E-4b}$$

$$y \to \infty \quad \Rightarrow \quad k_{mix} = k_{max} \quad \text{(maximum thermal conductivity)} \,, \text{and} \tag{E-4c}$$

$$y \to -\infty \quad \Rightarrow \quad k_{mix} = k_{min} \quad \text{(minimum thermal conductivity)} \,. \tag{E-4d}$$

The only value of *y* which cannot be used is *y*=0. The effect of gas pores in a solid fuel pellet is considered by some authors to deteriorate the fuel conductivity according to $k_f(1-P)^{2.5}$, and this is achieved using Eq. (E-3) by setting *y*=0.2.

The calculation of h_{mix} is therefore determined by two variables: Nu_{mix} and *y*. Nu_{mix} has the same value as Nu_{la} defined above, i.e. $\mathrm{Nu}_{mix} = 5$. *y* determines how the mixture thermal conductivity k_{mix} is calculated from the thermal conductivities of the individual components of the mixture. A value *y*=-0.2 is recommended.

E.3. Forced Convection Heat Transfer for Turbulent Flow in a Tube

Heat transfer from a turbulent liquid or gas to a tube wall is calculated using theoretical considerations and empirical correlations derived for single-phase fluids. The fluid is assumed to form a hydrodynamic and thermal boundary layer adjacent to the wall surface. The thickness of the thermal boundary layer with respect to the hydrodynamic layer depends on the Prandtl number of the fluid, which can range between 0.003 and 10 in SIMMER-III applications. Selected heat transfer correlations must be applicable over a suitable range of Prandtl number.

(1) Reynolds-Colburn analogy

A common theoretical approach to obtaining a Nusselt number correlation is the Reynolds-Colburn analogy, which can be found in many text books e.g. Ref. 2). The approach establishes a simple correlation between heat transfer and fluid friction by assuming that the molecular and turbulent heat and momentum diffusivities are identical. The simplest form is:

$$\mathrm{St}\,\mathrm{Pr}^{2/3} = \frac{C_f}{2}. \tag{E-5}$$

Equation (E-5) is attractive because it would appear to ensure consistency between the heat transfer and momentum transfer modeling. However, if the smooth tube turbulent friction factor is inserted into Eq. (E-5), the following Nusselt number correlation is obtained:

$$\mathrm{Nu}_D = 0.0395\,\mathrm{Re}_D^{3/4}\,\mathrm{Pr}^{1/3}, \tag{E-6}$$

A comparison of Eq. (E-6) with empirical correlations (see below) illustrates some drawbacks of the Reynolds-Colburn analogy. Firstly, the Prandtl number-dependence of the Nusselt number given by Eq. (E-6) is incorrect for liquid metals. This is because in equating momentum and heat diffusivities the Reynolds-Colburn analogy assumes the Prandtl number of the fluid is ~ 1, whereas for low Pr fluids boundary layer theory predicts a dependence on Peclet number. Secondly, Eq. (E-6) overpredicts measured Nusselt numbers significantly even for fluids with Pr ~ 1.

Equation (E-6) is useful for justifying the simplest Nusselt number correlation which can be used to model heat transfer to structure, i.e.:

$$\mathrm{Nu}_D = a\mathrm{Re}_D^b\mathrm{Pr}^c. \tag{E-7}$$

However, the values of constants *a*, *b* and *c* are best obtained from empirical correlations. Suitable correlations are discussed below.

(2) Empirical correlation for moderate and high Prandtl number fluids

The Dittus-Boelter correlation is recommended in Ref. 2 for fully developed turbulent flow in smooth pipes:

$$\mathrm{Nu}_D = 0.023\,\mathrm{Re}_D^{0.8}\,\mathrm{Pr}^n, \tag{E-8}$$

where n = 0.4 for heating, and n = 0.3 for cooling. Equation (E-8) is said to be valid for fluids with Prandtl numbers between about 0.6 and 100, and with moderate temperature differences between the wall and the bulk fluid. Physical properties should be evaluated at the bulk temperature.

Equation (E-8) is convenient to use in SIMMER-III and its validity range is not too restrictive, except for low Prandtl number (see below) and where a large temperature difference exists between the structure surface and the bulk fluid. Correlations to correct for the effect of large temperature differences in the fluid on physical properties are available, such as that proposed by Sieder and Tate.[2] However, these correlations are inconvenient to use in SIMMER-III because they require that the interface temperature between structure and fluid be known before the HTCs are calculated.

In summary, it is recommended to apply Eq. (E-8) to liquid fuel, the gas/vapor components and water.

(3) Correlation for low Prandtl number fluids

Seban and Shimazaki calculated theoretical heat transfer rates from turbulent fluid flow to a smooth pipe with a constant temperature wall.[1] The calculation used a radial distribution of eddy diffusivities for heat and momentum obtained from the Prandtl-Nikuradse velocity distribution. The Seban-Shimazaki correlation was obtained by fitting a simple correlation to the results of the more detailed calculations:

$$\mathrm{Nu}_D = 0.025\mathrm{Pe}_D^{0.8} = 0.025\,\mathrm{Re}_D^{0.8}\,\mathrm{Pr}^{0.8}\,. \tag{E-9}$$

Equation (E-9) is said to be valid for Pr < 0.1 and turbulent fluid flow. Interestingly the equation gives Nusselt numbers similar to the Dittus-Boelter correlation even for fluids with Pr ~ 1. It is recommended to apply Eq. (E-9) to liquid steel and sodium.

E.4. Heat Transfer from a Film to Structure in Annular Flow

(1) Stationary film

In the case of a stationary or slow-moving liquid film on structure the heat transfer rate is obtained using the centroid of the liquid film W_c as the appropriate length scale:

$$h = \frac{k\mathrm{Nu}_{la}}{W} = \frac{k}{W_c}\,, \tag{E-10}$$

where W is the film thickness. Equation (E-10) implies that the Nusselt number can be obtained from simple geometrical considerations:

$$\mathrm{Nu}_{la} = \frac{\left(\frac{W}{R}\right)}{1-\left[1-\frac{W}{R}\left(1-\frac{W}{2R}\right)\right]^{1/2}}\,. \tag{E-11}$$

However, for void fractions even as low as 35% (where bubbly flow would in fact be envisaged) the Nusselt number can be well approximated by $\mathrm{Nu}_{la} \cong 2$.

(2) Convection heat transfer

The approach is taken from Nigmatulin.[3] The heat transfer from a liquid film is assumed to be identical to the heat transfer in the outer annulus of single-phase liquid filling a channel. The velocity and temperature distributions are assumed to follow a 1/7-th law. The Nusselt number correlation derived in Ref. 3) is:

$$\mathrm{Nu}_D^* = 0.016\mathrm{Re}_W^{0.8}\mathrm{Pr}^{0.4}\left(\frac{W}{R}\right)^{-0.057}. \tag{E-12}$$

However, Eq. (E-12) is not in an appropriate form for two reasons: (a) the lengthscale to convert the Nusselt number to an HTC is hydraulic diameter, not the film thickness, and (b) the correlation describes heat transfer between the inner surface of a liquid film and the wall. We require the HTC between the radially averaged film temperature and the wall. Using the 1/7 law, the required Nusselt number correlation is equated to Nigmatulin's correlation by:

$$\mathrm{Nu}_W = Nu_D^*\frac{8}{7}\frac{1}{\left[1-\frac{8}{15}\left(\frac{W}{R}\right)\right]}. \tag{E-13}$$

Equation (E-13) can be rewritten as a factor F which multiplies the Dittus-Boelter correlation:

$$\mathrm{Nu}_W = 0.023\mathrm{Re}^{0.8}\mathrm{Pr}^{0.4}F\left(\frac{W}{R}\right), \tag{E-14}$$

where the factor F is a function of film thickness:

$$F(W/R) = \left(\frac{W}{R}\right)^{0.743}\frac{\left[1-\frac{8}{15}\right]}{\left[1-\frac{8}{15}\left(\frac{W}{R}\right)\right]}. \tag{E-15}$$

The factor behaves reasonably in the limits $W \to R$ and $W \to 0$. To compare the heat transfer described by Eq. (E-14) with the large amount of experimental data collected by Nigmatulin, it is necessary to reconvert Eq. (E-14) to a Nusselt number across the whole liquid film, and to evaluate using a liquid Prandtl number of 1.75, like Nigmatulin:

$$\mathrm{Nu}_D^* = 1 + 0.020\mathrm{Re}_W^{0.8}\left(\frac{W}{R}\right)^{-0.057}. \tag{E-16}$$

Although the equation is a function of liquid film thickness, the dependence is weak. Equation (E-16) overpredicts the experimental data slightly, but the disagreement is not too large, and the dependence of heat transfer with Reynolds number seems to be reasonably reproduced.

Note that the above approach is appropriate for liquids with Prandtl numbers close to, or exceeding unity, and its application to liquid metals is dubious. Another dubious quantity in SIMMER-III calculations is the film velocity in annular dispersed flow. The source of uncertainty in annular dispersed flow in SIMMER-III arises because relatively large velocities can be assigned to the liquid film since the film and entrained droplets (of the same liquid) are assigned to the same velocity field. For this reason, an additional

user-input multiplier is recommended so that excessive convection heat transfer from a liquid film can be suppressed if necessary.

E.5. Effects Not Addressed by the Forced Convection Correlation

The forced convection heat transfer correlation discussed above is obtained for a single-phase fluid assuming a hydrodynamic and thermal boundary layer is formed adjacent to a tube wall. The correlation does not take into account the effects of particles in the flow, nor heat transfer in other geometries, nor natural convection heat transfer in boiling pool geometry.

(1) Natural convection heat transfer in a pool

Natural convection heat transfer from a pool of liquid to the walls of its container is currently not explicitly modeled by SIMMER-III. This section describes the connection between the forced convection heat transfer correlation and natural convection heat transfer, and discusses how natural convection heat transfer might be better modeled by reference to two different approaches to modeling boiling pools.

A Nusselt number correlation for natural convection heat transfer through a turbulent film to a vertical plane is given in Ref. 4). If the conduction term is neglected the expression is:

$$\mathrm{Nu}_x = \frac{0.15\mathrm{Ra}_x^{1/3}}{[1+(0.492/\mathrm{Pr})^{9/16}]^{16/27}}, \tag{E-17}$$

where the Grashof number is defined from the length to the top of the plate, x (or the distance to the pool free surface in the case of a liquid pool in a container):

$$\mathrm{Gr}_x = \frac{g\beta\Delta T x^3}{\upsilon^2}. \tag{E-18}$$

For a boiling pool, Chawla et al.[5] essentially recommend Eq. (E-18), but with the Grashof number modified to take account of the buoyancy force due to bubbles:

$$\mathrm{Gr}_x = \frac{g\left(\beta\Delta T + 3\alpha_g\right)x^3}{\upsilon^2}. \tag{E-19}$$

The void fraction is weighted by a factor "3" in Eq. (E-19) because the boundary layer on the wall is assumed to be entirely liquid, whereas the temperature difference between the wall and the bulk fluid varies across the boundary layer. The Chawla-Chan correlation predicts a constant HTC along the walls of the container given the averaged void fraction and temperature difference in the boiling pool. However, for SIMMER-III we require the local HTC, determined as a function of local flow conditions.

Equation (E-17) is a weak function of Prandtl number of fluids with Pr ~ 1. Inserting Eq. (E-19) into (E-17), and evaluating the denominator at Pr=1 gives:

$$\mathrm{Nu}_x = 0.11\left[\frac{g\left(\beta\Delta T + 3\alpha_g\right)x^3}{\upsilon^2}\right]^{1/3}\mathrm{Pr}^{1/3}. \tag{E-20}$$

According to Chawla et al. the liquid boundary layer thickness is proportional to distance, $\delta \propto x$, and the velocity maximum in the liquid boundary layer is given by:

$$V_m = \left[g\left(\beta\Delta T + 3\alpha_g\right)g\delta\right]^{1/2} . \quad \text{(E-21)}$$

Substitution of Eq. (E-21) into Eq. (E-20) gives:

$$\mathrm{Nu}_\delta = 0.11\left[\frac{V_m^2\delta^2}{\upsilon^2}\right]^{1/3}\mathrm{Pr}^{1/3} \propto \mathrm{Re}_\delta^{2/3}\mathrm{Pr}^{1/3} . \quad \text{(E-22)}$$

Equation (E-22) expresses the local Nusselt number as a function of the local boundary layer thickness and a characteristic velocity in the liquid boundary layer (the HTC is a function only of the characteristic velocity). The encouraging feature of Eq. (E-22) is that the form and value of the exponents are similar to Eqs. (E-7) and (E-8), implying that the forced convection correlations can be used to estimate natural convection and boiling pool heat transfer. However, the lengthscale is different (the local boundary layer thickness) and an appropriate velocity which characterizes the liquid boundary layer should be used.

The Chawla-Chan model has been criticized for being too simplistic to represent the dynamics of a boiling pool.[6] A more realistic model envisages a dynamic liquid film layer to exist adjacent to the walls of a boiling pool. Heat transfer occurs both by convection due to the flow of liquid and also by condensation across the thin liquid film existing between wave peaks.[7] Ignoring the effect of condensation (though according to Ref. 7) it is in fact the most important effect), the convection heat transfer from the waves on the moving liquid film is given by:

$$\mathrm{Nu}_\lambda = 0.023\,\mathrm{Re}_\lambda^{0.6}\,\mathrm{Pr}^{0.3} . \quad \text{(E-23)}$$

Equation (E-23) is again similar to the familiar forced convection correlation, but the lengthscale is the wave thickness and the characteristic velocity the velocity of the waves.

The point of discussing the above models for a boiling pool is firstly to point out that the mechanism of heat transfer from a boiling pool to the container walls is still unresolved. However, convection heat transfer seems to be reasonably estimated by a forced convection heat transfer in the form given by Eq. (E-7). Nevertheless, it is crucial to use the correct lengthscale in place of hydraulic diameter and the correct velocity. The choice of lengthscale and velocity depends on the physical model assumed. The heat transfer modeling from a boiling pool needs to be examined further in the future.

(2) Effect of discontinuous components

The influence of discontinuous components on heat transfer from the continuous fluid is currently neglected in SIMMER-III. It is effectively assumed that the thermal boundary layer next to the wall is composed of the continuous phase fluid only. This may be true of some situations (for example the boundary layer on walls enclosing a water boiling pool is treated by some workers as being composed almost entirely of liquid water). However, one can also envisage situations where the discontinuous components disrupt the boundary layer by making random contacts with the structure, which introduces turbulence in the boundary layer, and which promotes heat transfer to the structure.

For bubbly flow in pipes the bubbles enhance turbulence in the liquid, which influences the radial velocity profile of the liquid close to the wall. However, the way in which the velocity profile is affected still

seems unresolved. Marie and Lance[8] have derived an expression for the enhancement of heat transfer in water/air bubbly flow for low void fractions (< 10%). Comparison with experiments indicates that heat transfer from an air/water mixture at a velocity of 0.5 m/s containing a 30% void fraction is increased by about 80%, which is clearly not insignificant. However, the general applicability of the derived expressions is unclear.

The turbulent influence due to discontinuous components is currently not explicitly modeled in SIMMER-III. The feasibility of doing so should be examined.

(3) Transient flows

The correlations described above are valid for quasi-steady state flows, whereas SIMMER-III is also applied to transient flows. The effect of pressure transients on turbulent flows in pipes has been investigated for fluids of moderate Prandtl number.[9] The main conclusion is that the use of quasi-steady state correlations is approximately valid in a decelerating flow. However, in accelerated flows the thermal boundary layer takes time to respond to new flow conditions and, during this time, heat transfer can be significantly overestimated using quasi-steady state formulae.

In any case, transient conditions cannot be solved accurately and reliably without modeling in detail the thermal boundary layer at the structure surface. Since this complexity is out of the scope of SIMMER-III, no correction can be made for transient conditions.

E.6. Recommendations for SIMMER-III

(1) Continuous fluid-structure heat transfer

The HTC describing the heat transfer from continuous phase liquids in SIMMER-III is calculated as follows:

$$h_{CP} = h_{mix} + \frac{k\mathrm{Nu}_D}{D_h}, \tag{E-24}$$

where h_{mix} is determined by Eq. (E-2), k is the thermal conductivity of the continuous liquid and Nu_D is determined by Eq. (E-7). The first term on the RHS of Eq. (E-24) represents heat transfer from the stationary or slow-moving multi-component mixture. The second term becomes more important at high velocities and represents heat transfer through a boundary layer established by the continuous phase fluid. For liquid fuel, it is recommended that Nu_D be defined by the Dittus-Boelter correlation, Eq. (E-8). For liquid sodium and steel Nu_D should be defined by the Seban-Shimazaki correlation, Eq. (E-9).

The HTC describing the heat transfer from gas and vapor in the dispersed flow regime is:

$$h_{gas} = \frac{k_{gas}}{D_h}(\mathrm{Nu}_{la} + \mathrm{Nu}_D), \tag{E-25}$$

where k_{gas} is the thermal conductivity of gas/vapor mixture, $\mathrm{Nu}_{la} = 5$ and Nu_D is determined by Eq. (E-7). It is recommended that Nu_D be defined by the Dittus-Boelter correlation, Eq. (E-8) for the gas/vapor mixture.

(2) Discontinuous fluid-structure heat transfer

The HTC describing the heat transfer from fluid particles in SIMMER-III depends on whether the flow regime is laminar or turbulent:

$$h_{DP} = h_{mix} \quad \text{for} \quad \mathrm{Re}_{CP} < 3000 \text{ , and} \tag{E-26a}$$

$$h_{DP} = \frac{5k}{R_p} \quad \text{for} \quad \mathrm{Re}_{CP} \geq 3000 \text{ ,} \tag{E-26b}$$

where R_p is particle radius. The mixture HTC (determined by Eq. (E-2)) is used in Eq. (26a) for all components in a stationary or slow-moving multi-component mixture. Equation (E-26b) describes conduction heat transfer inside a single rigid particle, using a constant Nusselt number. Although this HTC can be large, and is appropriate only for droplets which are in contact with structure, the IFA between the droplets and the wall is small and can represent the probability of droplet-wall contact in a timestep. In turbulent flow conditions the droplets are well mixed so that individual droplets cannot be distinguished, and it is valid to represent them by a "characteristic" droplet.

(3) Solid particles-structure heat transfer

The HTC describing heat transfer from solid particles to structure in SIMMER-III depends on the topology of the particles:

$$h_{SP} = h_{mix} \quad \text{for} \quad \frac{\alpha_{PP}}{(1-\alpha_{ST})} \geq \alpha_{MP} \text{ , or} \tag{E-27a}$$

$$h_{SP} = 0 \quad \text{for} \quad \frac{\alpha_{PP}}{(1-\alpha_{ST})} < \alpha_{MP} \text{ ,} \tag{E-27b}$$

where α_{PP} is the particles' volume fraction, α_{ST} is the structure volume fraction and α_{MP} is the maximum packing fraction for spheres. The particles at low volume fractions are treated as rigid spheres (which have negligible contact area with structure). In this case the HTC is simply set to zero because heat transfer between the particles and structure is negligible in comparison with other heat transfer routes. However, when the particles' volume fraction exceeds the maximum packing fraction for spheres, the "particles" cannot be regarded as spherical. In the latter case the solid should be seen as "solder", which can have appreciable contact area with structure, and the HTC of the particles is set to the mixture HTC (determined by Eq. (E-2)).

(4) Liquid film-structure heat transfer

The recommended HTC describing heat transfer from a liquid film to structure is:

$$h_{ann} = \frac{k\mathrm{Nu}}{W} \text{ , where } \quad \mathrm{Nu} = \mathrm{Nu}_{la} + a\,\mathrm{Re}_D^b\,\mathrm{Pr}^c \times F(W/R) \times C_{mul} \text{ ,} \tag{E-28}$$

where $\mathrm{Nu}_{la} = 2$, the constants *a*, *b* and *c* determine the forced convection heat transfer from the continuous liquid, the function *F*(*W*/*R*) is given by Eq. (E-15) and C_{mul} is a user-input multiplier.

Natural convection heat transfer modeling for a boiling pool and the effect of discontinuous components on heat transfer from the continuous fluid could be investigated further.

References for Appendix E

1) Seban, R.A., Shimazaki, T.T., Heat transfer to a fluid flowing turbulently in a smooth pipe with walls at constant temperature, Trans. ASME, Vol. 73, No. 6, 1951, pp. 803–807.

2) Holman, J.P., Heat Transfer, McGraw-Hill, 1989, 752p.

3) Nigmatulin, R.I. et al., Dynamics of multiphase media, Vol. II, Hemisphere Pub. Corp., 1991, p. 220.

4) Churchill, S. W., Chu, H.H.S., Correlating equations for laminar and turbulent free convection from a vertical plate, Int. J. Heat Mass Transfer, Vol. 18, No. 1, 1975, pp. 1323–1329.

5) Chawla, T.C., et al., Heat transfer from vertical/inclined boundaries of heat-generating boiling pools, ANL/RAS 81-17, 1981.

6) Seiler, J.M., et al., Synthesis of research on boiling pool thermalhydraulics, Proc. of IAEA Material Relocation technical meeting, O-arai, 1994, pp. 309–330.

7) Bede, M., One component, volume heated, boiling pool thermohydraulics, Proc. of the 6th Int. Top. Meetings on Nuclear Reactor Thermal Hydraulics (NURETH-6), 1993.

8) Marie, J.L., Lance, M., Derivation of the skin friction and heat transfer laws for turbulent 2-component bubbly flows in pipes, Proc. of the 8th Int. Heat transfer conf., 1986, pp. 2337–2342.

9) Kawamura, H., Transient hydraulics and heat transfer in turbulent flow, Nucl. Technol., Vol. 30, No. 3, 1976, pp. 246–255.

Nomenclature for Appendix E

c	Specific heat capacity of fluid	
C_f	Friction factor	
D	Diameter of the pipe or tube	
D_h	Hydraulic diameter	$D_h = \frac{4A}{W_p}$
F	Function defined by Eq. (E-15)	
Gr	Grashof number	
h	Heat transfer coefficient (HTC)	
k	Thermal conductivity of the external fluid	
Nu	Nusselt number:	
P	Porosity	
Pe	Peclet number	$\mathrm{Pe} = \mathrm{RePr}$
Pr	Prandtl number	
r	Coordinate in the radial direction	
R	Tube radius	$R = D/2$
Ra	Rayleigh number	$\mathrm{Ra} = \mathrm{GrPr}$
R_p	Particle radius	
Re	Reynolds number	$\mathrm{Re}_D = \frac{\rho V D_h}{\mu}$, $\mathrm{Re}_W = \frac{\rho V W}{\mu}$, $\mathrm{Re}_\delta = \frac{\rho V \delta}{\mu}$
St	Stanton number	$\mathrm{St} = \frac{h}{\rho c V}$
T	Temperature:	
T_i	Interface temperature	
ΔT	Temperature difference between wall and bulk fluid in a pool	
V	Fluid bulk velocity in the tube	
W	Width of annular liquid film	
W_c	Distance from the structure surface to the centroid of the liquid film	
W_p	Wetted perimeter of structure	
x	Distance from pool free surface, or top of a plate	
y	Variable to determine mixture conductivity (Eqs. (F.3) and (E-4))	

Greek symbols

α	Volume fraction (α_g: void fraction)	
β	Thermal expansion coefficient	
δ	Liquid boundary layer in a molten or boiling pool	
μ	Viscosity of fluid	
ρ	Density of particle	
ν	Kinematic viscosity	$\nu = \mu/\rho$

Subscripts

cp	Continuous phase
dp	Dispersed phase
D	Lengthscale is hydraulic diameter
i	Interface/structure surface
l	Liquid (film)
la	Laminar flow
mix	Multi-component mixture
δ	Liquid boundary layer in a molten or boiling pool
λ	Wave thickness for liquid film in a boiling pool

Appendix F: A Film Boiling Model

F.1. Introduction

The objective of this Appendix is to recommend a film boiling model suitable for implementation in the SIMMER-III code. A film boiling model is required where the temperature difference between a hot energy component and a liquid component is sufficient to separate the two components by a stable vapor film. The vapor acts as an insulating layer and can significantly reduce the heat transfer rate compared with the case of perfect wetting. A steady-state model is required. A further aim of this Appendix is to include the derivation and justification of the model comprehensively, and to discuss uncertainties in the model, for future reference.

In SIMMER-III topology, film boiling is of concern when very hot fuel droplets are surrounded by liquid sodium or steel, or when steel droplets are in liquid sodium. The continuous, more volatile, liquid cannot wet the droplet when the droplet is sufficiently hot so as to maintain a thin vapor film as an insulating barrier between the two liquids. In this case, the heat transfer coefficient (HTC) is overestimated if the role of the vapor film is not accounted for. Experiments of sodium boiling on a sphere[1)] indicate that the HTC can be overestimated by at least an order of magnitude at the minimum boiling temperature unless film boiling is modeled. Note that the volatile liquids in SIMMER-III calculations are often liquid metals.

Treatment of a continuous vapor film enveloping a sphere is generally subdivided into natural convection and forced convection models. The former models are applicable to SIMMER-III topology when the two liquids occupy the same velocity field, or when the relative velocity difference between the droplet and continuous liquid is low. In natural convection models the dominant pressure gradient in the vapor film is determined by buoyancy. In forced convection models the pressure gradient is imposed by the flow of the continuous liquid over the vapor film. The pressure gradient contributes to the film thickness, which in turn determines the heat flux from the droplet surface to the vapor-liquid interface. Both model types are discussed in Section F.4.

In addition to proposing theoretical models, it is necessary to define the circumstances in which film boiling can occur i.e. the minimum film boiling temperature. This is done in Section F.3. The role of film boiling in terms of a boiling curve is briefly discussed in Section F.6. It is also necessary to review the relevant experimental data which can be used to validate models, and which has been used to guide model development. This is done in Section F.2, and validation is discussed in Section F.5.

F.2. Some Experimental Observations

Most measurements of film boiling have been conducted with a wire, or flat plate, immersed in water. However, the experiments most useful for the development of a film boiling model for SIMMER-III are those in which small spheres were immersed in liquids, preferably in liquid metals. The most relevant experiments were performed by Farahat and Eggen,[1)] in which hot, tantalum spheres were quenched in liquid sodium at various subcoolings. From the measurements were obtained boiling curves, correlations for critical heat flux, minimum heat flux and film boiling temperature, and observations of the effects of subcooling and sphere diameter. Visual observations of film boiling must be obtained from the quenching of spheres in water or

freon. Dhir and Purohit[2] in particular provide natural and forced convection data for film boiling of a sphere in water. Other observations of forced convection film boiling on spheres were made by: Walford[3], Orozco and Witte[4] and Aziz et al.[5]. All of the experiments used solid spheres, typically of diameter 1 or 2 cm (Walford used the smallest sphere size: diameter 6 mm).

The role of film boiling in the boiling curve is discussed in Section F.6.3. Nevertheless, it is helpful to compare a "textbook" boiling curve with a boiling curve measured for liquid sodium.[1] It was shown that pool boiling occurs for liquid metals in a similar way to that observed for low thermal conductivity liquids such as water, and that film boiling does occur for liquid metals. It was also shown that the boiling curve varies with liquid subcooling. It is therefore desirable to take subcooling into account both in a film boiling model and in a correlation for minimum film boiling temperature. Farahat and Eggen also investigated the effect of varying the initial sphere temperature and halving the sphere diameter, but these had no appreciable effect on the film boiling heat flux.

Dhir and Purohit[2] also measured a dependence of the minimum film boiling temperature on liquid subcooling for water boiling on spheres. In forced flow conditions, the minimum film boiling temperature was found to be independent of the flow velocity. When the sphere was oxidized or the surface was pitted, premature vapor film collapse was observed. The dependence of vapor film formation on surface conditions cannot be taken into account when developing a model for SIMMER-III.

Steady-state natural convection film boiling on a sphere involves a vapor film covering the bottom hemisphere, with vapor bubbles forming at the top of the sphere. The area producing vapor bubbles depends upon the size of the sphere and the properties of the liquid.[6] SIMMER-III calculations will generally involve droplets less than millimeter-size. The appropriate geometry for small-sphere natural convection film boiling in SIMMER-III is therefore hot droplets contained within a single, elongated vapor dome.

In forced convection film boiling a thin vapor film covers the portion of the sphere facing the fluid flow. Vapor is removed from the film into a wake at the rear of the sphere. The size of the wake is a function of differential velocity and degree of liquid subcooling, but Orozco and Witte[4] made a particular distinction between two types of wake. For a thin wake (high surface temperatures) the dominant heat transfer mechanism is considered to be conduction across the vapor film. However, for a thick wake it was conjectured that nucleate/transition boiling occurred in the wake region. For this reason, Orozco and Witte concluded that wake heat transfer cannot be ignored when modeling forced convection film boiling.

Walford[3] made some interesting observations from the translation of a small nickel sphere through water at Reynolds number values of about 14000. Several heat transfer modes were identified as the sphere cooled. For a hot sphere the vapor film on the front was seen to be smooth and stable, with the film being less than 15-μm thick on the front. As the sphere cooled, disturbances on the vapor-liquid interface were seen, which grew larger until they collapsed into "violent nucleate boiling". Aziz et al.[5] identified a microbubble regime of film boiling in which small vapor bubbles were generated at the liquid/vapor interface and ejected into the bulk liquid. Significant pressure variations in the microbubble and disturbed flow regimes were conjectured to explain the, sometimes violent, sideways movements of spheres in free-fall. Whether the microbubble regime also applies to liquid metals is not known.

The above observations indicate that the boiling curve is not as simple as textbook curves, and that several types of film boiling can occur. A further complication is that intermittent liquid-solid contacts have been shown to occur in the film boiling regime.[7] The contacts were extremely infrequent for subcooled liquid, but occurred several times a second in saturated water film boiling, with their frequency increasing as the transition boiling regime was approached. Transient liquid-solid contacts therefore seem to contribute to heat transfer around the minimum film boiling temperature for liquids close to saturation.

Two important mechanisms in SIMMER-III calculations which would tend to disrupt vapor films, but which are not present or are minimized in the above experiments, are: turbulence in the continuous fluid, and transient contacts with the other discontinuous components. These would promote transient liquid-liquid contacts, and thus enhance heat transfer, and also effectively increase the minimum film boiling temperature. Pressure waves could also force vapor film collapse. The thinnest vapor films would be most susceptible to disruption (although very thin films do not pose much of a barrier to heat transfer in any case). There is no experimental evidence on whether there is a minimum sphere size which can support film boiling, although some data suggests a minimum vapor film size (see Section F.3.3).

Transient formation and destabilization of vapor films cannot be treated sufficiently generally in SIMMER-III. Nevertheless, for reference, Kim and Corradini[8] used experimental results to develop a model in which the vapor film is assumed to go through a cycle of growth and collapse without vapor release. Stevens and Witte[9] observed both precipitous and progressive destabilization of vapor films.

F.3. The Minimum Film Boiling Temperature

F.3.1. Minimum film boiling theories

The minimum film boiling temperature is the temperature at which the heat flux from a hot object immersed in a pool is at a minimum. The Leidenfrost temperature is related to the minimum film boiling temperature, but more properly concerns droplets of liquid placed on a hot surface. The difference between the two definitions is geometry and the ratio of liquid and heater heat capacities. In practice measurements of the Leidenfrost and minimum film boiling temperatures usually coincide.

There are basically two competing theories as to what determines the minimum film boiling temperature. The hydrodynamic theory was originally proposed by Berenson[10] and later modified by Henry[11] to take account of transient wetting. This model asserts that vapor removal from a film is due to the formation of Taylor instabilities on the vapor/liquid interface and that film collapse occurs at the most dangerous wavelength. In contrast the thermodynamic theory, which was originally proposed by Spiegler et al.[12] asserts that the minimum film boiling temperature corresponds to the maximum superheat temperature of the liquid. The basic assumptions of both of these models will be examined first.

Henry[11] created a dimensionless grouping from theoretical considerations, and fitted the group of parameters to the then available experimental data. Henry's correlation is in good agreement with Farahat's sodium boiling data. Unfortunately the hydrodynamic model is not strictly applicable to spheres with diameters less than the dangerous wavelength of the liquid (which is centimeter size for sodium and steel). This is because vapor bubble release from small droplets is determined by the droplet diameter, not by Taylor

instabilities on the vapor-liquid interface. Thus, the assumptions underlying Henry's correlation, whilst good for large spheres and flat plates, are not valid for the sizes of droplets which must be treated in a SIMMER-III calculation.

Thermodynamic theory involves calculating the maximum superheat temperature of the liquid, which is the vaporization temperature in the absence of nucleation sites or impurities. When the wall temperature exceeds the liquid maximum superheat temperature, film boiling is deemed to occur. Baumeister[13] adjusted Spiegler's original model by including transient conduction to better estimate of the wall surface temperature, and by revising the equation of state for a liquid metal. Gunnerson and Cronenberg[14] followed a similar procedure but used an alternative equation of state to calculate the maximum superheat temperature of liquid metals.

The minimum film boiling temperature can also be estimated from an empirical correlation. Olek et al.[15] noted that minimum film boiling temperatures for a wide variety of liquids can be correlated simply by the geometric mean of the normal boiling point and the critical temperature. The correlation is in agreement with sodium data. However, the authors acknowledge that the correlation has no theoretical basis and does not take account of geometry.

Gunnerson and Cronenberg[6] developed a model to calculate the minimum heat flux in spherical geometry. The minimum film boiling temperature can be obtained from the minimum flux if the heat transfer coefficient is known (for example given by the film boiling model described in Section F.4). The model makes assumptions about the frequency of bubble release and heat transfer due to transient wetting. The calculation of the minimum film boiling temperature by this method is rather involved.

F.3.2. Formulation of minimum film boiling temperature criterion

The minimum film boiling temperature criterion will be based upon the thermodynamic theory. This theory really provides an upper limit to the minimum film boiling temperature of saturated liquids, but it is sensible to use this limit given the features of the film boiling model which is proposed in Section F.4. This film boiling model assumes no transient wetting by the coolant, and so is most applicable in the high wall temperature limit. However, it also seems sensible to parameterize the calculation to allow the choice of a more realistic criterion if desired.

The maximum superheat of a liquid is calculated from its EOS: let $(\partial P/\partial V) = 0$ at constant temperature, and evaluate at $P = 0$. For a Van der Waals liquid, this procedure yields:

$$T_m = \frac{27}{32} T_c \,. \tag{F-1}$$

Equation (F-1) was improved upon by Leinhard[14] both theoretically and by correlating with experimental data. The rather more complicated expression behaves more sensibly in the region of the critical temperature:

$$\frac{T_m - T_s}{T_c} = \left(1 - \frac{T_s}{T_c}\right) - 0.095\left[1 - \left(\frac{T_s}{T_c}\right)^8\right]. \tag{F-2}$$

The minimum film boiling temperature, T_m in Eq. (F-2), represents the maximum possible wall temperature at which film boiling temperature can be initiated. The lowest minimum film boiling temperature is, in

principle, the saturation temperature of the liquid. In practice the minimum film boiling temperature of a saturated liquid lies somewhere between these two extremes:

$$T_s \leq T_{min} \leq T_m \,. \tag{F-3}$$

Equation (F-3) is not terribly satisfactory as a precise definition of the minimum film boiling temperature. The proponents of thermodynamic theory contend that T_m is actually a good approximation to the minimum film boiling or Leidenfrost temperatures, i.e. that film boiling depends entirely upon the properties of the liquid. Unfortunately, it does not hold for liquid metals. For example, film boiling of saturated sodium was measured by Farahat at 1590 K[1]; however, the maximum superheat temperature predicted by Eq. (F-1) is 2270 K.

To calculate more accurate Leidenfrost temperatures, some workers have noted that the Van der Waals EOS is not applicable to liquid metals. Gunnerson and Cronenberg[14] recommend an alternative calculation of the maximum superheat temperature for liquid metals, and their recommendation was followed in AFDM.[16] Unfortunately, the revised value of T_m for sodium is 2140 K, which is not much of an improvement on Eq. (F-1). Given that the maximum superheat value for iron (maximum superheat of 6780 K, critical temperature 8500 K) is also not much different from Eq. (F-1), there seems little advantage in using Gunnerson's alternative formula. Besides, the homogeneous nucleation temperature of sodium is about 2300 K, which indicates that the maximum superheat temperature is in fact well above the film boiling temperature measured by Farahat. (The spontaneous nucleation temperature is another indication of the maximum superheat of a liquid.)

Baumeister et al.[13] proposed that the discrepancy in liquid metal data could be explained by taking account of solid and liquid surface energies since liquid metals tend to have higher values of surface tension. However, a formula suitable for liquid-liquid interaction (hot droplets in a volatile liquid) was not derived.

It is therefore proposed that the minimum film boiling temperature is a function of a single parameter applied to the minimum film boiling temperature obtained from Eq. (F-2):

$$\Delta T_{min} = C_{mfb}(T_m - T_s) \,. \tag{F-4}$$

Equation (F-4) is not very different from the approach adopted in AFDM. If the minimum film boiling temperature is equated to the maximum superheat temperature, then C_{mfb} should be set to 1. Alternative suggestions for the value of C_{mfb} are discussed in Section F.3.3. Note that there is no dependence on liquid subcooling in Eq. (F-4), except if the wall temperature is calculated assuming transient wetting (i.e. a conduction-controlled interface temperature is calculated).

F.3.3. Validation

Olek's correlation of the minimum film boiling temperature[15] is:

$$C_{mfb} = \frac{1}{2}\frac{(T_c - T_s)}{(T_m - T_s)}. \tag{F-5}$$

For film boiling of saturated sodium at atmospheric pressure, Olek's correlation suggests a value $C_{mfb} = 0.60$; for water $C_{mfb} = 0.64$.

It is worthwhile examining the minimum film boiling temperatures measured in Ref. 1) for sodium boiling on spheres. The measurements were made by a single thermocouple on the surface of a tantalum sphere. Farahat's empirical correlation appears to agree with Henry's correlation. However, the dependence of the correlation on subcooling is caused by a single data point at the highest subcooling, which lies above the maximum superheat temperature for sodium. If the data point is erroneous then the data do not have an obvious dependence on subcooling and Olek's correlation is a reasonable approximation of the minimum film boiling temperature. If the data point is "good" then it reveals a large amount of scatter in the data at large subcoolings.

The minimum film boiling temperatures were measured by Dhir and Purohit[2] for water. The experiments involved quenching various hot metal spheres in water at various subcoolings and measuring the temperature at which the vapor film collapsed. The temperature of film collapse is taken to be the minimum film boiling temperature. The thermocouple was located in the center of the spheres but the surface temperatures of the sphere could be calculated with little error. The data show a pronounced dependence of minimum film boiling temperature on liquid subcooling, much more so than predicted by Henry. Furthermore, vapor film collapse was observed with surface temperatures greater than the critical point of water. Dhir and Purohit's results therefore also contradict the thermodynamic theory at high liquid subcoolings. The above correlation of minimum film boiling temperature with maximum superheat temperature is apparently valid only at low subcoolings.

Dhir and Purohit's results at high subcoolings can be explained using the film boiling models developed in Section F.4. A vapor film will collapse, even at high surface temperatures, when the heat transfer across the film is matched by the heat transfer within the subcooled liquid, i.e. when no vapor is being generated at the vapor-liquid interface. Maximum heat transfer will occur if there is a limiting vapor film thickness. From Eqs. (F.A-9) and (F.A-14) in Appendix F.A the criteria for vapor film collapse are:

$$\Delta T_s < \frac{\gamma Nu_c \delta_{min} \Delta T_{sc}}{D}, \tag{F-6a}$$

when radiation heat transfer is negligible, or

$$\Delta T_s < \frac{\gamma Nu_c \Delta T_{sc}}{(D/\delta_{min} + Nu_r)}, \tag{F-6b}$$

when radiation is not negligible. The limiting vapor thickness is of course not known a priori. It could be influenced by surface roughness or by the amplitude of waves on the vapor-liquid surface. For both Dhir and Purohit's data (using 19 and 25 mm diameter spheres) and Bradfield's data (using 63 mm diameter spheres) the vapor film collapse temperature can be correlated with $\delta_{min} \approx 100\ \mu m$.

F.3.4. Recommendation

The recommended minimum film boiling temperature is an amalgamation of Eqs. (F-4) and (F-6):

$$\Delta T_{min} = C_{mfb}(T_m - T_s) + \frac{\gamma Nu_c \Delta T_{sc}}{(D/\delta_{min} + Nu_r)}. \tag{F-7}$$

The maximum superheat temperature T_m is defined by Eq. (F-2). The constant C_{mfb} is a parameter which determines the minimum film boiling temperature at low subcoolings. A value of $C_{mfb} = 0.60$ provides a good fit to both sodium and water data. The second term on the RHS of Eq. (F-7) takes account of the increase of minimum film boiling temperature with liquid subcooling. The chief unknown is the minimum film thickness. A value of $\delta_{min} = 1.0 \times 10^{-4}$ is suggested by water boiling on metal spheres. However, a value appropriate for hot droplets immersed in a volatile liquid is not known. The equation is in reasonable agreement with water data, and provides an upper bound to the sodium data.

F.4. A Film Boiling Model for SIMMER-III

F.4.1. Natural convection film boiling

The natural convection film boiling model in AFDM originates from theoretical work by Farahat and El Halfawy. [17] The term "natural convection" refers to the behavior of the coolant when a hot sphere is immersed in it, and differentiates it from the situation where coolant is forced over the sphere.

The derivation of the film boiling HTC in Ref. 17) is repeated in Appendix F.A (there are several mistakes in the original paper). The main assumptions are: (a) axi-symmetric, spherical geometry, (b) a vapor film covers the entire sphere surface except for a small removal area at the top, (c) the vapor film thickness is variable with height but is always small compared with the sphere size, (d) vapor is generated at the vapor/liquid interface and flows upward to the removal region, (e) vapor flow is laminar and driven by buoyant and shear forces, (f) heat is transferred across the vapor film by conduction and radiation only, and (g) vapor generation is constant per unit area. The overall Nusselt number for film boiling is:

$$(\mathrm{Nu}_t - \gamma \mathrm{Nu}_t \Phi)(\mathrm{Nu}_t - \mathrm{Nu}_r)^3 = \frac{\mathrm{Ra}^*}{0.71\beta}. \tag{F-8}$$

The film boiling model in the AFDM code is essentially Eq. (F-8). The physical meaning of the terms in the equation are discussed in Appendix F.A.

Equation (F-8) is appropriate for large spheres, where the vapor removal area is small compared with the whole sphere area. For smaller spheres a vapor film would cover just the bottom hemisphere whist a vapor dome would, at least periodically, effectively insulate the upper hemisphere. A crude criterion to differentiate between large and small spheres can be obtained by equating the buoyancy and surface tension forces for a departing bubble[6]:

$$D_s = \left[\frac{12\sigma}{g(\rho_l - \rho)}\right]^{1/2}. \tag{F-9}$$

The size criterion of spheres in liquid sodium is about 1.2 cm for a wide range of temperatures; for liquid steel the criterion is about 1.8 cm. In SIMMER-III calculations droplets will almost always be much less than centimeter size, and so a small sphere model is applicable. However, for the purpose of validating the model, the sizes of spheres used in experiments need to be considered. Farahat's film boiling experiments with liquid sodium were conducted with sphere sizes between 1.6 and 2.5 cm, and so were approximately in

the large sphere range. For water at room temperature the size criterion is 0.9 cm. Thus, the data from Dhir and Purohit's experiments also belong to the large-size regime.

In the small sphere film boiling model the HTC is approximately halved in comparison with the large sphere model (see Appendix F.A):

$$\left(\mathrm{Nu}_t - \frac{1}{2}\gamma \mathrm{Nu}_t \Phi\right)\left(\mathrm{Nu}_t - \frac{1}{2}\mathrm{Nu}_r\right)^3 = \frac{1}{8}\frac{\mathrm{Ra}^*}{0.71\beta}. \tag{F-10}$$

F.4.2. Forced convection film boiling

A forced convection film boiling model is derived in Appendix F.B by ignoring buoyancy and assuming that the pressure gradient in the vapor film is determined by the potential flow of liquid over the sphere. An insulating wake is assumed to envelop the rear hemisphere. The overall heat transfer coefficient is:

$$\left(\mathrm{Nu}_t - \frac{1}{2}\gamma \mathrm{Nu}_c \frac{\Delta T_{sc}}{\Delta T_s} - \frac{1}{2}\mathrm{Nu}_w\right)\left(\mathrm{Nu}_t - \frac{1}{2}\mathrm{Nu}_r\right)^3 = \frac{0.886\omega^4}{\beta'}\mathrm{Re}^2\,\mathrm{Pr}^*. \tag{F-11}$$

Heat transfer to the wake is an uncertainty which can, in principle, be solved by fitting the equation to experimental data. In practice heat transfer to the wake will be neglected:

$\mathrm{Nu}_w = 0$.

F.4.3. Integrated film boiling model

In Section F.4.1 a model was proposed to calculate the film boiling heat transfer coefficient where buoyancy governs vapor removal from around a sphere. In Section F.4.2 the film boiling HTC was calculated for the scenario where the liquid velocity is very high. It is convenient, though not strictly correct, to add these two expressions to obtain a general formula:

$$\left(\mathrm{Nu}_t - \frac{1}{2}\gamma \mathrm{Nu}_t \Phi\right)\left(\mathrm{Nu}_t - \frac{1}{2}\mathrm{Nu}_r\right)^3 = F(\mathrm{Ra}^*, \mathrm{Re}), \tag{F-12}$$

where:

$$F(\mathrm{Ra}^*, \mathrm{Re}) = \frac{1}{8}\frac{\mathrm{Ra}^*}{0.71\beta} + \frac{0.886\omega^4\,\mathrm{Re}^2\,\mathrm{Pr}^*}{\beta'}.$$

A more convenient, but approximate, expression can be obtained by expanding the power series in Eq. (F-12):

$$\mathrm{Nu}_t \approx (F(\mathrm{Ra}^*, \mathrm{Re}))^{1/4} + \frac{1}{8}\gamma \mathrm{Nu}_c \frac{\Delta T_{sc}}{\Delta T_s} + \frac{3}{8}\mathrm{Nu}_r. \tag{F-13}$$

Equations (F-12) and (F-13) represent the film boiling model recommended for SIMMER-III. Criticisms of the model are discussed in Section F.6.1.

F.5. Validation of the Film Boiling Model

F.5.1. Correlations for natural convection film boiling in non-metals

First, experimental correlations discussed in the open literature are compared with the natural convection model derived in Section F.4.1. The correlations have generally been obtained for water film boiling in non-spherical geometries. The film boiling model proposed in Section F.4 is then compared directly against film boiling of water on spheres.

References 1) and 17) quote correlations which have been obtained for non-metallic liquids. These are repeated in Eqs. (F-14) to (F-16). Bromley studied film boiling from cylinders to saturated liquid pools. He recommended the following equation to take account of radiation:

$$h_t = h_{fb} + 0.75h_r \,. \tag{F-14}$$

An experimental correlation by Daniels is:

$$\overline{\mathrm{Nu}} = 0.71(\mathrm{Ra}^*)^{1/4} \,. \tag{F-15}$$

Hamill and Baumeister investigated film boiling on flat plates and proposed the following correlation:

$$h_t = h_{fb} + 0.88h_r + 0.12h_c \frac{\Delta T_{sc}}{\Delta T_s}. \tag{F-16}$$

However, the most detailed and relevant data are from Ref. 2) for natural convection film boiling of water from metallic spheres. The data was well-correlated by the expression:

$$\overline{\mathrm{Nu}} = 0.8(\mathrm{Ra}^*)^{1/4}\left(\frac{\lambda}{\lambda^*}\right)^{1/4} + \gamma\overline{\mathrm{Nu}_c}\frac{\Delta T_{sc}}{\Delta T_s} + C_l\frac{D}{k}\frac{\sigma_{SB}(T_w^4 - T_s^4)}{\Delta T_s}, \tag{F-17}$$

where $C_l \approx 1$, and the average natural convection Nusselt number used was:

$$\overline{\mathrm{Nu}_c} = 0.9\left(\frac{g\rho_l^2 c_{pl}\beta_l \Delta T_{sc} D^3}{\mu_l k_l}\right)^{1/4} = 0.9(\mathrm{Gr}_l\mathrm{Pr}_l)^{1/4} \,.$$

The above experimental correlations shall be compared with the large-sphere natural convection formula derived in Section F.4.1, rather than the small-sphere model. This is because the dimensions of the spheres etc. used to derive the above correlations were centimeter-size or larger.

The proposed film boiling model for SIMMER-III is based on Eq. (F-11). The approximate expansion can be used for water because the contribution of radiation to the total heat transfer is relatively small (~10%) and the heat transfer into the subcooled liquid is generally less than the heat used in generating vapor. Substituting recommended correlations (Appendix F.C) gives:

$$\begin{aligned}\mathrm{Nu}_t \approx\ & 0.83(\mathrm{Ra}^*)^{\frac{1}{4}} + 0.25\gamma\left[2 + 0.75(\mathrm{Gr}_l\mathrm{Pr}_l)^{\frac{1}{4}}\right]\frac{\Delta T_{sc}}{\Delta T_s} \\ & + 0.75\frac{\varepsilon_w\varepsilon_c}{(\varepsilon_w + \varepsilon_c - 1)}\frac{D}{k}\frac{\sigma_{SB}(T_w^4 - T_s^4)}{\Delta T_s}.\end{aligned} \tag{F-18}$$

The factor "0.83" on the first term of Eq. (F-18) is in fair agreement with the factor "0.71" in Daniels' correlation (Eq. (F-15)). The factor "0.75" on the radiation heat transfer is in agreement with the prediction by Bromley (Eq. (F-14)) and is in fair agreement with the "0.88" in Hammill and Baumeister's formulation (Eq. (F-16)). However, the factor "0.25" on the subcooling term in Eq. (F-18) is twice the factor in the Eq. (F-16). Nevertheless, it is encouraging that Eq. (F-18) contains the right functional dependency, and can be applied successfully to a variety of geometries.

Detailed comparison of Eqs. (F-18) and (F-17) is useful since (F-17) was obtained for spherical geometry. The first terms on the RHS of both equations are almost identical. The last terms, representing radiative heat transfer, differ only in the multiplicative constant. Anyhow radiation was a comparatively insignificant process in these experiments. The subcooling terms in Eqs. (F-17) and (F-18) have the same functional dependency when the (minor) conduction factor "2" is dropped. However, the experimental correlation has a subcooling term which is a factor of 5 larger. The proposed correlation significantly underestimates the measured heat transfer at large subcoolings. (Dhir and Purohit also developed a natural convection film boiling model which underestimated heat transfer at high subcoolings.)

F.5.2. Sodium data for natural convection film boiling

A correlation for the film boiling heat transfer coefficient was obtained by Farahat and Eggen from experiments of sodium boiling off a tantalum sphere [1]:

$$h_t = h_{fb} + \frac{17.9}{(\Delta T_{sc})^{0.7}} h_c \frac{\Delta T_{sc}}{\Delta T_s} + 0.88 h_r \,. \qquad \text{(F-19)}$$

This equation has a similar functional form to the proposed model for SIMMER-III in Eq. (F-18).

In evaluating data using the proposed film boiling model for SIMMER-III the biggest uncertainty is in the values of the emissivities of the wall and sodium in the radiative term. The proposed SIMMER-III model calculates slightly lower heat transfer coefficients than measured, but this could be due to using low emissivity values in the calculation. Nevertheless, there is fairly good agreement between the model proposed for SIMMER-III and the experimental data for a wide range of liquid subcoolings and wall surface temperatures.

It is interesting to contrast film boiling in sodium and water. In the water film boiling experiments performed by Dhir and Purohit radiative heat transfer was estimated to contribute no more than about 10% of the total heat transfer coefficient. In Farahat's sodium boiling experiments the contribution of radiation was about 30% at the minimum film boiling temperature for saturated liquid, and rapidly rose to become the dominant heat loss mechanism. Another notable feature of the sodium data is that less than 20 K subcooling was required at the minimum film boiling temperature for the heat transfer across the vapor film to be absorbed by heat transfer within the coolant. For film boiling in liquid metals it is clearly important to model the radiative and subcooling heat transfer terms correctly.

F.5.3. Forced convection film boiling models

Kobayasi[18] developed a model for forced convection film boiling in saturated liquids where the liquid velocity is vertical. If the gravitational term in the resulting formula is ignored, and heat transfer is restricted through a vapor film covering the front hemisphere only, the correlation can be expressed as:

$$\frac{\mathrm{Nu}}{\omega \mathrm{Re}^{1/2}} = 0.454(\mathrm{Pr}^*)^{1/4} \tag{F-20}$$

The numerical constant on the RHS of Eq. (F-20) increases as the separation point for the vapor film is assumed to move further back (0.454 at $\varphi = 90°$ from the front stagnation point, 0.67 at $\varphi = 141°$, 0.81 at $\varphi = 135°$, etc.). Kobayasi's model has not been used as the basis of a SIMMER-III model because heat transfer in subcooled liquid was not considered and radiative heat transfer is treated as a sort of additive correction term to the main model.

Epstein and Hauser[19] developed a numerical solution to solve the forced flow of liquid around the front of a sphere, where the pressure gradient in the liquid was assumed to be determined by potential flow. If vapor film separation from the sphere is assumed at $\varphi = \pi/2$ from the front stagnation point (as in the model proposed for SIMMER-III) then the following analytical solution is obtained for heat transfer to a saturated liquid:

$$\frac{Nu}{\omega Re^{1/2}} = 0.553(\mathrm{Pr}^*)^{\frac{1}{4}}. \tag{F-21}$$

The main drawback of Epstein's approximate model is that, for subcooled liquids, the temperature of the liquid is assumed to vary appreciably only in a thin region adjacent to the vapor-liquid interface. This is not generally true for liquid metals and so the model cannot be transplanted directly into SIMMER-III. Additionally radiation heat transfer is neglected and the model assumes a constant vapor film thickness (which is not assumed in the model proposed in Section F.4).

Both of the above theoretical models can be compared with the model derived in Section F.4.2 for SIMMER-III. When radiation heat transfer is ignored Eq. (F-11) gives the heat transfer to a saturated liquid:

$$\frac{\mathrm{Nu}}{\omega \mathrm{Re}^{1/2}} = 0.74(\mathrm{Pr}^*)^{\frac{1}{4}}. \tag{F-22}$$

Equation (F-22) predicts higher heat transfer coefficients than the other two models. However, the most striking similarity between all the models is that they have the same functional dependency.

The main reason why the constant in the model proposed for SIMMER-III differs from the other two models is that the shear stress at the vapor-liquid boundary is represented by an empirical constant in the vapor momentum equation. This makes the derivation considerably simpler, and makes the resulting equation more flexible because the vapor-liquid boundary conditions are actually uncertain. The constant 0.74 in Eq. (F-22) is obtained using a value of the slip parameter of $\beta = 3$, which assumes no shear stress at the interface and thus maximizes vapor removal and heat transfer. If shear stress is assumed to result in a larger value of the slip parameter, $\beta = 12$, then the numerical constant in Eq. (F-22) becomes 0.52, which is in better

agreement with the Kobayasi and Epstein models (which implicitly include slip by matching the vapor and liquid interface velocities).

Nevertheless, there is a practical reason for keeping a value $\beta = 3$. The model proposed for SIMMER-III assumes vapor film separation, with wake formation, at $\phi = \pi/2$ from the front stagnation point. In practice the separation occurs between positions $\varphi = \pi/2$ and $\varphi = 3\pi/2$.[19] Kobayasi's model gives some indication how the heat transfer increases with the angle of separation (see discussion above). It can be seen that a value $\beta = 3$ in the SIMMER-III model approximately accounts for a separation angle greater than $\varphi = \pi/2$.

F.5.4. Forced convection film boiling data

Quantitative heat flux measurements were obtained by Dhir and Purohit[2] for moving spheres in water. There is no forced convection data for liquid metals. Saturated water film boiling data could be correlated by the expression:

$$\mathrm{Nu} = \mathrm{Nu}_0 + 0.8(\mathrm{Re}^*)^{1/2}\,, \tag{F-23}$$

where the constant Nu_0 represents natural convection film boiling, and was compared successfully with the proposed SIMMER-III model in Section F.5.1. The Reynolds number dependency of the proposed SIMMER-III model can be obtained by evaluating Eq. (F-23) for water (materials properties obtained from Ref. 20):

$$\mathrm{Nu} = 0.90(\mathrm{Re}^*)^{1/2}\,. \tag{F-24}$$

Thus the predicted Reynolds number dependency in the proposed SIMMER-III model is in fair agreement with the measured dependency by Dhir and Purohit.

For forced flow of subcooled water Dhir and Purohit recommend the following expression:

$$\mathrm{Nu} = \mathrm{Nu}_0 + 0.8(\mathrm{Re}^*)^{1/2}\left(1 + \frac{k_l}{k}\frac{\Delta T_{sc}}{\Delta T_s}\right). \tag{F-25}$$

The subcooling term in the model proposed for SIMMER-III is:

$$\frac{\gamma}{8}\mathrm{Nu}_c\frac{\Delta T_{sc}}{\Delta T_s} \approx 0.1\,\mathrm{Re}^{\frac{1}{2}}\frac{k_l}{k}\frac{\Delta T_{sc}}{\Delta T_s}\,, \tag{F-26}$$

where Eq. (F-26) was evaluated using the following forced convection HTC:

$$\mathrm{Nu} = 2 + 0.6\,\mathrm{Re}^{1/2}\,\mathrm{Pr}_l^{1/3} \approx 0.6\,\mathrm{Re}^{1/2}\,\mathrm{Pr}_l^{1/3}\,. \tag{F-27}$$

The functional dependence of the SIMMER-III model is the same as the empirical correlation. However, the numerical constant is low by a factor of 8.

F.5.5. Summary of validation

The proposed natural convection film boiling model is in good agreement with water and sodium data at low subcoolings. The model also gives encouraging agreement for objects other than spheres. The validation against liquid sodium is particularly valuable since it verifies the proposed film boiling model in conditions of liquid metal boiling on a sphere.

The proposed forced convection film boiling model is in encouraging agreement with, and more flexible than, the "state-of-the-art" analytical models available in the open literature. The model is in good agreement with forced convection film boiling data for saturated water. The main discrepancy for both the natural and forced convection models is the dependence on subcooling when compared with water data.

F.6. Discussion

F.6.1. Critique of the model

The model derived in Section F.4 is relatively simple compared with other analytical solutions because the boundary conditions at the liquid-vapor interface are not precisely formulated when solving the vapor film momentum equation. Assumptions about stress and velocity continuity are contained in a (constant) parameter. However, this is also an advantage because the conditions at the interface are unknown: it is not certain whether slip can occur at the interface. Also the effect of externally imposed pressure gradients on the vapor flow is ignored.

The model was developed with solid spheres in mind, rather than for hot droplets immersed in a more volatile liquid (which is the SIMMER-III scenario). One effect of considering droplets would be to compound the uncertainty in the "wall"-vapor boundary conditions since the droplet surface might be able to move. However the greatest uncertainty is probably in the composition of the vapor film. A hot droplet would be able to evaporate into the surrounding vapor film and this would be a heat transfer process in addition to conduction across the film. Furthermore the material properties of the vapor film would be altered. The problem is perhaps amenable to theoretical analysis, but there are no quantitative measurements of film boiling on droplets which could verify the more complicated model.

There are phenomena associated with film boiling, such as waves on the liquid-vapor interface, which have not been considered. However a particularly large uncertainty is heat transfer to the wake, in forced flow boiling, or to the upper vapor dome for natural convection boiling on a small sphere. This has been ignored in the model derived in Section F.4. However, Orozve and Witte[4)] argue that wake heat transfer is significant, and may even be a type of transition boiling. Furthermore, the separation point of the wake is known to vary with Reynolds number and subcooling, whereas it is kept constant in the proposed model.

A criticism that can be leveled at the validation performed in Section F.5 is that the natural convection model was validated only for large spheres. The small sphere model was not validated, and thus may underestimate heat transfer by up to a factor of two. No validation was performed because there is no experimental data. It would be interesting to know if there is a minimum sphere size which can support film boiling.

The model developed in Section F.4 considers spherical droplets to be insulated by a vapor film without external influences. In fact, it is quite feasible that the presence of other discontinuous components in a SIMMER-III calculation could interact with the droplets, causing transient collapse of the vapor film. If this happened frequently the heat transfer process from the droplets to the surrounding liquid would resemble transition boiling rather than film boiling. It might be possible to simulate this process by calculating the frequency of interactions and using it to compute a "weighted" HTC from the film boiling and single-phase

HTCs, but this method is not realistic. Use of a film boiling HTC in multi-component flows is thus likely to tend to underestimate the heat transfer.

The transient growth of a vapor film is of course not considered since SIMMER-III requires quasi-steady state HTCs. Similarly, the effect of a collapsing vapor film is not considered, although it could contribute to droplet fragmentation.

It is argued in AFDM[16] that no film boiling should be initiated in a single-phase cell since the amount of vapor is insufficient to form a complete vapor blanket around the droplets. However, experimental results show that film boiling occurs in subcooled liquids. In this case, it is necessary to decide how to treat the vapor generated by a film boiling model in SIMMER-III formulation.

Having made the above criticisms, it is worthwhile reiterating the advantages of implementing a film boiling model. For high temperature droplets, such as fuel droplets, immersed in a volatile liquid, a film boiling model provides a mechanistic means of calculating heat transfer between the two components. The model realistically imposes an insulating vapor film between the components which enables the calculation of more realistic heat transfer coefficients than the current SIMMER-III modeling (which uses single-phase HTCs). Application of the model to the best available experimental data yields encouraging agreement. The film boiling may not be very accurate in many conditions, but it is better than having no model at all.

F.6.2. Single-phase heat transfer by natural convection

Currently in SIMMER-III heat transfer in a liquid heated by hot particles and droplets in the same velocity field is calculated assuming conduction only. In fact steady-state heat transfer would be enhanced by natural convection around the particles. Thus a more realistic minimum heat transfer coefficient in the liquid would be obtained by using the natural convection Nusselt number formulations in Appendix F.C.

For liquid fuel a suitable formula is:

$$\mathrm{Nu}_{nc} = 2 + 0.75(\mathrm{GrPr})^{1/4} . \tag{F-28}$$

For liquid metals the effect of the thicker thermal boundary layer must be considered:

$$\mathrm{Nu}_{nc} = 2 + 0.75(\mathrm{GrPr}^2)^{1/4} . \tag{F-29}$$

It is recommended that Eqs. (F-28) and (F-29) be incorporated into SIMMER-III, at least until turbulence enhanced heat transfer is modeled.

F.6.3. The SIMMER-III boiling curve

Currently in SIMMER-III, boiling heat transfer between two liquid energy components is not modeled: the maximum interface temperature is limited (unphysically) by the saturation temperature of the most volatile component. The implementation of a film boiling model introduces the question of how phase changes at the interface of two liquid components generally influence exchange coefficients. For heat transfer a boiling curve must be recommended.

For hot droplets immersed in a more volatile liquid, the recommended HTC with no phase change is listed in Section F.6.2. A film boiling model has been described at length in Sections F.4 and F.5. It is

necessary to ensure a smooth transition from the single-phase to the film boiling heat transfer coefficient as a function of droplet temperature. One way of ensuring this would be to cap the single-phase HTC by the film boiling HTC:

$$\mathrm{Nu}_{nc} \leq \mathrm{Nu}_t \,. \tag{F-30}$$

This approach ignores the shape of the boiling curve. In particular, the large heat transfer rates during nucleate boiling and transition boiling are neglected. The approach adopted in AFDM is to continue to use the single-phase HTC throughout the nucleate boiling regime and then to interpolate HTCs between the departure from nucleate boiling temperature to the minimum film boiling temperature. This gives three heat transfer regimes, corresponding approximately to nucleate boiling, transition boiling and film boiling, respectively:

$$h = \begin{cases} h_c & \text{for } \Delta T_w \leq \Delta T_{DNB} \\ \dfrac{h_c(\Delta T_{min} - \Delta T_w) + h_i(\Delta T_w - \Delta T_{DNB})}{(\Delta T_{min} - \Delta T_{DNB})} & \text{for } \Delta T_{DNB} < \Delta T_w < \Delta T_{min} \\ h_t & \text{for } \Delta T_w \geq \Delta T_{min} \end{cases} . \tag{F-31}$$

The temperature difference at the departure from nucleate boiling must be defined by the user.

Even for a high thermal conductivity liquid like sodium, it is obvious that the real boiling curve is not satisfactorily modeled using single-phase HTCs. Heat transfer rates in the nucleate boiling and transition boiling regimes are significantly underestimated. (Note also that the single-phase HTC correlations are outside the range of their validity when used above the saturation temperature.) Nevertheless it is proposed that Eq. (F-31) should be implemented in SIMMER-III.

In fact there are several complications concerning boiling on liquid droplets. Boiling is a violent process of vapor bubble growth and detachment. The pressure gradients associated with boiling, and the collapse of surrounding liquid onto a droplet surface would contribute to the fragmentation of droplets. The challenge in modeling the boiling process is as much how to treat droplet fragmentation as how to obtain appropriate heat transfer coefficients. It might be possible to learn lessons from FCI models in this area, since the collapse of a vapor film coincident with droplet fragmentation is a propagation phase of the FCI process.

F.6.4. Implementation in SIMMER-III

If the model proposed in Section F.4 is to be included in a version of SIMMER-III, it is worthwhile making some observations before constructing an algorithm.

(a) The interface temperature between two liquid components is required in advance since a film boiling model should be called only when the interface temperature exceeds the minimum film boiling temperature. Interface temperatures are currently calculated in the heat and mass transfer suite of subroutines of SIMMER-III. It therefore seems sensible to calculate film boiling in a subroutine which is called at this location, rather than repeat or move the interface temperatures calculations to subroutine 'htc'. An alternative option is to calculate a film boiling HTC in subroutine 'htc', and merely choose between single-phase and film boiling HTCs in the heat and mass transfer routines. Note that the current SIMMER-III code must be altered to allow interface temperatures which exceed the saturation temperature of the most volatile component.

(b) The film boiling models imply that a portion of the heat transferred from the hot droplet generates vapor, and the remaining portion is transferred into the subcooled liquid. This suggests that some heat and mass should be transferred directly to the vapor field, and the remaining heat is transferred to the surrounding coolant. In fact it is probably more convenient in SIMMER-III to calculate all heat transfer to the surrounding coolant (for a sub-cooled liquid this is the same as assuming that the vapor immediately condenses). The latter approach was adopted in AFDM.

(c) The wall temperature in the model - or the droplet surface temperature - needs to be defined. The two convenient options are the average droplet temperature, or an instantaneous interface temperature based on direct contact between the droplet and the coolant. It is recommended that the latter temperature is used because transient contacts between wall and coolant occur near the minimum film boiling temperature, and because the HTC should be continuous from the single-phase HTC to the film boiling HTC as the vapor film thickness decreases.

(d) A large number of materials properties need to be calculated, which probably necessitates a call to the EOS routines. The vapor properties need to be evaluated at a temperature midway between the saturation temperature and the wall temperature. Liquid properties should strictly be calculated at a temperature midway between saturation and the bulk temperature.

F.7. Conclusions

A film boiling model suitable for inclusion in SIMMER-III is recommended. The model is appropriate for high temperature droplets - such as fuel droplets - immersed in a more volatile liquid. It should ensure a more realistic calculation of heat transfer coefficients than the current SIMMER-III modeling (which uses single-phase HTCs). The model is in encouraging agreement with the most suitable experimental data. A simple boiling curve is recommended, but it significantly underestimates heat fluxes in the nucleate boiling regime.

The proposed film boiling model is an improvement over the model in AFDM in the following areas:

(a) The minimum film boiling temperature criterion takes account of coolant subcooling. Otherwise minimum film boiling temperatures would be underestimated.

(b) The natural convection film boiling model takes account of the droplet size with respect to the vapor bubble departure area. This virtually halves the heat transfer coefficient.

(c) A forced convection film boiling model has been developed to treat the situation when there is a relative velocity between the droplets and the continuous liquid.

(d) All the above models have been validated to some extent by comparing predictions with water and sodium experimental data in the open literature.

A full derivation of the models is included in the text, and areas of uncertainty have been highlighted.

Appendix F.A: Natural Convection Film Boiling Models

The models derived in this appendix are variations on the approach used by Farahat and El Halfawy.[17] The derivation is repeated, for large spheres, because of mistakes in the original reference. The models are appropriate for film boiling around solid spheres; differences expected for film boiling around droplets are discussed in the main text. The term "natural convection" refers to the behavior of a subcooled liquid when a hot, stationary sphere is immersed in it, and is used to distinguish the models from the scenario where fluid is forced over a sphere.

F.A.1. Model for large particles

A sphere with uniform surface temperature is immersed in a volatile liquid (a coolant). The surface temperature is assumed to be sufficiently high to sustain a stable vapor film which entirely envelops the sphere. Heat transfer across the film generates vapor at the liquid-vapor interface, which is at the saturation temperature of the coolant. The vapor flows up and around the sphere and is removed over a small area at the top of the sphere. The problem is axi-symmetric.

(1) Momentum equation

The force balance for the vapor film in the θ direction is:

$$-\frac{dP}{d\theta}2\pi R\delta \sin\theta = \rho_l g 2\pi R^2 \delta \sin^2\theta + 2\pi R^2 \delta \sin^2\theta\,(\tau_w - \tau_i). \tag{F.A-1}$$

Since the vapor film is stable and in steady-state, there are no transient terms in the force-balance, and no vapor motion in the r-direction. The driving force in the vapor film is assumed to be buoyancy alone:

$$-\frac{dP}{d\theta} = \rho_l g R \sin\theta\,. \tag{F.A-2}$$

The vapor flow is assumed to be laminar and incompressible. The shear stress is represented empirically:

$$\tau_w - \tau_i = \frac{\beta \mu \bar{v}_\theta}{\gamma}. \tag{F.A-3}$$

The form of Eq. (F.A-3) is the solution obtained for laminar flow between two parallel plates. The value of the slip parameter β is debatable since it contains assumptions about the boundary conditions at the vapor-liquid and vapor-solid interfaces. A value of $\beta = 12$ is appropriate for a parabolic vapor velocity profile between two stationary plates, i.e. the slip condition; a value of $\beta = 3$ results when the shear stress at one of the plates is assumed to be zero, i.e. the no-slip condition. These values of the slip parameter are derived in Appendix F.C.

Define the vapor mass flow rate as m:

$$m = \rho \bar{v}_\theta 2\pi R \sin\theta \tag{F.A-4}$$

Then substituting Eqs. (F.A-2), (F.A-3) and (F.A-4) into (F.A-1) gives an expression for the vapor film thickness as a function of θ:

$$\delta^3 = \frac{\beta\mu m}{2\pi R\rho\Delta\rho g \sin^2\theta}. \quad \text{(F.A-5)}$$

Equation (F.A-5) differs from the equivalent equation in Ref. 17) by having a $\sin^2\theta$ term on the denominator in place of a $sin\,\theta$ term.

(2) Energy equation

The energy equation at angle θ in the vapor film is:

$$2\pi R^2 \sin\theta\, d\theta \left(\frac{k}{\delta} + h_r\right)\Delta T_s = \lambda^* dm + 2\pi R^2 \sin\theta\, d\theta \Delta T_{sc} h_c\,, \quad \text{(F.A-6)}$$

where the term on the LHS of (F.A-6) represents heat transfer by conduction and radiation across the vapor film and ΔT_s is the temperature difference across the film. The first term on the RHS of (F.A-6) represents the vapor generation at the vapor/liquid interface. The second term represents heat transfer from the interface into the subcooled liquid. ΔT_{sc} is the liquid subcooling. Appropriate HTCs for radiative and liquid heat transfer are discussed in Appendix F.C.

It is now necessary to define the variable that is required from this analysis, which is the overall heat transfer coefficient for the sphere. Let the heat flux, q, out of the sphere be defined by:

$$q = h_t \Delta T_s = \frac{m_t \lambda^*}{4\pi R^2} + h_c \Delta T_{sc}\,. \quad \text{(F.A-7)}$$

The first term on the RHS of (F.A-7) represents the heat released in generating vapor bubbles at the top of the sphere. The second term represents the overall heat transfer into a subcooled liquid. This is interesting with respect to SIMMER-III topology because it implies that heat transfer from a hot sphere should be divided between the vapor energy field and the liquid energy field.

Equation (F.A-7) generates two new variables, h_t and m_t, and so a further equation is required to relate the total vapor production to the local vapor production. This is done by assuming that the rate of vapor production per surface area is constant, which is based upon an observation of film boiling. around cylinders by Bromley[18]:

$$m = \frac{1}{2} m_t (1 - \cos\theta). \quad \text{(F.A-8)}$$

A useful solution is obtained after an orgy of algebra: (F.A-5) is substituted into (F.A-6) to eliminate δ; (F.A-8) is then substituted to eliminate m. The resulting equation is then integrated over the whole area of the sphere to eliminate θ. Finally, h_t is substituted for m_t using (F.A-7). The solution is then:

$$\left(\frac{h_t D}{k} - \frac{h_c D}{k}\frac{\Delta T_{sc}}{\Delta T_s}\right)\left(\frac{h_t D}{k} - \frac{h_r D}{k}\right)^3 = \frac{\rho\Delta\rho g\lambda^* D^3}{0.71\beta\mu k\Delta T_s}. \quad \text{(F.A-9)}$$

Equation (F.A-9) can be expressed more pithily by a reformulation in terms of Nusselt numbers:

$$(\mathrm{Nu}_t - \gamma \mathrm{Nu}_t \Phi)(\mathrm{Nu}_t - \mathrm{Nu}_r)^3 = \frac{\mathrm{Ra}^*}{0.71\beta}. \quad \text{(F.A-10)}$$

Equation (F.A-10) is very similar, but not identical to, one used in Ref. 17). The equation is a quartic in h_t and so requires iteration to obtain a solution. A more malleable, but approximate, form can be obtained by expanding the terms in brackets. First rewrite (F.A-9) as:

$$h_t\left(1-\frac{h_c}{h_t}\frac{\Delta T_{sc}}{\Delta T_s}\right)^{1/4}\left(1-\frac{h_r}{h_t}\right)^{3/4}=h_f\,, \tag{F.A-11a}$$

where

$$h_f=\frac{k}{D}\left(\frac{\mathrm{Ra}^*}{0.71\beta}\right)^{1/4}=\left(\frac{\rho\Delta\rho g\lambda^* k^3}{0.71\beta\mu D\Delta T_s}\right)^{1/4}\,. \tag{F.A-11b}$$

Then expand the two terms in brackets as a power series, and assume that second order terms in $1/\mathrm{h_t}$ can be dropped:

$$h_t\approx h_f+\frac{1}{4}h_c\frac{\Delta T_{sc}}{\Delta T_s}+\frac{3}{4}h_r\,. \tag{F.A-12}$$

Equation (F.A-12) is not only easier to solve, it also highlights the physical meaning of the film boiling heat transfer coefficient. The first term on the RHS is the HTC for a saturated liquid where radiative heat transfer is unimportant; conduction across the vapor film goes entirely into vapor production. The second term represents the heat transfer in the subcooled liquid. The third term represents the contribution by radiation heat transfer.

The use of equation (F.A-12) in place of the less convenient (F.A-9) is strictly valid only when the following relations apply:

$$\frac{h_c}{h_t}\frac{\Delta T_{sc}}{\Delta T_s}<<1\ \text{ and }\ \frac{h_r}{h_t}<<1\,. \tag{F.A-13}$$

In fact expansion of the radiative heat transfer term is not unreasonable because comparison of Eqs. (F.A-12) and (F.A-9) shows that it would introduce a 25% error at most. Unfortunately, the same cannot be said for the subcooling term without evaluating its magnitude with respect to the minimum film boiling and radiative HTCs. For a low thermal conductivity liquid like water the expansion is generally valid because the bulk of the heat transported to the liquid-vapor interface generates vapor. However, for sodium the heat transfer in subcooled liquid is usually important and the subcooling term even dominates the overall heat transfer coefficient in some circumstances.

Equation (F.A-9) can also be used to calculate the conditions in a subcooled liquid when a vapor film cannot be maintained because all the heat is being conducted away by the coolant. This occurs when the term in the first bracket of Eq. (F.A-9) becomes negative:

$$\Delta T_{sc}>\frac{\mathrm{Nu}_t\Delta T_s}{\gamma\mathrm{Nu}_c}\,. \tag{F.A-14}$$

F.A.2. Model for small particles

The above model describes vapor removal from the very top of a sphere, where the area of removal is small. Whilst this model is plausible for large spheres, that is spheres of centimeter-size or larger in liquid metals, the removal area cannot be ignored for small spheres. In fact a vapor dome is likely to form over the top half of a small sphere, restricting heat transfer mainly to conduction across a thin vapor film over the bottom half of the sphere.

If heat transfer is limited to just the bottom half of the sphere, the analysis in Section F.A.1 needs to be modified slightly. Equations (F.A-1) to (F.A-6) remain valid, but Eq. (F.A-7), which defines the overall heat transfer coefficient, becomes:

$$h_t \Delta T_s = \frac{m_t \lambda^*}{4\pi R^2} + \frac{1}{2} h_c \Delta T_{sc} \,. \tag{F.A-15}$$

The total rate of vapor production, in Eq. (F.A-8), becomes:

$$m = m_t (1 - \cos\theta) \,. \tag{F.A-16}$$

The solution is now:

$$\left(\frac{h_t D}{k} - \frac{1}{2}\frac{h_c D}{k}\frac{\Delta T_{sc}}{\Delta T_s}\right)\left(\frac{h_t D}{k} - \frac{1}{2}\frac{h_r D}{k}\right)^3 = \frac{1}{8}\frac{\rho \Delta\rho g \lambda^* D^3}{0.71 \beta \mu k \Delta T_s} = \frac{1}{8}\frac{Ra^*}{0.71\beta} \,, \tag{F.A-17}$$

where all terms are defined in Section F.A.1.

The expansion of the brackets yields the following approximate solution:

$$h_t \approx \frac{h_f}{2^{3/4}} + \frac{1}{8} h_c \frac{\Delta T_{\mathrm{sc}}}{\Delta T_s} + \frac{3}{8} h_f \,. \tag{F.A-18}$$

As expected, the heat transfer coefficient is reduced by almost a factor of 2 compared with the solution obtained in Section F.A.1.

Appendix F.B: A Forced Convection Film Boiling Model

A hot sphere is submerged in a liquid with uniform velocity far from the sphere. A vapor film is formed over the hemisphere facing into the oncoming liquid, and insulates the sphere. A wake is assumed to envelop the back hemisphere, from the location of the equatorial plane. Heat transfer from the sphere is assumed to be dominated by conduction across the thin vapor film on the front of the sphere. The problem is symmetric about the axis parallel to the liquid velocity.

(1) Momentum equation

The momentum equation in the vapor film is:

$$-\frac{dP}{d\varphi}2\pi R\delta \sin\varphi = 2\pi R^2 \sin\varphi\,(\tau_w - \tau_i)\,. \tag{F.B-1}$$

Equation (F.B-1) is the same as (F.A-1) in Appendix F.A except that the gravity term is dropped. As this term is small compared with the buoyancy force, and buoyancy shall be neglected compared with the imposed pressure gradient, then this assumption is valid.

The pressure gradient in the vapor film is assumed to be imposed by the potential flow of the liquid around the sphere[21]:

$$P = P_0 + \frac{\rho_l u^2}{2}\left(1 - \frac{9}{4}\sin^2\varphi\right). \tag{F.B-2}$$

Potential flow means incompressible, inviscid fluid flow, which is true in the limit of large Reynolds number. The imposition of the pressure gradient in the liquid on the vapor flow is a consequence of boundary layer analysis. Thus the model implicitly assumes a no-slip condition at the liquid-vapor interface.

The buoyancy force has been ignored in Eq. (F.B-2) because the gravitational axis need not coincide with direction of liquid flow. This is an implicit assumption that the liquid velocity is sufficiently high to swamp the buoyancy term. The ratio of the potential flow gradient to the gradient caused by buoyancy when the two are acting in the same direction (i.e. vertically) is:

$$\frac{dP/d\varphi_{forced}}{dP/d\varphi_{buoyancy}} = \frac{9u^2}{4gR}\cos\varphi\,. \tag{F.B-3}$$

Thus, after integration over a hemisphere, a rough criterion for when the forced convection pressure gradient dominates the natural convection gradient is:

$$u > \frac{2}{3}(gR)^{1/2}\,. \tag{F.B-4}$$

The criterion in equation (F.B-4) can be achieved for relatively low velocities for small spheres.

The pressure gradient in the vapor film is obtained from (F.B-2):

$$\frac{dP}{d\varphi} = -\frac{9}{4}\rho_l u^2 \sin\varphi\cos\varphi\,. \tag{F.B-5}$$

As in the natural convection model in Appendix F.A, the shear stress is treated empirically:

$$\tau_w - \tau_i = \frac{\beta' \mu \bar{v}_\varphi}{\delta}. \tag{F.B-6}$$

Using the same definition of vapor mass flow rate as in Appendix F.A, the vapor film thickness is obtained by substituting Eqs. (F.B-5) and (F.B-6) into Eq. (F.B-1):

$$\delta^3 = \frac{2\beta' \mu m}{9\pi \rho_l \rho u^2 \sin^2\varphi \cos\varphi}. \tag{F.B-7}$$

Note that equation (F.B-7) gives physically realistic values only up $\varphi = \pi/2$. This is a consequence of the potential flow assumption since the pressure distribution is symmetric about $\varphi = \pi/2$. For practical purposes this means that a pressure gradient provided by potential flow alone cannot be used to calculate the vapor motion in a film enveloping the whole sphere.

(2) Energy equation

The energy equation across the vapor film is the same as in the natural convection model (Eq. (F.A-6)):

$$2\pi R^2 \sin\varphi \, d\varphi \left(\frac{k}{\delta} + h_r\right) \Delta T_s = \lambda^* dm + 2\pi R^2 \sin\varphi \, d\varphi \Delta T_{sc} h_c . \tag{F.B-8}$$

However, the overall energy equation is appropriate for the hemisphere boiling model:

$$\Delta T_s = \frac{m_t \lambda^*}{4\pi R^2} + \frac{1}{2} h_c \Delta T_{sc} + \frac{1}{2} h_w \Delta T_s . \tag{F.B-9}$$

The total rate of vapor production is:

$$m = m_t (1 - \cos\varphi) . \tag{F.B-10}$$

The solution is obtained by inserting Eqs. (F.B-7), (F.B-9) and (F.B-10) into (F.B-8) and integrating from $\varphi = 0$ to $\varphi = \pi/2$:

$$\left(\frac{h_t D}{k} - \frac{1}{2}\frac{h_c D}{k}\frac{\Delta T_{sc}}{\Delta T_s} - \frac{1}{2}\frac{h_w D}{k}\right)\left(\frac{h_t D}{k} - \frac{1}{2}\frac{h_r D}{k}\right)^3 = \frac{0.886 \rho_l \rho u^2 \lambda^* D^2}{\beta' \mu k \Delta T_s}. \tag{F.B-11}$$

Equation (F.B-11) can be expressed in terms of Nusselt numbers:

$$\left(\mathrm{Nu}_t - \frac{1}{2}\gamma \mathrm{Nu}_c \frac{\Delta T_{sc}}{\Delta T_s} - \frac{1}{2}\mathrm{Nu}_w\right)\left(\mathrm{Nu}_t - \frac{1}{2}\mathrm{Nu}_r\right)^3 = \frac{0.886\omega^4}{\beta'} \mathrm{Re}^2 \mathrm{Pr}^* . \tag{F.B-12}$$

Equation (F.B-12) can be simplified by taking a series expansion and dropping all but first order terms in Nu_t:

$$\mathrm{Nu}_t = \frac{0.97\omega}{\beta'^{1/4}} [(\mathrm{Re}^*)^2 \mathrm{Pr}^*]^{1/4} + \frac{1}{8}\gamma \mathrm{Nu}_c \frac{\Delta T_{sc}}{\Delta T_s} + \frac{3}{8}\mathrm{Nu}_r + \frac{1}{8}\mathrm{Nu}_w . \tag{F.B-13}$$

The terms on the RHS of Eq. (F.B-13) lend themselves to physical interpretation. The first term contains the Reynolds number dependency of heat transfer from a particle in a moving liquid. The second and third terms represent the heat transfer in the subcooled liquid and by radiation across the vapor film respectively. The

last term is the heat transfer to the wake. In practice the latter term is unknown and so will be ignored when calculating Nu_t; it is included in the derivation of Eq. (F.B-13) in order to illustrate how heat transfer to the wake might be included in the formulation if future results should demand it.

Appendix F.C: On Nusselt Numbers and Other Empirical Correlations

(1) Radiative Nusselt number

For a thin vapor film around a sphere, it can easily be shown that the radiative heat transfer coefficient can be expressed as:

$$h_r = \frac{\varepsilon_w \varepsilon_c}{(\varepsilon_w + \varepsilon_c - 1)} \frac{\sigma_{SB}[T_w^4 - T_s^4]}{\Delta T_s} . \quad \text{(F.C-1)}$$

The radiative Nusselt number is defined by:

$$\mathrm{Nu}_r = \frac{h_r D}{k} . \quad \text{(F.C-2)}$$

The main uncertainty in evaluating Eq. (F.C-1) is deciding what values are appropriate for the emissivities. A means of calculating the emissivity of liquid metals is quoted in Ref. 1):

$$\varepsilon = -\frac{1.0 \times 10^{-5} T}{\sqrt{k_l}} . \quad \text{(F.C-3)}$$

(2) Natural convection Nusselt numbers

A review of empirical natural convection coefficients by Amato and Trien[22] lead to the following recommendation:

$$\mathrm{Nu}_c = 2 + 0.5(\mathrm{Gr}_l \mathrm{Pr}_l)^{1/4} . \quad \text{(F.C-4)}$$

However, Farahat and El Halfawy[17] used a higher coefficient when performing calculations using their film boiling model:

$$\mathrm{Nu}_c = 2 + 0.75(\mathrm{Gr}_l \mathrm{Pr}_l)^{1/4} . \quad \text{(F.C-5)}$$

Dhir and Purohit[2] state that the difference in the numerical constant is due to assumptions about slip between the coolant and the sphere. In fact, Eq. (F.C-5) fits the experimental data better, and so this is the equation recommended for use with non-metals.

For liquid metals the Nusselt number is a function of Boussinesq number rather than Rayleigh number. This is because the thicker thermal boundary in liquid metals makes natural convection more difficult. Thus, the recommended Nusselt number for liquid metals is:

$$\mathrm{Nu}_c = 2 + 0.75(\mathrm{Gr}_l \mathrm{Pr}_l^2)^{1/4} . \quad \text{(F.C-6)}$$

(3) Forced convection single-phase Nusselt numbers

For correlations suitable for the forced convection of fluid past a sphere, the recommended formula for non-metals is:

$$\mathrm{Nu}_c = 2 + \left(0.4\mathrm{Re}^{1/2} + 0.06\mathrm{Re}^{2/3}\right)\mathrm{Pr}^{0.4} . \quad \text{(F.C-7)}$$

For metals the following is recommended:

$$\mathrm{Nu}_c = 2 + 0.386\mathrm{Re}^{1/2}\mathrm{Pr}^{1/2} . \quad \text{(F.C-8)}$$

(4) Heat transfer to the wake

There is no quantitative data on heat transfer from a sphere to its wake during film boiling. Therefore assume that the wake heat transfer is negligible:

$$\mathrm{Nu}_w = 0 . \quad \text{(F.C-9)}$$

(5) The slip parameter β

The slip parameter is used to relate the shear stresses acting on the vapor film to the average vapor velocity (Eq. (F.A-3)). Suitable values for β are obtained by analogy with the solutions for the laminar flow of vapor between two parallel plates.

Let coordinate *x* be parallel to the plates and *y* be the perpendicular axis. The steady-state laminar flow of a fluid is determined by:

$$\frac{\delta P}{\delta x} = \frac{\delta \tau}{\delta y}, \quad \text{(F.C-10)}$$

where the pressure is P and the shear stress is defined by $\tau = \mu(\partial u/\partial y)$. Assuming constant material properties and noting that $\partial P/\partial x$ is independent of *y* allows Eq. (F.C-10) to be integrated:

$$\left(\frac{\delta P}{\delta x}\right)\frac{y^2}{2} = \mu u + Ay + B , \quad \text{(F.C-11)}$$

where A and B are numerical constants to be determined from the boundary conditions.

Case 1 (no slip condition; parabolic velocity profile)

Consider vapor flowing between two stationary plates with no vapor slip at the boundaries. The plates are distance w apart. The boundary conditions are therefore:

$$u = 0 \text{ at } y = 0 , \text{ and } u = 0 \text{ at } y = w . \quad \text{(F.C-12)}$$

Boundary conditions in Eq. (F.C-12) result in a parabolic velocity profile. Integrating to obtain the average velocity gives:

$$\bar{u} = \frac{-w^2}{12\mu}\left(\frac{\partial \tau}{\partial y}\right). \quad \text{(F.C-13)}$$

Comparison with Eq. (F.A-3) shows that in this case the value of the slip parameter is 12.

Case 2 (slip condition; linear velocity profile)

Now let there be no slip at the interface with only one of the plates. The new boundary conditions are:

$$u = 0 \text{ at } y = 0, \text{ and } \frac{\partial u}{\partial y} = 0 \text{ at } y = w. \tag{F.C-14}$$

Integrating to obtain the average velocity gives:

$$\bar{u} = \frac{-w^2}{3\mu}\left(\frac{\partial \tau}{\partial y}\right). \tag{F.C-15}$$

Comparison with Eq. (F.A-3) shows that in this case the value of the slip parameter is 3.

For natural convection Case 1 represents a maximum value of the slip parameter because the liquid-vapor interface is not stationary for a subcooled liquid (due to natural convection etc.). Gunnerson and Cronenberg[6] therefore constructed a linear relation of slip based on subcooling:

$$\beta = \begin{cases} 12 - \dfrac{18\Delta T_{sc}}{\left(T_s - T_{mp}\right)} & \text{for } 0 \le \Delta T_{sc} \le \dfrac{\left(T_s - T_{mp}\right)}{2} \\ 3 & \text{for } \Delta T_{sc} > \dfrac{\left(T_s - T_{mp}\right)}{2} \end{cases}. \tag{F.C-16}$$

In fact Eq. (F.C-16) seems a rather arbitrary construction. The slip parameter from Case 2 is actually preferred since it better fits the data (see Section F.5). In the case of forced convection, Case 2 is recommended because it compensates to some extent for a higher vapor film separation angle (see Section F.5.3). Thus the recommendation for the slip parameters is simply:

$$\beta = \beta' = 3. \tag{F.C-17}$$

References for Appendix F

1) Farahat, M., Eggen, D.T., Pool Boiling in Subcooled Sodium at Atmospheric Pressure, Nucl. Sci. Eng., Vol. 53, No. 2, 1974, pp. 240–254.

2) Dhir, V.K., Purohit, G.P., Subcooled film boiling heat transfer from spheres, Nucl. Eng. Des., Vol. 47, No. 1, 1978, pp. 49–66.

3) Walford, F.J., Transient heat transfer from a hot nickel sphere moving through water, Int. J. Heat Mass Transfer, Vol. 12, No. 12, 1969, pp. 1621–1625.

4) Orozco, J.A., Witte, L.C., Flow film boiling from a sphere to subcooled Freon-11, J. Heat Transfer, Vol. 108, No. 4, 1986, pp. 934–938.

5) Aziz, S., et al., Heat transfer regimes in forced convection film boiling on spheres, Proc. 8th Int. Heat Transfer Conf., San Francisco, 1986, pp. 2149–2154.

6) Gunnerson, F.S., Cronenberg, A.W., On the minimum film boiling conditions for spherical geometries, J. Heat Transfer, Vol. 102, No. 2, 1980, pp. 335–341.

7) Kikuchi, Y., et al., Measurement of liquid-solid contact in film boiling", Int. J. Heat Mass Transfer, Vol. 35, No. 6, 1992, pp. 1589–1594.

8) Kim, B.J., Corradini, M.L., Recent film boiling calculations: implications on fuel-coolant interactions, Int. J. Heat Mass Transfer, Vol. 29, No. 8, 1986, pp. 1159–1167.

9) Stevens, J.W., Witte, L.C., Transient film and transition boiling from a sphere, Int. J. Heat Mass Transfer, Vol. 14, No. 3, 1971, pp. 443–450.

10) Berenson, P.J., Film boiling heat transfer from a horizontal surface, J. Heat Transfer, Vol. 83, No. 3, 1961, pp. 351–356.

11) Henry, R.E., A correlation for the minimum film boiling temperature, AIChE Symp. Ser. Vol. 70, No. 138, 1974, pp. 81–90.

12) Spiegler, P., et al., Onset of stable film boiling and the foam limit, Int. J. Heat Mass Transfer, Vol. 6, No. 11, 1963, pp. 987–989.

13) Baumeister, K.J., Simon, F.F., Leidenfrost temperature - its correlation for liquid metals, cryogens, hydrocarbons and water, J. Heat Transfer, Vol. 95, No. 2, 1973, pp. 166–173.

14) Gunnerson, F. S., Cronenberg, A.W., On the thermodynamic superheat limit for liquid metals and its relation to the Leidenfrost temperature, J. Heat Transfer, Vol. 100, No. 4, 1978, pp. 734–737.

15) Olek, S., et al., A simple correlation for the minimum film boiling temperature, J. Heat Transfer, Vol. 113, No. 1, 1991, pp. 263–264.

16) Berthier, J. et al., AFDM: An Advanced Fluid Dynamics Model, Volume III: AFDM Heat-Transfer and Momentum-Exchange Coefficients, LA-11692-MS, Vol. III, Los Alamos National Laboratory, 1990.

17) Farahat, M.M.K., El Halfawy, F.Z., Film boiling heat transfer from spherical particles to subcooled liquids, Atomkernenergie, Vol. 26, No. 4, 1975, pp. 235–241.

18) Kobayasi, K., Film boiling heat transfer around a sphere in forced convection, J. Nucl. Sci. Technol., Vol. 2, No. 2, 1965, pp. 52–67.

19) Epstein, M., Hauser, G.M., Subcooled forced convection film boiling in the forward stagnation region of a sphere or cylinder, Int. J. Heat Mass Transfer, Vol. 23, No. 2, 1980, pp. 179–189.

20) Holman, J.P., Heat Transfer, McGraw-Hill, 1989, 752p.

21) Clift, R. et al., Bubbles, Drops, and Particles, Academic Press, 1978, 380p.

22) Amoto, W.S., Tien, C.L., Free convection heat transfer from isothermal spheres in water, Int. J. Heat Mass Transfer, Vol. 15, No. 2, 1972, pp. 327–339.

Nomenclature for Appendix F

C_{mfb} Constant used to calculate the minimum film boiling temperature

c_p Specific heat capacity of vapor

c_{pl} Specific heat capacity of liquid (coolant)

D Diameter of a sphere

D_s Size criterion for large sphere/small sphere regime

G Acceleration due to gravity

Gr Grashof number $\mathrm{Gr}_l = \dfrac{g\rho_l^2\beta_l\Delta T_{sc}D^3}{\mu_l^2}$

h Heat transfer coefficient (HTC):

h_c is the HTC in the coolant surrounding the sphere

h_r is the radiative HTC

h_t is the total HTC

$$h_f = \frac{k}{D}\left(\frac{\mathrm{Ra}^*}{0.71\beta}\right)^{1/4} = \left(\frac{\rho\Delta\rho g\lambda^* k^3}{0.71\beta\mu D\Delta T_s}\right)^{1/4}$$

k Vapor thermal conductivity

k_l Liquid (coolant) thermal conductivity

m Vapor mass flow rate at angle θ

m_t Total vapor production rate

Nu Nusselt number:

$\mathrm{Nu}_c = h_c D/k_l$ is in the coolant surrounding the vapor film

$\mathrm{Nu}_r = h_r D/k$ is the radiation Nusselt number

$\mathrm{Nu}_t = h_t D/k$ is the total Nusselt number

Nu_w is for heat transfer to a wake

Nu_0 is the Nusselt number at low Reynolds number

P Pressure

P_0 Pressure at the front stagnation point of a sphere in forced flow

Pr Prandtl number $\mathrm{Pr}^* = \dfrac{\lambda^*\mu}{k\Delta T_s}$, $\mathrm{Pr}_l = \dfrac{\mu_l c_{pl}}{k_l}$

R Radius of a sphere $R = D/2$

Ra Rayleigh number $\mathrm{Ra}^* = \dfrac{\rho\Delta\rho g\lambda^* D^3}{\mu k\Delta T_s}$

Re Reynolds number $\mathrm{Re} = \dfrac{\rho_l u D}{\mu_l}$

T Temperature:

T_w is the wall (hot surface) temperature

T_s is the liquid (coolant) saturation temperature

T_m is the liquid (coolant) maximum superheat temperature

T_c is the liquid (coolant) critical temperature

T_{min} is the minimum film boiling temperature

T_{mp} is the liquid melting point

ΔT Temperature difference relative to the liquid (coolant) saturation temperature:

$\Delta T_{min} = T_{min} - T_s$ is the minimum film boiling temperature (difference)

$\Delta T_s = T_w - T_s$ is the temperature difference across the vapor film

$\Delta T_{sc} = T_s - T_c$ is the liquid subcooling

u Coolant velocity far from the sphere

V Volume

$\bar{v}_\theta$ Average vapor velocity at angle θ

Greek symbols

β Slip parameter for vapor flow in natural convection models (Eq. (F.A-3))

β' Slip parameter for vapor flow in forced convection model (Eq. (F.B-6))

β_l Thermal expansivity of the liquid (coolant)

γ Ratio of liquid/vapor thermal conductivities ($= k_l/k$)

δ Vapor film thickness

δ_{min} Minimum vapor film thickness

ε Emissivity

ε_w is the emissivity of the wall (hot surface)

ε_c is the emissivity of the coolan

λ Latent heat of vaporization

$\lambda^* = \pi + 0.5 c_p \Delta T_s$

μ Vapor viscosity

μ_l Liquid (coolant) viscosity

ρ Vapor density

ρ_l Liquid density

$\Delta\rho$ Density difference between liquid and vapor ($= \rho_l - \rho$)

σ Surface tension

σ_{SB} Stefan-Boltzmann constant

τ_w Shear stress at the wall (i.e. the hot surface)

τ_i Shear stress at the vapor-liquid interface

Φ Subcooling ratio $\nu = \Delta T_{sc}/\Delta T_s$

ω $\omega = \left[\frac{\rho}{\rho_l}\left(\frac{\mu_l}{\mu}\right)^2\right]^{1/4}$

θ Angle from the vertical in natural convection film boiling model

φ Angle from the direction of liquid velocity in forced convection model

Subscripts

l Liquid (Vapor properties do not have subscripts)